การจำลองเชิงตัวเลขสำหรับการขยายตัวของรอยร้าวล้าในคานเหล็กที่มีแผ่นเสริมตั้งเชื่อมข้างคาน

นายวันเฉลิม เตรียมล้ำเลิศ

วิทยานิพนธ์นี้เป็นส่วนหนึ่งของการศึกษาตามหลักสูตรปริญญาวิศวกรรมศาสตรมหาบัณฑิต
สาขาวิชาวิศวกรรมโยธา ภาควิชาวิศวกรรมโยธา
คณะวิศวกรรมศาสตร์ จุฬาลงกรณ์มหาวิทยาลัย
ปีการศึกษา 2558

NUMERICAL SIMULATION FOR FATIGUE CRACK PROPAGATION IN STEEL BEAMS WITH WELDED TRANSVERSE STIFFENERS

Mr. Wanchalerm Triamlumlerd

A Thesis Submitted in Partial Fulfillment of the Requirements
for the Degree of Master of Engineering Program in Civil Engineering
Department of Civil Engineering
Faculty of Engineering
Chulalongkorn University
Academic Year 2015

Thesis Title	NUMERICAL SIMULATION FOR FATIGUE CRACK PROPAGATION IN STEEL BEAMS WITH WELDED TRANSVERSE STIFFENERS
By	Mr. Wanchalerm Triamlumlerd
Field of Study	Civil Engineering
Thesis Advisor	Associate Professor Akhrawat Lenwari, Ph.D.

Accepted by the Faculty of Engineering, Chulalongkorn University in Partial Fulfillment of the Requirements for the Master's Degree

.....Dean of the Faculty of Engineering
(Associate Professor Supot Teachavorasinskun, D.Eng.)

THESIS COMMITTEE

.....Chairman
(Professor Teerapong Senjuntichai, Ph.D.)

.....Thesis Advisor
(Associate Professor Akhrawat Lenwari, Ph.D.)

.....Examiner
(Assistant Professor Jirapong Kasivitamnuay, D.Eng.)

.....External Examiner
(Associate Professor Piya Chotickai, Ph.D.)

วันเฉลิม เตรียมล้ำเลิศ : การจำลองเชิงตัวเลขสำหรับการขยายตัวของรอยร้าวล้าในคานเหล็กที่มีแผ่นเสริมตั้งเชื่อมข้างคาน (NUMERICAL SIMULATION FOR FATIGUE CRACK PROPAGATION IN STEEL BEAMS WITH WELDED TRANSVERSE STIFFENERS) อ.ที่ปรึกษาวิทยานิพนธ์หลัก: รศ. ดร.อัครวัชร เล่นวารี, 104 หน้า.

วัตถุประสงค์ของงานวิจัยนี้ คือ เพื่อศึกษาการขยายตัวของรอยร้าวล้าของคานเหล็กหน้าตัดรูปตัวไอที่มีแผ่นเสริมตั้งเชื่อมข้างคาน โดยใช้การจำลองเชิงตัวเลขแบบ 3 มิติ ที่ถูกแรงกระทำในระนาบ นอกจากนี้เพื่อทำนายอายุของคานเหล็กในกรณีต่างๆ ได้แก่ คานเหล็กที่มีรอยร้าวเริ่มต้นต่างกัน มีขนาดช่องว่างของแผ่นเอวต่างกัน และคานเหล็กที่มีขนาดแผ่นเสริมตั้งเชื่อมข้างคานต่างกัน งานวิจัยนี้ได้นำโปรแกรม FRANC3D ที่เป็นระเบียบวิธีไฟไนต์เอลิเมนต์ มาช่วยในการคำนวณ และผลที่ได้จากการวิเคราะห์ของแต่ละแบบจำลองในกรณีต่างๆ ได้ผลว่าขนาดรอยร้าวเริ่มต้นที่มีขนาดเล็กจะสามารถรับแรงกระทำซ้ำซากได้จำนวนรอบที่มากและขนาดว่างของแผ่นเอวที่มีขนาดเล็กจะทำให้ตัวประกอบความเข้มของความเค้น (stress intensity factor) มีค่าสูงซึ่งส่งผลให้อายุของความล้าลดลง ในขณะที่แผ่นเสริมตั้งเชื่อมข้างคานที่มีความหนาน้อยจะมีผลทำให้คานเหล็กมีอายุที่ยาวนานขึ้น

ภาควิชา วิศวกรรมโยธา ลายมือชื่อนิสิต .....

สาขาวิชา วิศวกรรมโยธา ลายมือชื่อ อ.ที่ปรึกษาหลัก .....

ปีการศึกษา 2558

5770298221 : MAJOR CIVIL ENGINEERING

KEYWORDS: FATIGUE CRACK PROPAGATION / STEEL I-BEAM WITH WELDED TRANSVERSE STIFFENERS / INITIAL CRACK SIZE / WEB-GAP LENGTH / TRANSVERSE STIFFENER DIMENSION

WANCHALERM TRIAMLUMLERD: NUMERICAL SIMULATION FOR FATIGUE CRACK PROPAGATION IN STEEL BEAMS WITH WELDED TRANSVERSE STIFFENERS. ADVISOR: ASSOC. PROF. AKHRAWAT LENWARI, Ph.D., 104 pp.

The purposes of this study are to numerically simulate the 3D in-plane fatigue crack propagation in steel I-girders with welded transverse stiffeners and to predict the fatigue life of steel beams with different initial crack sizes and girder geometries, such as web-gap lengths and transverse stiffener dimensions. The FRANC3D software was used to perform calculation using the finite element analysis. Many cases were conducted and the results indicated that the propagation of very small crack required very high number of load cycles and the initial crack with smaller web-gap length had a higher value of stress intensity factor which shortened the fatigue life, whereas the thinner transverse stiffener had a tendency to decrease the fatigue life of steel I-beams.

Department: Civil Engineering Student's Signature .....
Field of Study: Civil Engineering Advisor's Signature .....
Academic Year: 2015

ACKNOWLEDGEMENTS

Although only my name appears on the cover of this thesis, a great many people have contributed to its production. It has been a period of intense learning for me but I also got a good way to do science research. These achievements would be very useful for my career and be one of my life's greatest lessons. I would like to reflect on the people who have supported and helped me so much throughout this period.

Firstly, the author would first like to express my sincere thanks to my thesis advisor, Assoc. Prof. Akhrawat Lenwari for giving me knowledge, invaluable help, and constant encouragement throughout this thesis. Without these supports, I could not have been successfully conducted.

Also, I would like to thank my thesis committee: Prof. Teerapong Senjuntichai, Asst. Prof. Jirapong Kasivitamnuay, and Assoc. Prof. Piya Chotickai for their encouragement, insightful comments, and valuable suggestions.

Besides, I really want to give special words of gratefulness to my scholarship. The scholarship from the graduate school, Chulalongkorn University to commemorate the 72nd anniversary of his Majesty King Bhumibala Aduladeja and the 90th Anniversary Chulalongkorn University Fund (Ratchadaphiseksomphot Endowment Fund) are gratefully acknowledged.

Finally, I would personally like to thank my friends and family who always encourage and support me throughout all the time. I am forever grateful because this accomplishment would not have been possible without them.

CONTENTS

Page

Page

Page

LIST OF FIGURES

Page

LIST OF TABLES

page

CHAPTER I
INTRODUCTION

1.1 Motivation and significance

Steel bridges are generally used in many applications, such as crossing the river, intersection, etc. Due to confrontation with a number of cycles of live load whose stress amplitudes are lower than yield stress, many fatigue cracks can occur in any positions of steel bridges, especially concentrated stress areas, and incomplete areas, which are welded or modified. The metropolis or the city that has high density of population is likely to have high cycle of live load. Thus, the rate of fatigue crack occurrence is increasing. There are many factors which cause fatigue crack to occur, such as magnitudes, irregularities of force, geometries of steel structure, discontinuities of materials, exposures to environment, and temperature changes. When fatigue crack occurs, it is quite difficult to control the direction of fatigue crack propagation. The fatigue cracks always grow in the critical direction and can damage the structure. Moreover, the prediction of fatigue crack propagation will protect the steel structures and know the approximate service life of a steel structure [1, 2].

In the design steps of steel beams, especially extra-long steel beams, many problems usually occur, especially insufficient shear capacity. Transverse stiffeners are used to solve these problems. In addition, in the fabrication procedure of transverse stiffeners on the steel beams was recommended to preserve the gap between bottom end of the transverse stiffeners and the tension flange called “web gap” in purpose of the convenience for welding the transverse stiffeners on web. The welding and the gap are the reasons that cause the damages of the steel beams from fatigue crack.

The design guides of AASHTO (2012) [3] recommended the use of four to six times as thick as web thickness for the strength of steel beams [4] but did not consider the effects of fatigue crack to the life span of the steel beams and might finally cause the fracture of the bridge. Moreover, the connection of two materials can cause the non-homogeneous area in the objects called “defects”. The sizes of defects depend on the quality of welding which also influence the life of the steel structures.

In addition, the transverse stiffeners must have sufficient rigidity to keep the cross section of steel beam in shape in order to ensure the nodal line formation during web buckling and develop the shear-buckling resistance. The web panel boundary was assumed not to deflect laterally perpendicular to the plane of web when steel beam was subject to external loads [5]. So, all transvers stiffeners were required to have proper rigidity in that direction whereas the effects of fatigue crack were not taken into consideration. Consequently, the fatigue crack may be the cause to fracture the steel structures as shown in Figure 1.1.

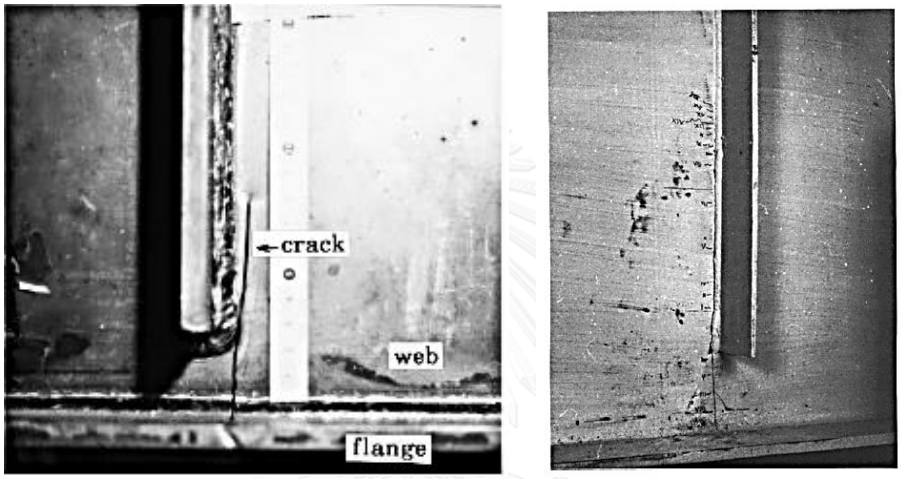

Figure 1.1 Fatigue crack propagation of steel I-beams with welded transverse stiffeners [6, 7]

Many studies have investigated the behavior of steel structures when the fatigue crack occurs. Fisher (1974) described the behavior of fatigue crack growth occurring at the welded toe of steel I-beam with welded transverse stiffeners. The fatigue crack can initiate at any locations and propagate in various patterns depending on the welding of the stiffeners to either only the web or welding of the web and the flanges.

Newman and Raju (1984) studied the fatigue crack growth patterns and predicted the lives of steel plates for three crack configurations. The first case was surface crack in steel plates subjected to remote tension and bending. The second and third steel plates subjected to remote tension loading were surface crack and corner crack at a circular hole respectively. Also, Zong, Shi, and Wang (2015) performed numerical simulation of fatigue crack propagation and predicted the life of steel plates using FRANC3D. In order to measure the fatigue growth rate parameter, numerical

simulation for fatigue crack propagation of CT specimens were used in these tests. Two material types used in test were base metal and butt weld joint. Moreover, Kotsikos and Grasso (2012) also used FRANC3D in simulation of fatigue crack in rail and investigated the fatigue crack behavior at the foot region of a rail.

Although many researches have investigated the fatigue crack behavior, more studies are needed to extend more complex patterns of steel structure in order to apply in many cases.

The purposes of this study are to numerically simulate the 3D in-plane fatigue crack propagation in steel I-girders with welded transverse stiffeners and to predict the fatigue life of steel beams with different initial crack sizes and girder geometries, such as web gap sizes, and transverse stiffener dimensions.

Because of many procedures and complex calculations of fatigue crack propagation, FRAND3D, which is one of commercial engineering software, was used to perform using the finite element analysis. The abilities of this software are the insertion of the initial crack configurations, static crack analysis for calculation of stress intensity factor K, crack growth analysis for computation and interpretation the fatigue crack extension with any criteria along the crack growth direction, etc. Many problems can be solved conveniently and shown in 3 dimensions. However, other software have to be used concurrently to draw solid work, define supports and loadings, and be the solver for FRANC3D. In this research selects ANSYS to work with. Furthermore, FRANC3D has the great option to remesh automatically, especially the critical point. The accuracy increases from this performance of the software.

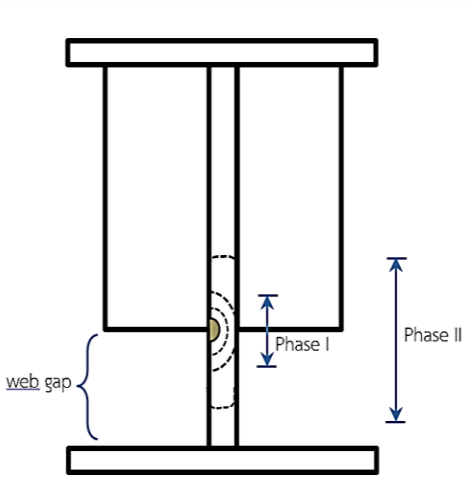

Figure 1.2 Phases of fatigue crack growth in steel I-beams with welded transverse stiffeners

Fatigue cracks usually initiate at the weld toe in the area of bottom end of transverse stiffener on the web surface and grow across the web thickness as a semicircular shape as shown in Figure 1.2. Afterward, the fatigue crack transforms the shape into two-tip through-thickness shape with both fronts growing up and down the web [6]. In this study, this behavior can be separated to be two phases. Phase I starts from fatigue crack initiation, semicircular shape, and propagates until penetrating through the web plate. Then, fatigue crack transforms the shape to be two-tip through-thickness shape which Phase II starts and propagates until reaching the fracture toughness as shown in Figure 1.3.

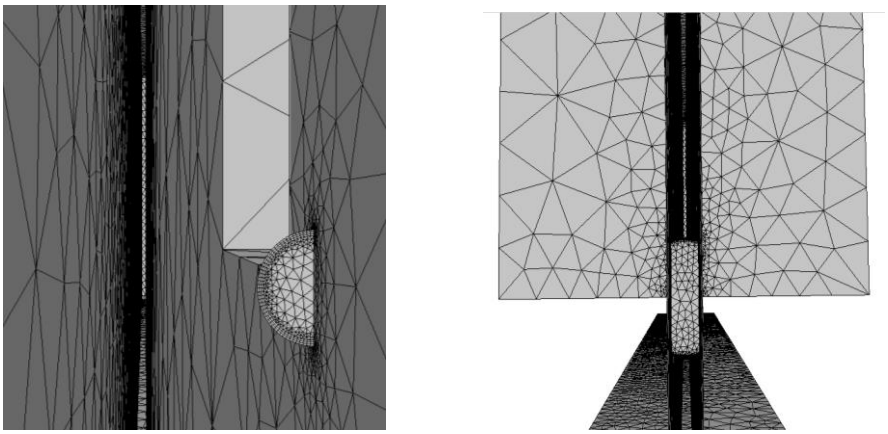

(a) (b)

Figure 1.3 Initial crack configurations of (a) phase I (b) phase II

The steel I-girders with welded transverse stiffeners are mainly used in construction of steel bridge and other steel structures. Accordingly, predictions of fatigue crack propagation life are very useful to maintain serviceability of steel structures.

1.2 Research objectives

1. To numerically simulate the 3D in-plane fatigue crack propagation in steel I-girders with welded transverse stiffeners.

2. To predict the fatigue life of steel beams with different initial crack sizes and girder geometries, such as web gap sizes, and transverse stiffener dimensions.

1.3 Scope of research

The research was limited in scope as follows:

1. Type of live load is cyclic loading which has constant magnitude.

2. The simulation of fatigue crack propagation is based on the linear-elastic fracture mechanics.

3. Fatigue crack occurs from influence of in-plane stress, therefore the distortion-induced fatigue is not considered in this research.

4. Residual stresses which arise from the welding are not considered in the simulations.

5. Environmental effects, e.g., temperature change, humidity, and corrosion are not considered to affect to fatigue crack propagation.

6. Numerical simulation is performed using the finite element analysis.

CHAPTER II
LITERATURE REVIEW

2.1 Fatigue crack propagation in steel structures

Fatigue is one of the main factors that cause the collapse of steel bridges. Since the steel bridges are subjected to a number of cycles of live load which has stress amplitudes lower than yield stress, fatigue crack initiation occurs in any area, especially joint in steel bridge and welding area. Life of the steel bridges and serviceability are significantly reduced. Consequently, the durability of steel bridges will be more effective if influence of fatigue crack is taken into consideration.

The important parameter to estimate service life of steel bridge is stress intensity factor (K). Newman and Raju (1979) [8] studied the stress intensity factor of steel plate with surface crack under tension or bending. A 3D finite-element stress analysis was used to compute mode-I stress intensity factor along the crack front.

Fatigue crack can grow in any directions depending on situations. Newman and Raju (1984) proposed fatigue crack propagation patterns and lives for surface crack, surface crack at holes, and corner cracks at holes of steel plates in three-dimensional crack bodies. Modified linear-elastic fracture mechanics concepts were used to predict these problems. Remote tension and bending were assigned to the first specimen, surface crack in a steel plate. Only remote tension was assigned to the specimens having surface crack and corner crack at circular hole respectively. Cyclic loads with constant amplitude were assigned with range of stress ratio (R) from -0.5 to 0.75. In the prediction of crack propagation used the equations of SIF improved by Newman and Raju (1979). [9]

Since the crack shapes were assumed to be either semi-elliptical or quarter-elliptical patterns, specimens needed to consider only the ranges of SIF at the maximum depth point and the tip of the crack at the surface.

Newman and Raju (1984) predicted the patterns and lives of fatigue crack growth in three specimens and compared with test data which was taken from their

literature. The first case was the plate having initial crack at surface subjected to remote tension loading and bending moment as shown in Figure 2.1. Figure 2.2 shows that the ratio of crack shape in width to length direction (a/c) decreased throughout the increasing of crack growth a/t for the case of plate was subjected to remote tension loading. In case of remote bending moment in Figure 2.3, the ratio of crack a/c increased in the beginning then went down when a/t was higher than 0.4. Moreover, Figure 2.4 shows that the obtained crack length from prediction depending on load cycles agree well with experiment.

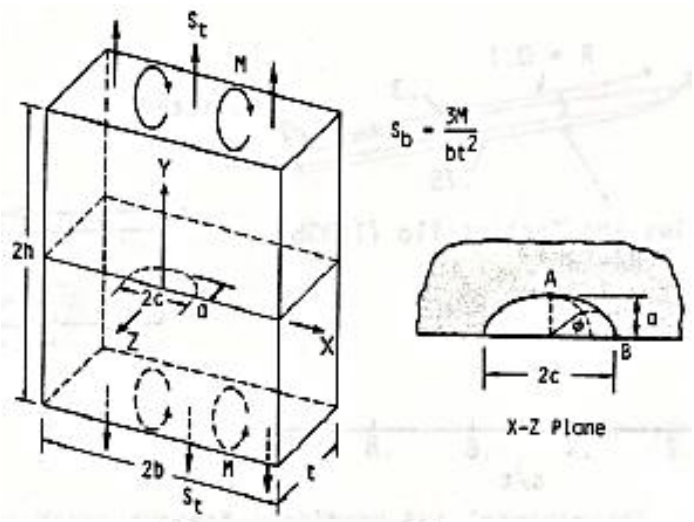

Figure 2.1 Surface crack in a steel plate [10].

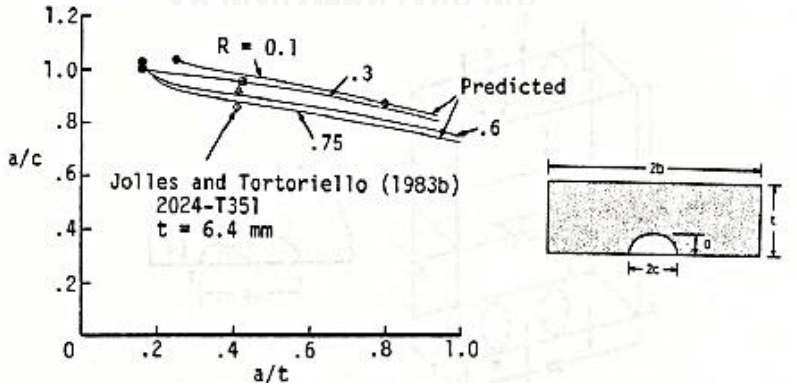

Figure 2.2 Prediction of fatigue patterns for a surface crack under remote tension compared to experiments [10].

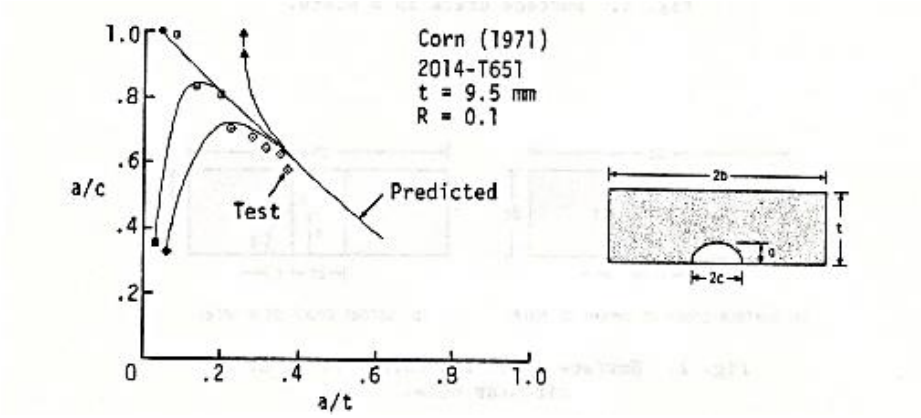

Figure 2.3 Prediction of fatigue patterns for a surface crack under remote bending compared to experiments. [10].

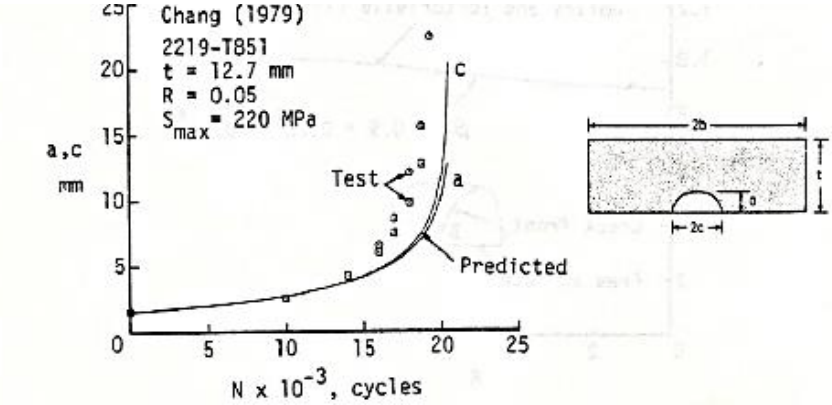

Figure 2.4 Prediction of fatigue life for the surface crack under remote tension compared to experiments [10].

The second case was the plate having initial surface crack at center of a circular hole under tension as shown in Figure 2.5. The results in Figure 2.6 show that the ratio of crack shape in width to length direction a/c decreased dramatically in the beginning and then slightly rose after a/t reached to 0.3. Crack length obtained from prediction depending on load cycles also agreed well with experiment as shown in Figure 2.7.

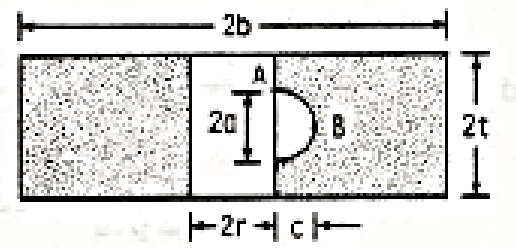

Figure 2.5 Surface crack at center of circular hole [10].

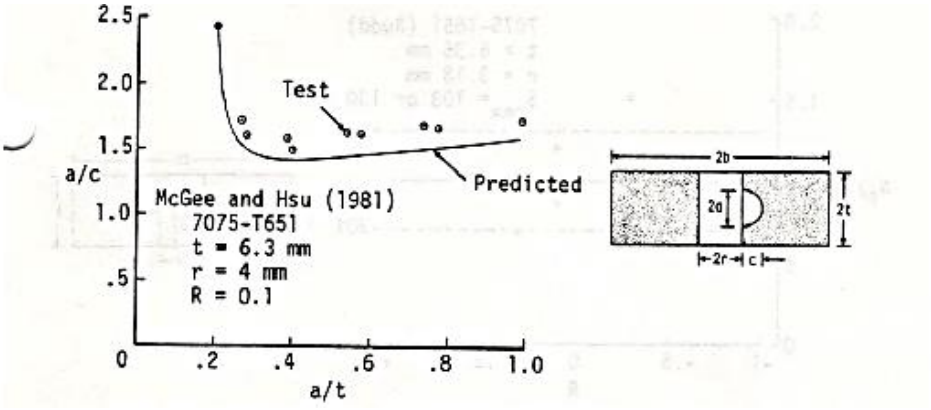

Figure 2.6 Prediction of fatigue patterns for a surface crack at a hole under remote tension compared to experiments [10].

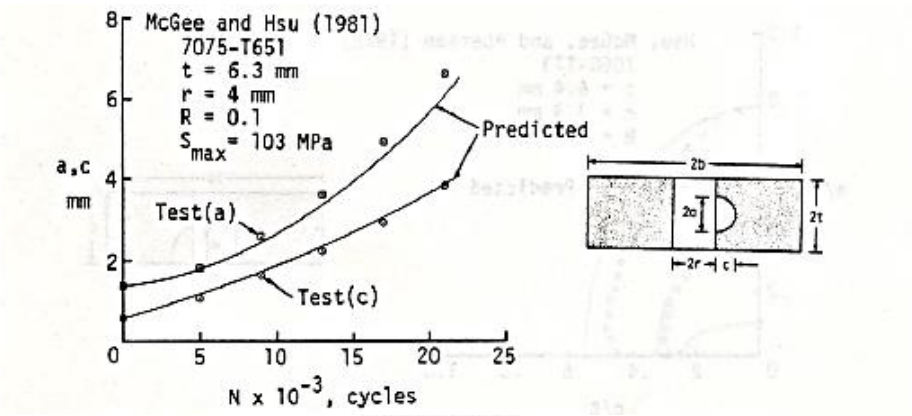

Figure 2.7 Prediction of fatigue life for a surface crack at a hole under remote tension compared to experiments [10].

The last case was the plate having initial surface crack at corner of circular hole subjected to remote tension loading as shown in Figure 2.8. The results in Figure 2.9 show the comparison of predicted crack shape to test result. Good agreement was observed between prediction and test at the small a/t value but the large a/t value was observed as fair agreement. Finally, Crack length obtained from prediction depending on load cycles also agreed well with experiment as shown in Figure 2.10.

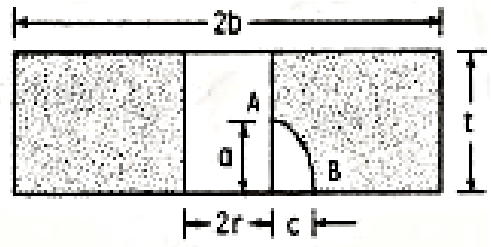

Figure 2.8 corner crack at a circular hole [10].

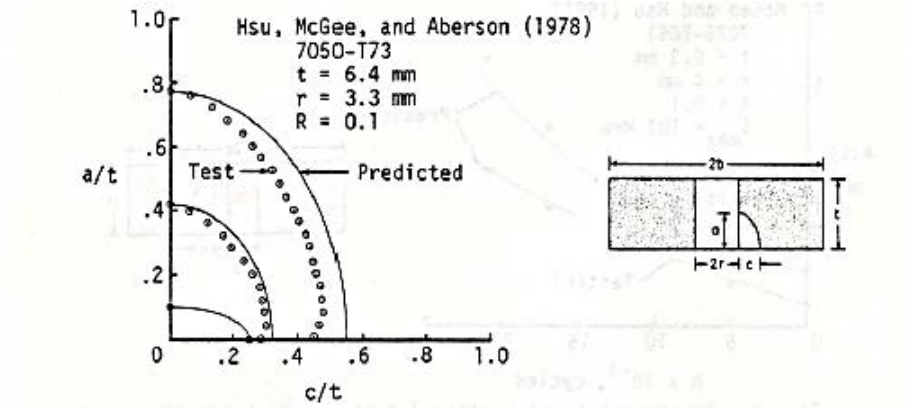

Figure 2.9 Prediction of fatigue pattern for a corner crack at a hole under remote tension compared to experiment [10].

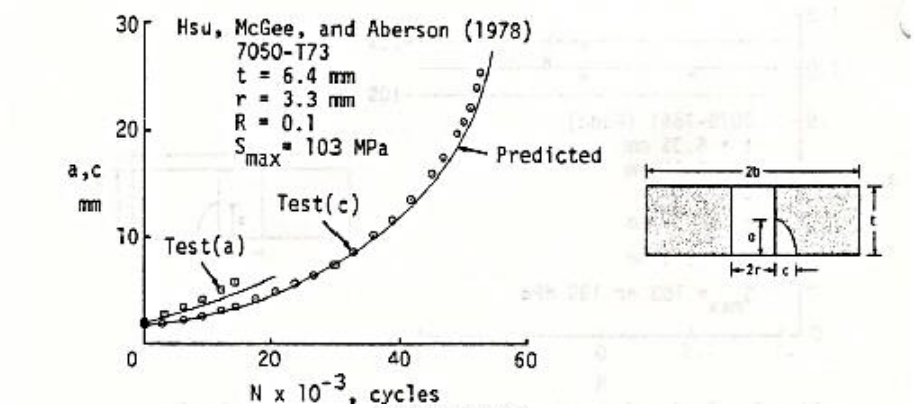

Figure 2.10 Prediction of fatigue life for a corner crack at a hole under remote tension compared to experiments [10].

Although Newman and Raju (1984) used the modified linear-elastic fracture mechanics concepts to predicted fatigue crack propagation, there were many other criteria which could be used to perform prediction of fatigue crack propagation as well. Bouchard, Bay, and Chastel (2003) performed many various applications to predict crack propagation path and compared by using three different crack growth criteria. Maximum circumferential stress criterion (MCSC), minimum strain energy density fracture criterion (MSEDC), and maximum strain energy release rate criterion (MSERRC) were chosen in research based on finite element methods. The crack propagation was calculated on the method of remeshing and nodal relaxation. [11]

The materials used in all examples were elastic with a Young's modulus E=98,000 MPa. and a Poisson ratio $\nu = 0.3$ [11]

1) A rectangular part with an oblique pre-crack was submitted to a vertical tensile test

1.1) The maximum circumferential stress criterion (MCSC)

The crack propagation in mode I had direction perpendicular to principal stress occurring from vertical applied load as shown in the Figure 2.11. The path of crack propagation obtained from this criteria grew in horizontal direction along the plate. [11]

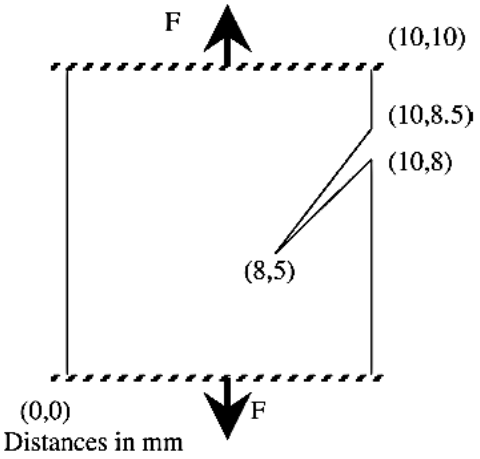

Figure 2.11 A rectangular part with an oblique pre-crack [11].

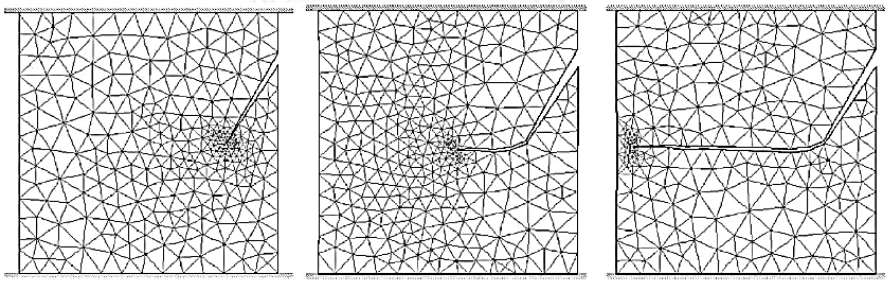

Figure 2.12 The fatigue crack path with the MCSC [11].

1.2) The minimum strain energy density fracture criterion (MSEDC)

The ring around crack trip had directly influence the accuracy of this criterion which was calculated for each element of the ring and the local minimum was calculated using S(θ) curve. According to different values between external element and internal element of the ring, separation of both values were required for better accuracy. Moreover, the calculation of the local minimum should compute as the minimum of parabola for improvement the accuracy as well. The crack may propagate in the direction that energy was minimum. [11]

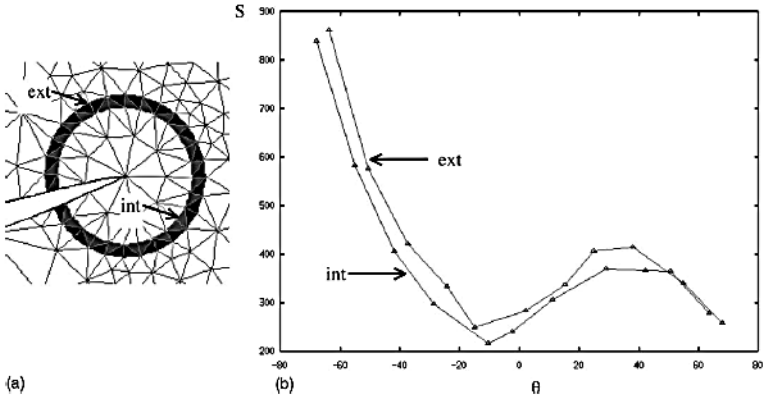

Figure 2.13 (a) Ring elements at the crack tip and (b) calculated S(θ) curve for the MSEDC with the numerical formulation [11].

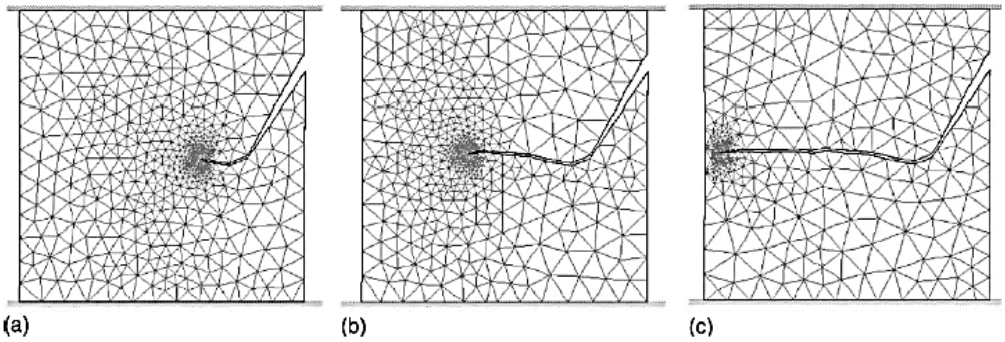

Figure 2.14 Crack propagation path with the MSEDC without numerical improvements [11].

The path of crack propagation calculated by MSED method was quite in the horizontal direction and grew steadily until the end of the plate as shown in Figure 2.14.

1.3) The maximum strain energy release rate criterion (MSERRC) using the G(θ) method

The maximum point of the G(θ) curve was considered to predict the path of crack propagation. However, the accuracy depended on the chosen angle step. [11]

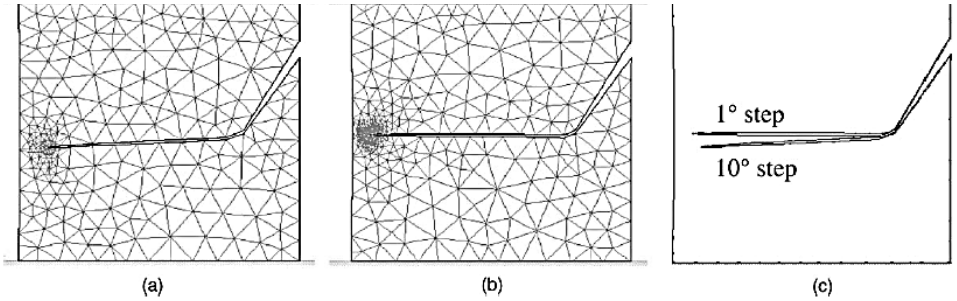

Figure 2.15 The fatigue crack path calculated with the MSERRC for an angle scan of (a) 10^{o}, (b) 1^{o} and (c) superimposed trajectories [11].

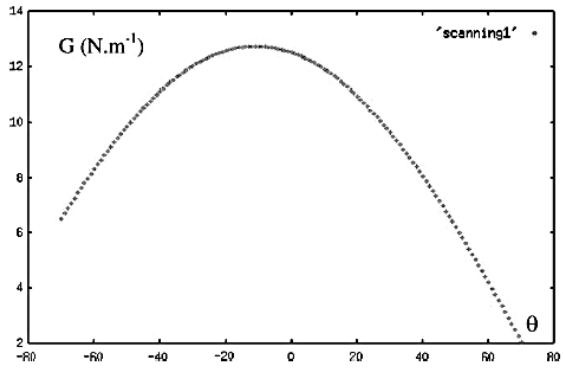

Figure 2.16 S(θ) curve [11].

According to these results, all criteria could give good results. The crack paths of each criteria were not significantly different. Thus, any criteria could be chosen for prediction of crack propagation by user depending on their convenience.

2) Two holes steel plate with pre-crack

This example studied crack propagation in planar domain with two holes as shown in the Figure 2.17. The crack path was under the influence of mode-I loading.

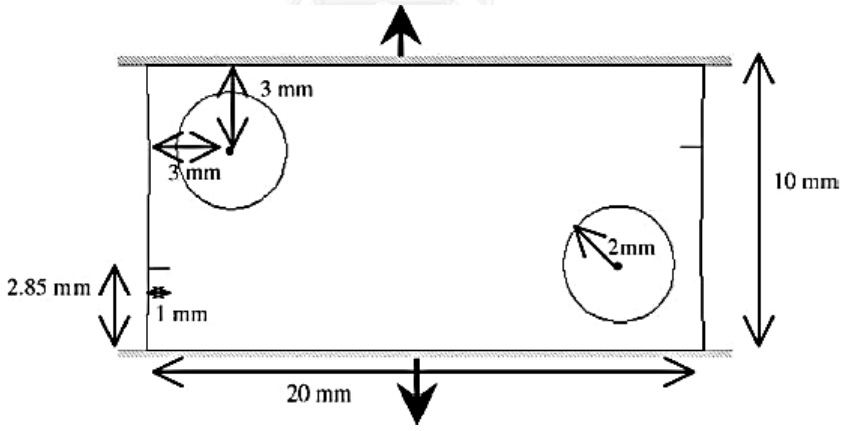

Figure 2.17 Pre-cracked part of steel plate with two holes [11].

2.1) The maximum circumferential stress criterion (MCSC)

Each crack grew in very near the holes in the beginning and changed to grow in horizontal direction. The opposite hole attracted the crack again.

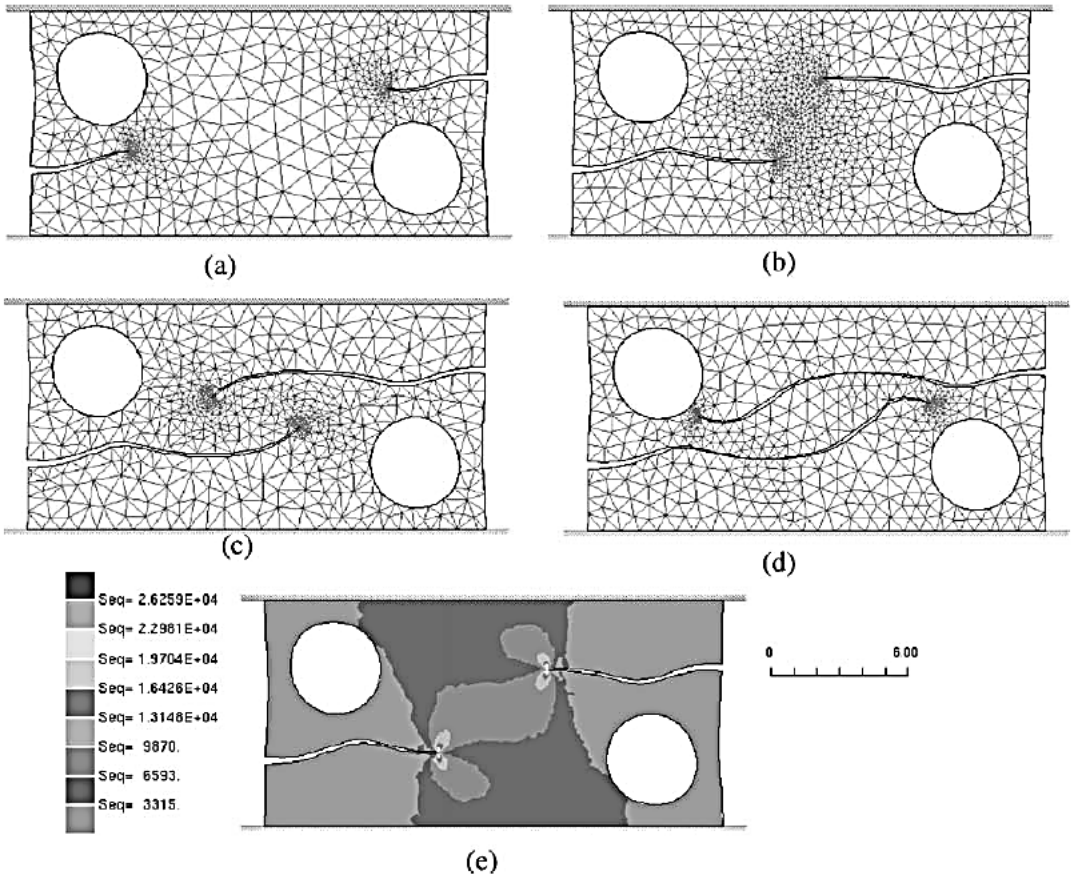

Figure 2.18 Crack paths in a pre-cracked part with two holes, calculated with the MCSC [11].

2.2) The minimum strain energy density fracture criterion (MSEDC)

Three simulations were operated with a small ring, medium ring, and large ring. The crack path of the small ring moved toward the holes and it would not change the direction to horizontal direction. The crack path of medium ring was the proper path in global propagation. The large radius gave a path in horizontal direction and grew to the opposite side of the steel plate as shown in Figure 2.19.

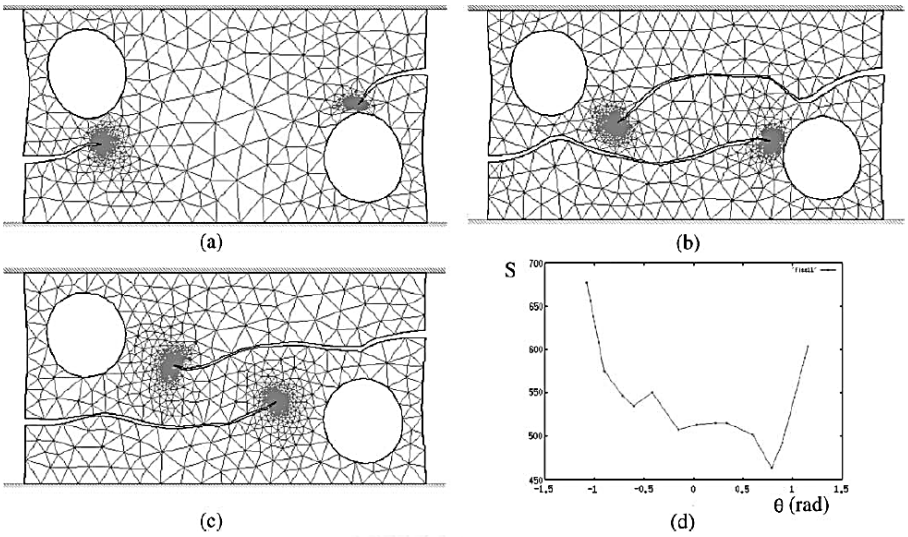

Figure 2.19 Crack paths calculated with the MSEDC with different ring radii. (a) a small ring around crack tip, (b) a medium one, (c) the large one [11].

2.3) The maximum strain energy release rate criterion (MSERRC) using the G(θ) method

Although this criterion also had three different sizes of ring, the G(θ) curve was still regular. The 10° scanning path of three criteria was quite similar. Therefore, the superposition of the crack path for these simulations presented the mesh-independent of this criterion.

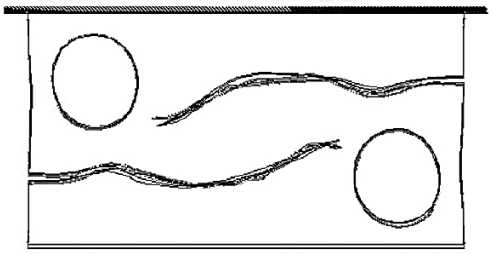

Figure 2.20 Superposition of crack trajectories calculated with the MSERRC, for three different mesh refinements [11].

Meshing in complex example was more important than simple example. The result of MSEDC depended on meshing but the others could give good results without mesh dependence. The comparison of crack path results between the MSEDC and MSERRC, and between the MSERRC and MCSC are shown in the Figure 2.21. Moreover, holes had more influence the local criterion of MCSC, but in the global result had no significant difference.

The results of CPU time computation of three criteria with the same automatic remeshing parameters show that the MSEDC was the slowest method spending time for the crack propagation. The two others criteria were time equivalent as shown in the Table 2.1.

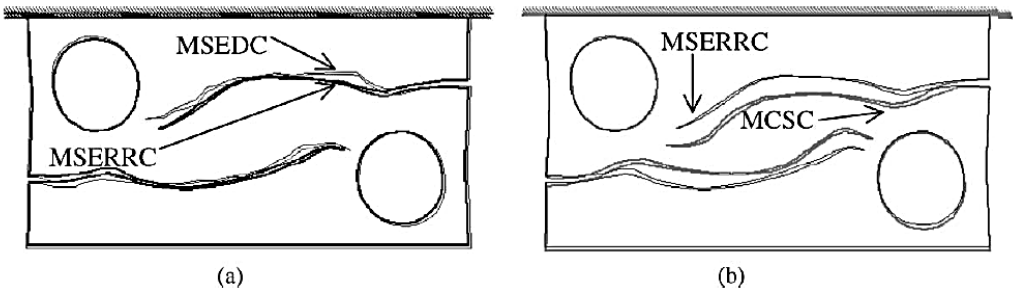

Figure 2.21 Crack trajectories comparison [11].

Table 2.1 CPU time comparison [11]

Criterion	MCSC	MSEDC	MSERRC
Number of nodes	3053	3075	3186
CPU time	t	$1.3t$	$1.08t$

3) Crack growth from a fillet weld

A structural member, I-beam, which had initial crack at a fillet, joint between web and flange in I-beam, was considered the path of crack propagation. The linear elastic plane strain was simulated using the MCSC with a Poisson ratio **V**=0.3 and a Young's modulus E=200 GPa. The initial crack length at the fillet was a0=5 mm. Accordingly, the bending stiffness could be changed by varying the size of bottom I-beam h = 15, 115, and 315 mm. respectively. The results of crack propagation were certainly different depending on bending stiffness as shown in the Figure 2.22.

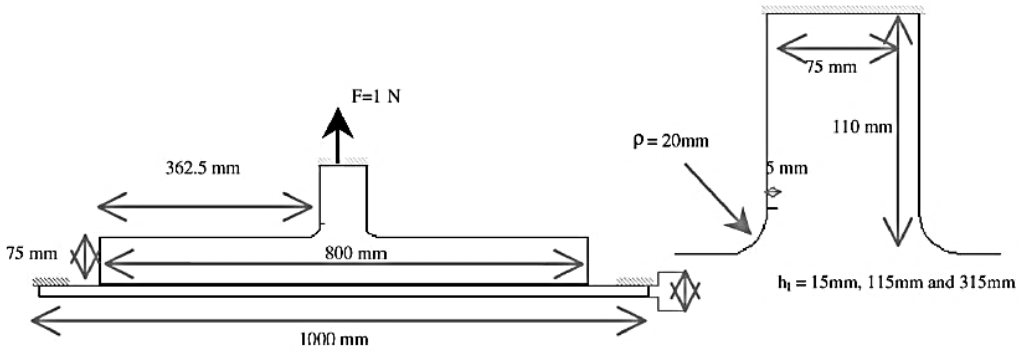

Figure 2.22 Crack growth from a fillet [11]

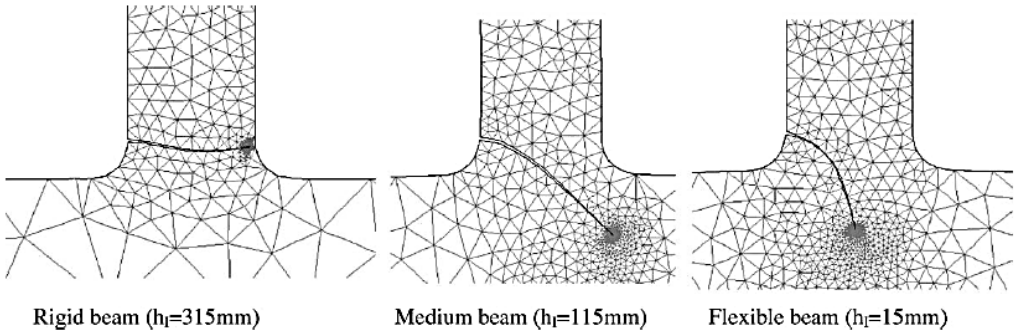

Figure 2.23 Influence of the bottom I-beam rigidity on the crack path [11]

The results in Figure 2.23 describe that path of crack propagation was different depending on the size of beam (h). The crack patterns of rigid, medium, and flexible beam grew in horizontal direction, declined, and considerably went down respectively.

Table 2.2 Comparison of the performance in each criteria

	Criteria 1 (MCSC)	Criteria 2 (MSEDC)	Criteria 3 (MSERRC)
Accuracy	high	Medium	high
Time computation	Medium	Slower than the 2 other criteria.	medium
Implement in finite element code	Easier than the 2 other criteria.	Medium	hard

Table 2.2 shows the comparison of three criteria in terms of accuracy, time computation, and implement in finite element code and probably conclude that MCSC was more suitable for prediction of the crack propagation path. Consequently, the MCSC method will be used in this study.

In this research, fatigue crack initiated as a semicircular shape at the weld toe and propagated to the end of web thickness called Phase I. Liao (1989) computed the values of stress intensity factor along semicircular surface for surface crack under tension or bending in three dimensional plates as shown in Figure 2.24.

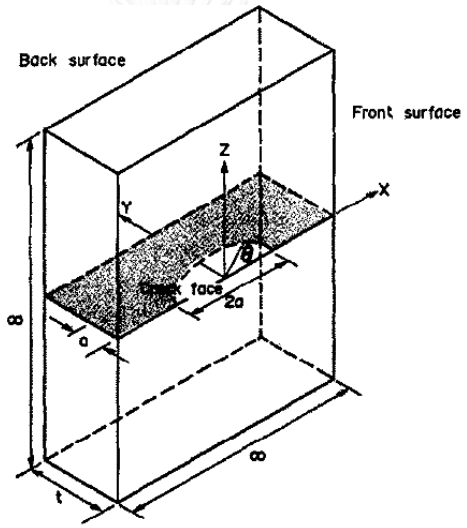

Figure 2.24 Semicircular flaw in an infinite plate of finite-thickness [12]

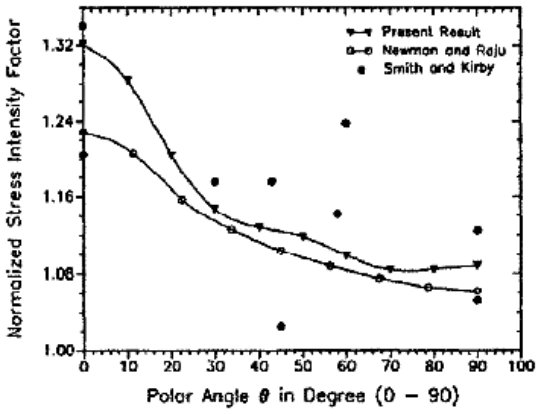

Figure 2.25 Semicircular flaw under tension [12], a/t=0.4

Numerical results of normalized stress intensity factor along polar angle under tension and bending at depth to thickness ratios a/t of 0.2, 0.4, 0.6, 0.8 were calculated and were compared with Newman and Raju (1979) solution. Figure 2.25 plotted the results of normalized stress intensity factor along polar angle of semicircular flaw under tension at a/t of 0.4. The stress intensity factor at surface front was the highest value and dropped substantially along crack front until the deepest point [12].

McFadyen, Bell, and Vosikovsky (1990) studied the stress intensity factor and life of steel plate with surface semi-elliptical defect by testing with pure bending as shown in Figure 2.26. The fatigue crack shapes results shown in Figure 2.27 describe that the crack size in c direction of semi-elliptical shape grew up faster than grew in a direction. Moreover, fatigue crack life of both directions was predicted and compared the results with Newman and Raju (1981) [13] as shown in Figure 2.28. The results show satisfactory in testing and supported the Newman and Raju solution [14].

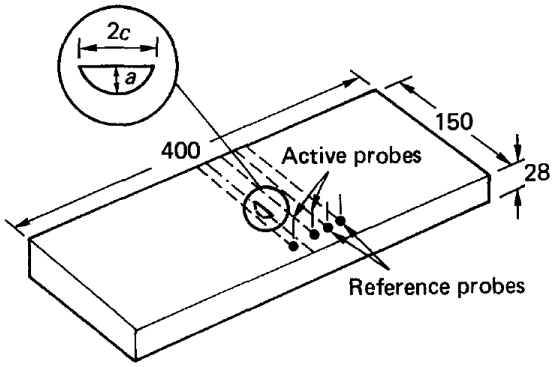

Figure 2.26 Specimen geometry and configuration [14] (dimension in mm)

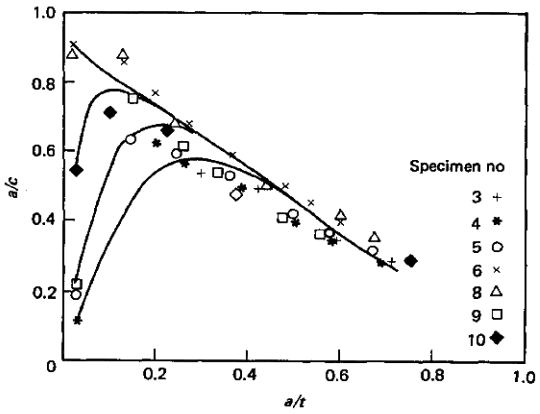

Figure 2.27 Predicted crack shape development for specimen [14], SIF from Newman and Raju solution [13]

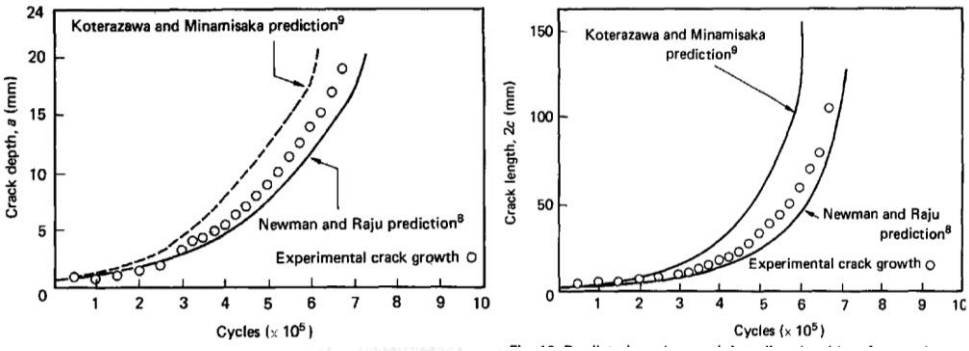

Figure 2.28 Predicted crack growth in a and c directions [14]

2.2 Fatigue of welded details in steel bridges

In order to develop accurate stress intensity factor solutions for steel I-beams under tension or bending, Albrecht, Lenwari, and Feng (2008) [15] studied the effects of parameters on correction factors for two-tip web crack as shown in Figure 2.29. The stress intensity factor for upper crack tip (K^A) and lower crack tips (K^B) of two-tip web crack were different caused by eccentricity. Three parameters that influenced correction factor for the upper crack tip of a web crack under bending were the flange-to-web area ratio (β), the normalized web crack length (λ_w), and the normalized crack eccentricity (ε) as shown in Figure 2.30.

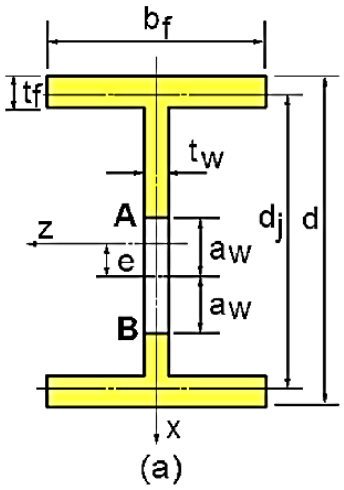

Figure 2.29 Coordinates and symbols of I-beam for two-tip web crack web crack [15]

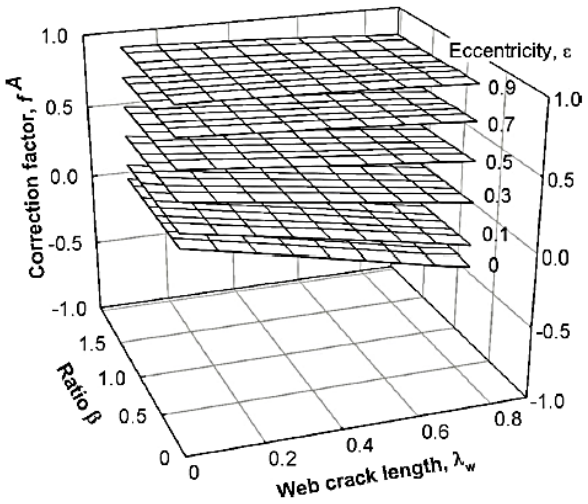

Figure 2.30 Correction factor for the upper tip of a web crack under bending [15]

In addition, constraining effect also influenced the correction factors of I-beams by comparison with single plate solutions [15]. The correction factor (f^{β}) of single-plate solutions always increase with the crack length but I-beams are always less than the single-plate solutions because of constraining effect. This effect is higher when crack length increase or the crack tip propagates closer to the flange-to-web junction.

Therefore, the best fitting equation to compute the correction factor of two-tip and of I-beam under tension and bending were (2.1) where coefficients were given in Table 2.3 [15].

$$f^{A,B}(\lambda_w, \varepsilon, \beta) = a_0 + a_1\varepsilon + a_2\beta\varepsilon + a_3\varepsilon^2 + a_4\lambda_w + a_5\beta\lambda_w + a_6\varepsilon\lambda_w + a_7\lambda_w^2 + a_8\beta\varepsilon\lambda_w + a_9\beta^2\varepsilon + a_{10}\beta\varepsilon^2 + a_{11}\lambda_w\beta^2 + a_{12}\lambda_w\varepsilon^2 + a_{13}\beta\lambda_w^2 + a_{14}\varepsilon\lambda_w^2 \quad (2.1)$$

Table 2.3 Coefficients for Two-Tip Web Cracks in I-beams [15]

	Tension		Bending	
Coefficient	Upper crack tip	Lower crack tip	Upper crack tip	Lower crack tip
a_0	1	1	0	0
a_1	−0.07184	−0.03591	1.02395	1.02052
a_2	0.05916	0.03257	−0.02824	−0.03142
a_3	0.07266	0.01609	−0.02660	−0.02841
a_4	0.16801	0.17113	−0.51095	0.48403
a_5	−0.15810	−0.17469	−0.00309	−0.02169
a_6	−0.09645	0.00540	0.66587	-0.19538
a_7	0.13248	0.19882	0.02106	0.10116
a_8	0.11124	0.10355	−0.03243	−0.02670
a_9	−0.01464	−0.01573	0.00337	0.00206
a_{10}	−0.03299	0.00399	0.02660	0.03282
a_{11}	0.04288	0.05901	0.00483	0.01704
a_{12}	−0.14373	−0.13149	−0.14302	−0.20652
a_{13}	−0.09648	−0.16125	−0.01281	−0.06069
a_{14}	−0.03380	−0.27916	−0.04610	−0.28079

2.3 Fatigue crack propagation at welded transverse stiffeners

Steel I-beams with transverse stiffeners are usually used in many steel structures, especially steel bridges that confront with a number of cycles of live load whose stress amplitudes are lower than yield stress, many fatigue cracks can occur.

In the design steps of steel beams, especially extra-long steel beams, many problems usually occur, e.g., insufficient shear capacity, concentrated loading, and lateral buckling. Transverse stiffeners are used to solve these problems. In addition, in the fabrication procedure of transverse stiffeners on the steel beams was recommended to preserve the gap between bottom end of the transverse stiffeners and the tension flange called “web gap” in purpose of the convenience for welding the transverse stiffeners on web. Therefore, the welding and the gap are the reasons that cause the damages of the steel beams from fatigue crack.

The design guides of AASHTO (2012) recommended the use of four to six times as thick as web thickness for the strength of steel beams but did not consider the effects of fatigue crack to the life span of the steel beams and might finally cause the fracture of the bridge. The steel I-beam with welded transverse stiffeners was classified as Category C' detail (AASHTO, 2012)[3]. This detail was partially studied by Fisher (1974). They studied the behavior of fatigue crack growth occurring at the welded toe of steel I-beam with welded transverse stiffeners. The fatigue crack can initiate at any locations and propagate in various patterns depending on the welding of the stiffeners to either only the web or welding of the web and the flanges.

Fisher (1974) discussed the type 2 stiffeners that were not welded to bottom flange in a region of pure bending. The plane of crack propagated in perpendicular to the longitudinal axis of the steel girder as shown in Figure 2.31.

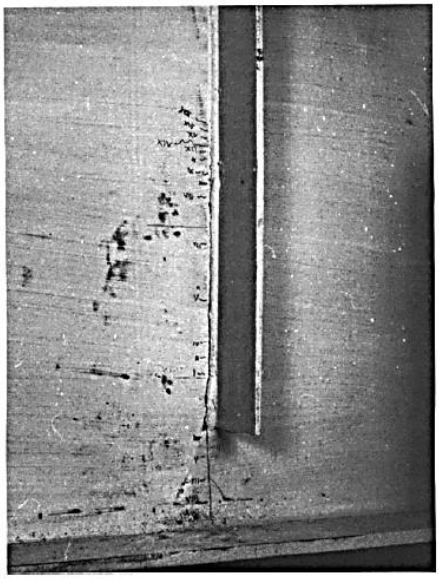

Figure 2.31 Typical failure at Type 2 stiffener [6]

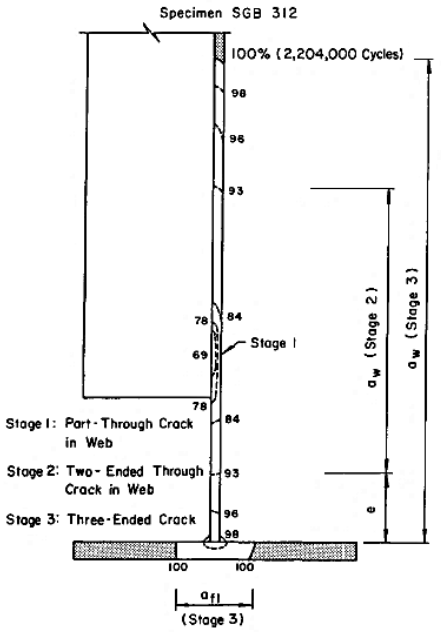

Figure 2.32 Stages of crack growth at Type 2 stiffener [6]

There were three stages of growth, as shown in Figure 2.32. In the first stage, fatigue crack initiated as the semielliptical shape and propagated until end of the web plate. Stage 2 started when the fatigue crack changed into a two-tip through-the thickness shape. In the last stage, the lower front had broken through the extreme fiber of the tensile flange. The fatigue crack propagated as a three-ended crack having two fronts at tensile flange and the other at the web. Approximately 80 percent of the total number of cycles were spent in growing the crack during stage 1. The second and third stages were approximately 16 and 4 percent, respectively.

Sakano and Wahab (1998) investigated the long-term fatigue of I-girder with welded transverse stiffeners under both constant and variable amplitude loading [7]. The material of web and flange plates are JIS SM490A steel whereas the stiffeners is JIS SS400 steel. Three specimens (Nos. 1–3) are tested under constant amplitude loading and two specimens (Nos. 4 and 5) under variable amplitude loading as shown in Figure 2.33. Stress repetition rate is 2–3 Hz. The maximum load is fixed at 333 kN for all specimens.

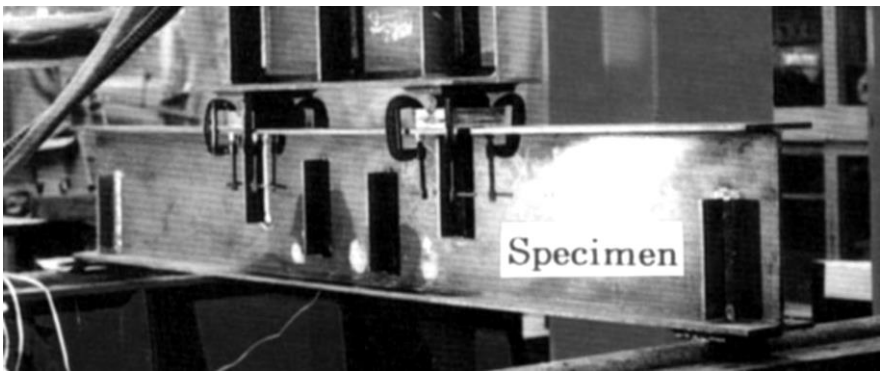

Figure 2.33 Steel beam specimen with attachments [7]

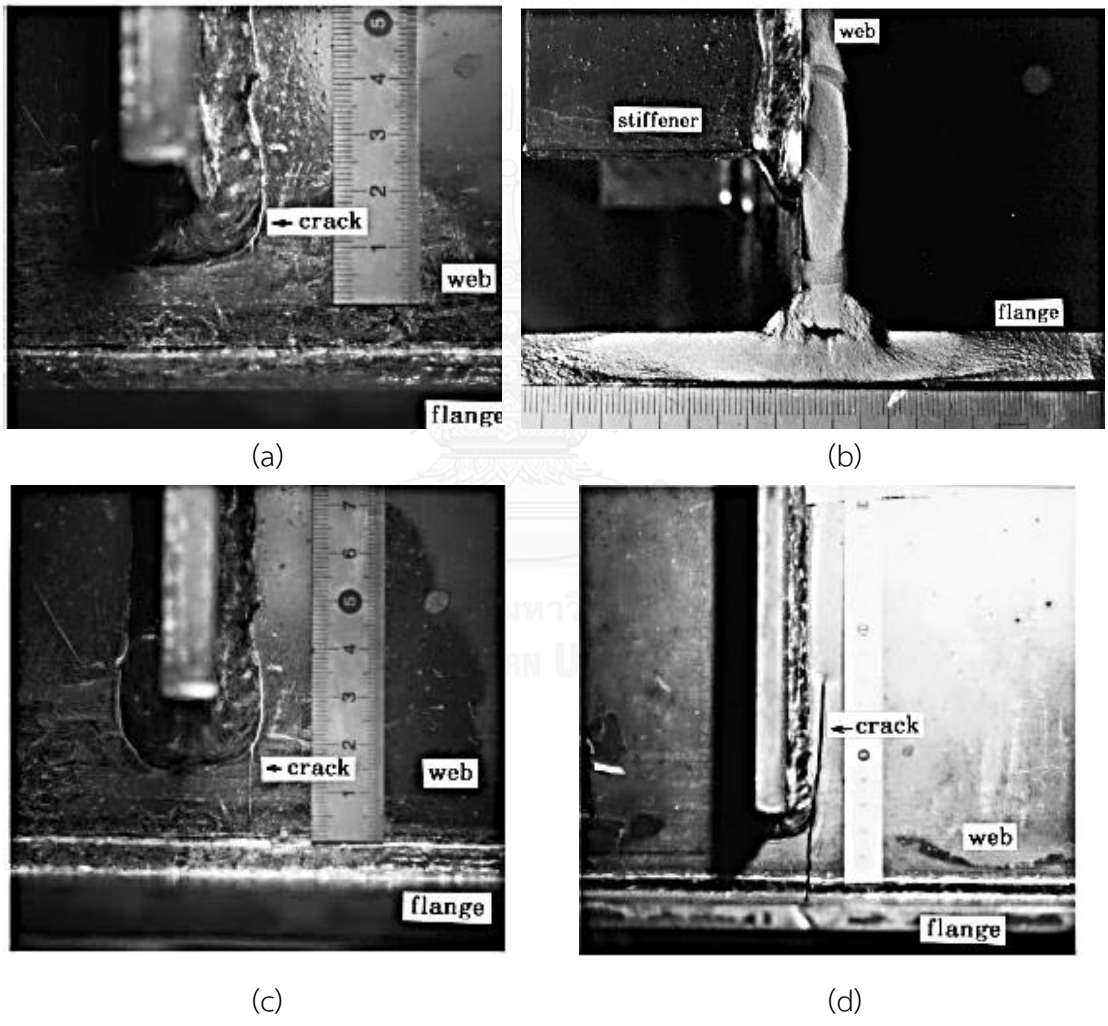

Figure 2.34 fatigue crack propagation (a) fatigue crack initiation (b) cross section at initial stage (c) growing crack (d) failure of flange [7]

Figure 2.32(a) presents the location of fatigue crack initiation at the fillet weld toe on the web plate beside lower end of the intermediate welded transvers stiffeners whose crack shape was semi-elliptical as shown in Figure 2.32 (b). The number of load cycles from beginning until detection of initial fatigue crack was approximately 2.77 million cycles. The fatigue crack propagated as a semi-elliptical shape until penetrating through the web plate then changed the shapes into two-tip through-thickness and both fatigue crack tips propagated in the vertical direction that was perpendicular to the direction of bending tensile stress that was approximately 3.40 million cycles. Finally, the crack propagated to fracture at the bottom flange at approximately 3.52 million cycles. The results show that the girders that were subject to variable amplitude loading had higher number of load cycles than constant amplitude loading.

2.4 Numerical simulation using FRANC2D and FRANC3D software

The software has many useful to compute any values in order to predict fatigue crack propagation paths and lives of steel structure. The fatigue crack test on large structure as bridge was quite difficult to conduct because several reasons. Accordingly, the software was used to obtain the results and reduced time computation in calculation therefore researcher can study in many cases.

Duchaczek and Manko (2014) researched in different methods to calculate stress intensity factor so as to predict service life of steel military bridges by several methods. [16]

The first method for calculation of the stress intensity factor was the direct method [16]. A simple beam which had 400 I-section, effective span l_e=5.00 m, and total length l_t=5.60 m. was used as the adopted calculation. The concentrated force of P and assembly holes were assigned to the middle span as shown in Figure 2.35.

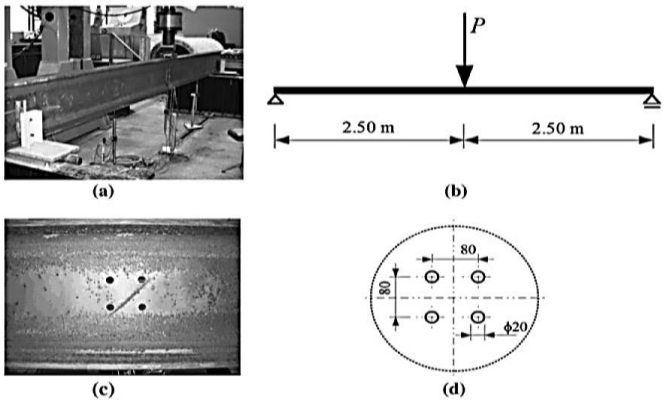

Figure 2.35 test of steel structure beam [16]: (a) test in laboratory, (b) the three points bending, (c) the assembly openings on the steel beam (d) their distribution

Duchaczek and Manko (2014) used the formula (2.2) to compute the stress intensity factor as a function of crack tip distance r.

$$K_I = \lim_{r \to 0} \left(\sigma_{22} \sqrt{2\pi r} \right) \tag{2.2}$$

where σ_{22} is a normal tensile stress

The other three methods for calculation the stress intensity factor K_I were used to compute the stress intensity factor in case of fatigue crack propagation in a linear elastic material with Poisson ratio ν=0.3 and Young's modulus E=210 GPa. The values of stress intensity factor K_I could be described in form of polynomial function depending on the crack length a. Moreover, FRANC2D was used to analyze these values. The results were shown in Figure 2.36 and Table 2.4.

(a) displacement correlation technique (DCT)

$$K_I = 3.591043x10^{-9}a^6 - 1.226492x10^{-6}a^5 + 1.607019x10^{-4}a^4 - 1.002931x10^{-2}a^3 + 0.305422a^2 - 3.477165a + 28.399837 \tag{2.3}$$

(b) modified crack closure integral technique (MCCIT)

$$K_I = 3.495912x10^{-9}a^6 - 1.193476x10^{-6}a^5 + 1.564181x10^{-4}a^4 - 0.977095x10^{-2}a^3 + 0.298066a^2 - 3.388440a + 28.077051 \tag{2.4}$$

(c) application of integral J

$$K_I = 3.474625x10^{-9}a^6 - 1.185022x10^{-6}a^5 + 1.550842x10^{-4}a^4 - 0.967008x10^{-2}a^3 + 0.294549a^2 - 3.343551a + 27.920652 \tag{2.5}$$

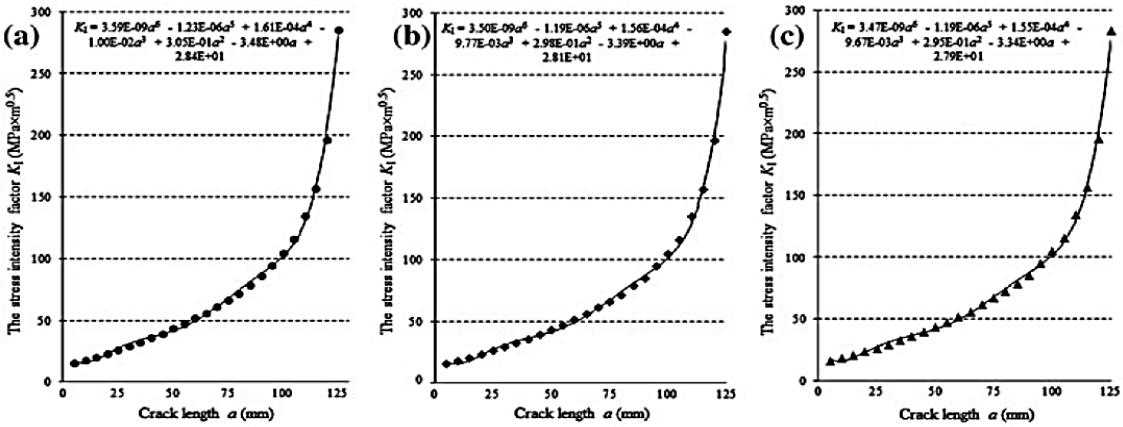

Figure 2.36 Three methods provide the values of stress intensity factor K_I based on the FRANC2D software [16]: (a) DCT, (b) MCCIT and (c) the J-integral technique

Table 2.4 Comparison of the value of stress intensity factor using four methods [16]

		The stress intensity factor K_I (MPa × m$^{0.5}$)			
		FRANC2D software basis			
No.	Crack length a (mm)	Displacement correlation technique (DCT)	Modified crack closure integral technique (MCCIT)	J-integral	Direct method (DM)
1.	5	15.504	15.514	15.504	14.944
2.	10	17.974	17.910	17.974	19.121
3.	15	20.160	20.323	20.157	21.594
4.	20	23.213	23.158	23.213	23.553
5.	25	26.058	25.891	26.058	25.528
6.	30	29.123	28.746	29.136	27.778
7.	35	32.544	32.512	32.544	30.409
8.	40	35.808	35.680	35.808	33.431
9.	45	38.944	39.072	38.944	36.798
10.	50	43.424	43.360	43.424	40.441
11.	55	47.168	46.944	47.168	44.289
12.	60	51.712	51.680	51.808	48.298
13.	65	55.840	55.584	55.968	52.459
14.	70	61.312	61.216	61.312	56.819
15.	75	66.368	66.432	66.080	61.483
16.	80	71.680	71.872	71.264	66.617
17.	85	78.496	78.400	78.912	72.442
18.	90	86.336	85.280	84.928	79.223
19.	95	94.528	94.816	94.944	87.248
20.	100	104.608	104.672	104.800	96.803
21.	105	116.032	115.808	116.320	108.132
22.	110	134.208	133.888	134.368	121.394
23.	115	156.608	156.320	156.512	136.609
24.	120	196.224	195.680	196.736	153.592
25.	125	285.600	283.328	284.736	171.879

The results of the stress intensity factors calculated by several methods show that all methods gave the values which were insignificantly higher than the value obtained from the direct method when crack length was not exceed 100 mm as shown in Table 2.4. Thus, the values of stress intensity factors can be obtained from any methods that crack lengths were not exceed 80 percent of web plate as shown in Figure 2.37. They were enough convergent to good results in the engineering fields.

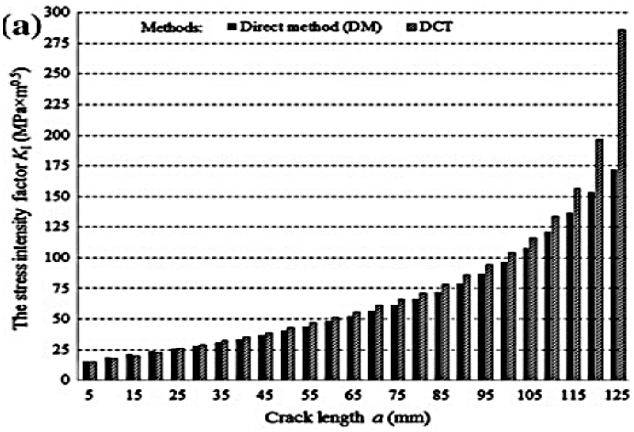

Figure 2.37 A comparison of the values of the stress intensity factor KI using Direct method and Displacement correlation technique [16].

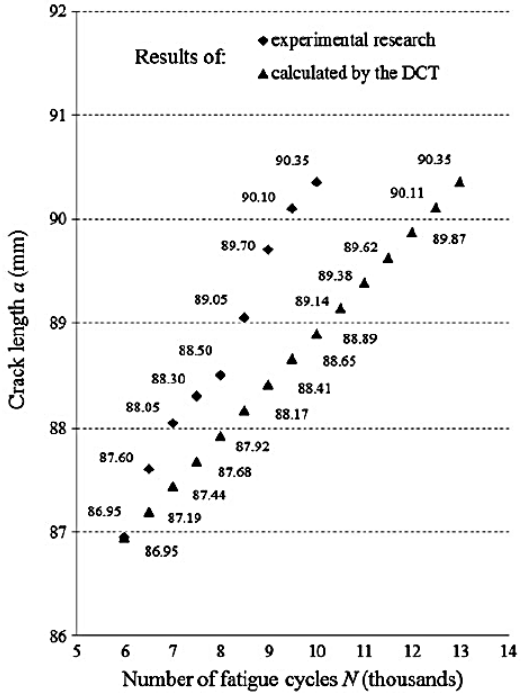

Figure 2.38 Increase in the fatigue crack length depending on the number of load cycles [16]

Paris and Erdogan Equation (1963) was applied to obtain an expression for the influence of number of load cycles N on increasing of crack length a. It was possible to describe that the results of calculation by the D2CT method was sufficiently close to experimental results. Therefore, the DCT method will be used to calculate the stress intensity factors for all cases.

Riddell, Ingraffea, and Wawrzynek (1997) studied the behavior of fatigue crack. The test had the geometry and boundary conditions as shown in Figure 2.39. Constant amplitude loadings were applied. There were 2 transition defined in this experiment. The first transition occurred when the crack tip 1 reached the corner α having the number of cycles of l_1 and the second transition occurred when the crack tip 2 reached the corner β having the number of cycles of l_2.

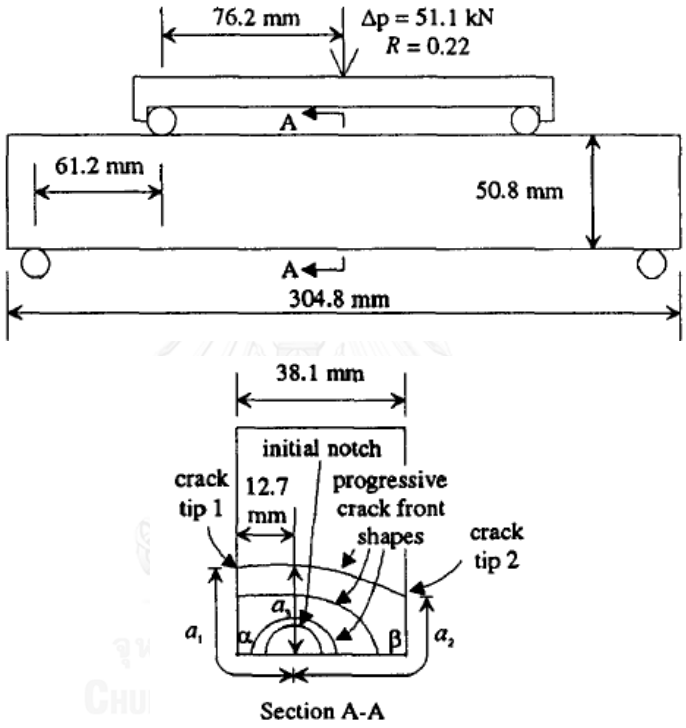

Figure 2.39 Geometry and boundary conditions for test [17]

Table 2.5 The number of cycles obtained from experiments and numerical simulations[17]

Simulation or experiment	l_1	l_2
Experimental upper-bound	39 500	81 700
Experimental average	55 600	107 400
Experimental lower-bound	86 400	158 200
NASCRAC®	51 000	67 500
NASA/FLAGRO	60 000	109 000
FRANC3D	39 200	68 900

Table 2.5 shows the results of number of cycles for both transitions obtained from each methods. The results obtained from FRANC3D were the minimum cycles. This research concluded that the fatigue life predicted from FRANC3D was conservative and reasonable for all test set investigated.

Rails are usually subjected to bending especially at the foot region and web corner [18]. Kotsikos and Grasso (2012) studied a predictive model with different initial small crack of a rail which was tested under four point bending was compared with an experiment.

The fatigue crack fronts were generated by finite element methods using ANSYS and FRANC3D. The average yield strength was 540 MPa and the ultimate strength was 940 MPa with an approximate elongation 12%. The results of crack front with different initial crack position by software is shown in the Figure 2.40 and by experiment is shown in Figure 2.41.

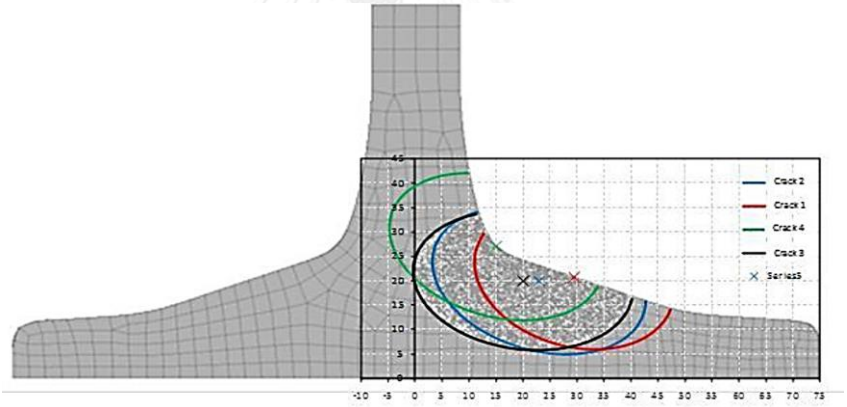

Figure 2.40 Outline of fatigue crack fronts at failure [18]

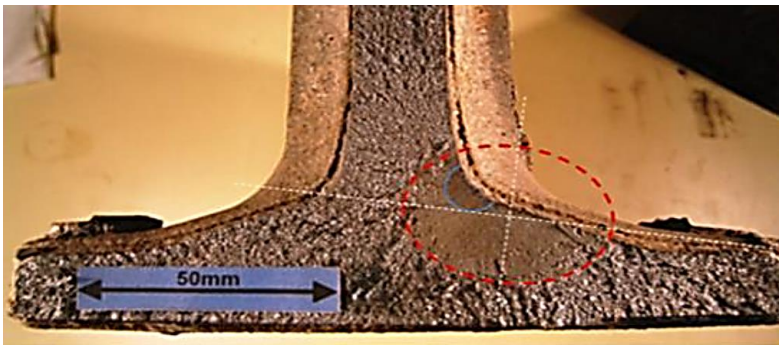

Figure 2.41 Fatigue tested rail showing semicircular crack near initiation site (solid line) and semi-elliptical crack at failure (dotted line) [18]

The initial crack which had a semi-circular profile changed to elliptical profile. The crack front grew toward the foot of the rail more than toward the web because the stress may increase further away from neutral axis toward the foot of the rail as shown in both the Figure 2.40 and Figure 2.41. Moreover, plastic region around the crack trip could be considered when ductile material was used in numerical simulation.

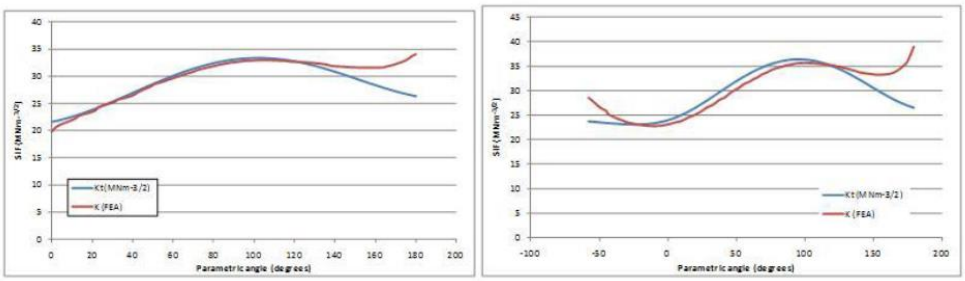

Figure 2.42 Comparison of SIF value from FEA and analytical solution for web corner crack1 (left) and crack2 (right) [18]

Figure 2.42 shows that there were a good agreement of the stress intensity factor between FRANC3D and analytical solution obtained from Newman and Raju (1979) [8].

Also, another research performed numerical simulation of fatigue crack propagation and predicted the life of steel plates using FRANC3D [19]. In order to measure fatigue growth rate parameter, numerical simulation on fatigue crack propagation of CT specimens were employed in these tests shown in Figure 2.43. Two material types used in test were base metal and butt weld joint whose properties are shown in Table 2.6.

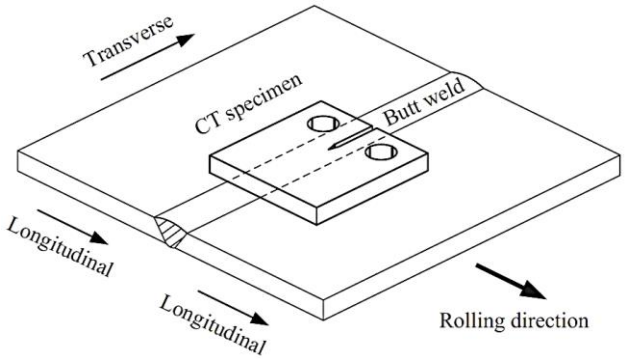

Figure 2.43 Sampling of CT specimens of butt weld [19].

Table 2.6 Average mechanical properties of WNQ570 base metal and butt welds [19].

	f_y (MPa)	f_u (MPa)	E (MPa)	A (%)	Z (%)
Base metal	495	568	207	45.6	62.3
Butt weld joint	569	665	225	23.6	70.1

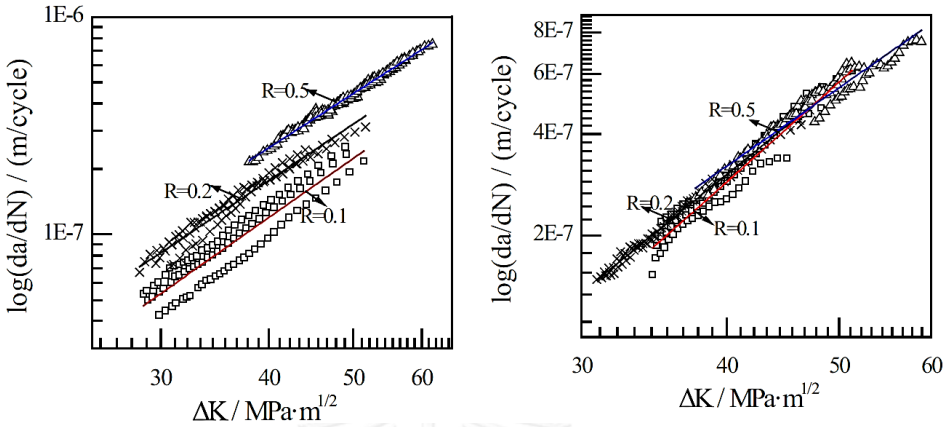

Figure 2.44 Fatigue crack growth rate test results of Base metals (left) Butt welds (right) [19].

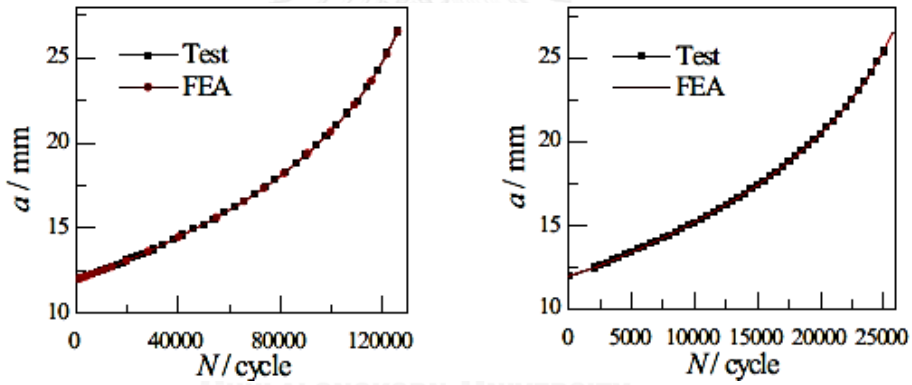

Figure 2.45 Numerical Simulation results of predicted and measured a-N curves for base metals (left) and butt welds (right) [19].

The experimental test results (Figure 2.44) show the effect of stress ratio on fatigue crack growth rate for WNQ570 base metals and butt welds. The measured results tended to decrease throughout the increasing of the stress ratio.

The stress intensity factor was calculated and the maximum tensile stress criterion (MTS) was adopt for the numerical simulation by FRANC3D. Finally, the measured fatigue crack growth rate parameters were also used to be the input for propagation model. The curve of complete crack length against number of cycle (a-N curves) were obtained as shown in Figure 2.45. Good agreement was observed between experimental investigation and numerical simulation by FRANC3D.

Additionally, the fatigue crack growth rate of base metal was lower than that of butt welds. While WNQ570 base metal had a lower the fatigue crack growth rate than other bridge steels. Therefore, this material had an excellent fatigue resistant capacity and was suitable for being in steel bridge materials [19].

Storgards, Simonsson, and Sjostrom (2015) also used FRANC3D to predict crack propagation and compare with the experiment under cyclic loads. Figure 2.46 shows the results of crack front shapes from FRANC3D (white line) on fracture surface from mechanical tests. For R=0.05 (left), the numerical results gave some difference from the test but for R=0.6, the numerical results and the actual test were almost no difference [20].

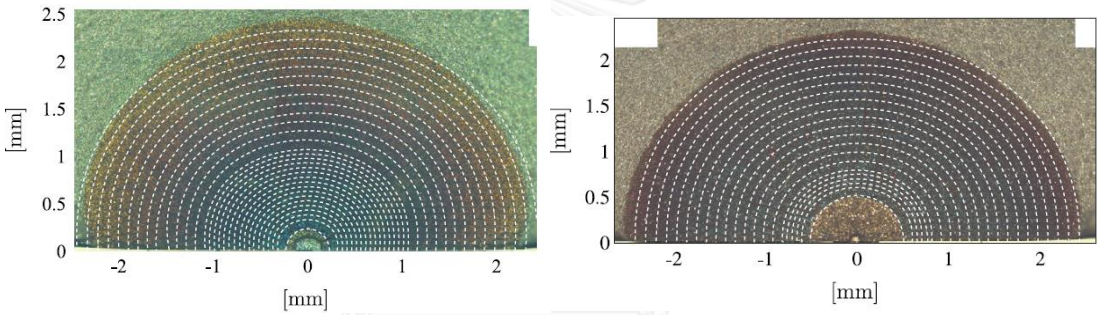

Figure 2.46 Cyclic test results for (left) R=0.05 and (right) R=0.6 [20]

Seifi and Omidvar (2013) studied fatigue crack growth in mixed mode I and III using modified CT specimens [21]. The fatigue behaviors depended on many parameters, such as, initial angle of crack, initial length of crack. The details of specimens shown in Figure 2.47. The numerical simulation also used FRANC3D with MTS criterion to determine the crack growth.

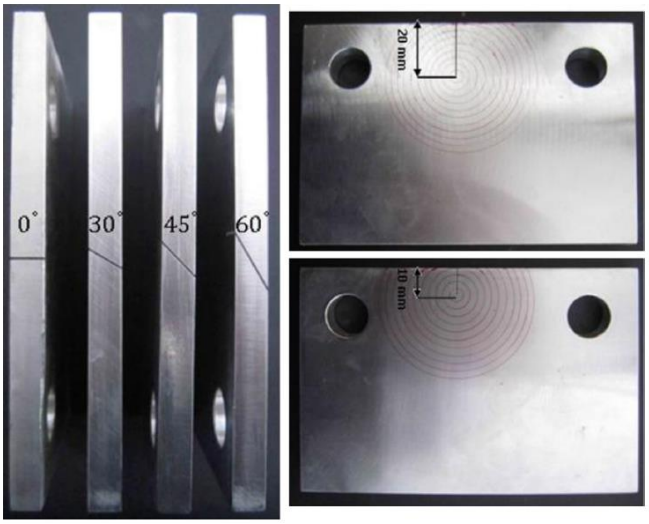

Figure 2.47 Details of specimens [21]

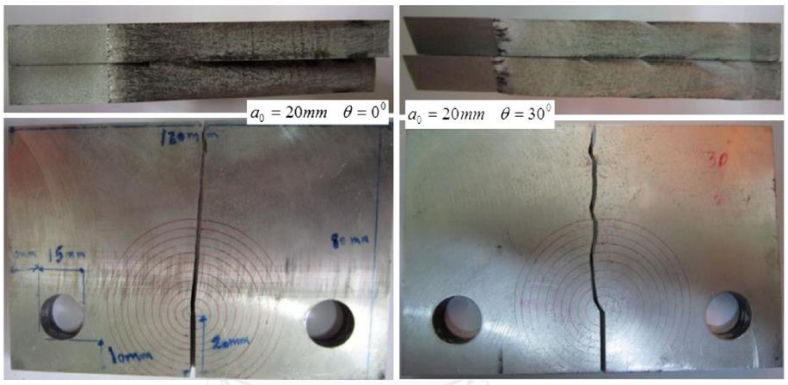

Figure 2.48 Crack growth paths and fracture surfaces [21]

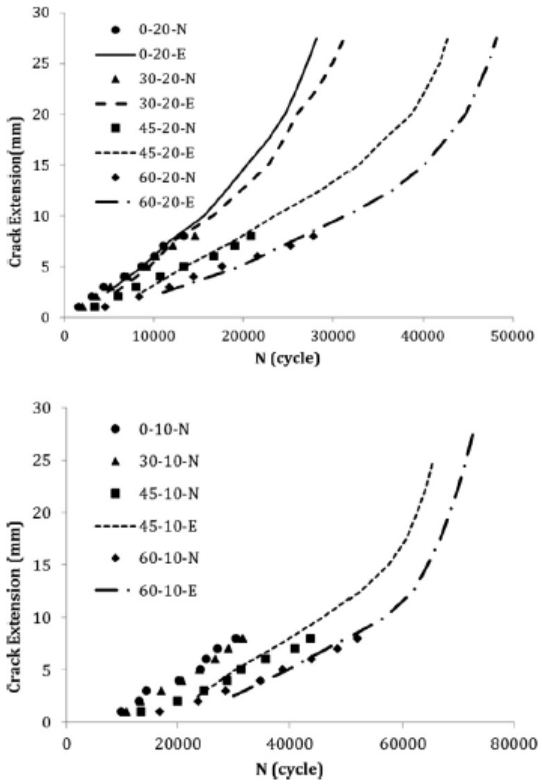

Figure 2.49 Numerical results (N) and experiment results (E) of fatigue crack life for specimens with pre-cracks of 20 mm (top) and 10 mm (bottom) in any angles [21]

The specimens contained a crack with inclination angle θ=0, 30, 45, and 60 degree with the initial crack lengths of 10 and 20 mm. Figure 2.48 shows fatigue crack propagation path and Figure 2.49 shows the fatigue crack life. The results describe that the fatigue life increased by increasing the crack angle. Therefore, mode I had a dominant influence mode III. On the other hand, the fatigue crack life decreased by increasing the pre-crack length [21].

CHAPTER III
THEORY

3.1 The finite element method

The distribution of stresses and strains in a body on which external loads and displacements subject is frequently essential to determine. A closed-form analytical solution can be obtained in particular cases, for example, isotropic elastic material is subjected to plane stress or plane strain loading. However, most of problems cannot be described by closed-form solutions; therefore, numerical techniques are used to estimate the stresses and strains in the body [22].

There are many numerical techniques used to estimate solid mechanics problems, for instance, finite element method, finite different method, and boundary integral equation method. In recent years, almost problems have been solved by using the finite element method and the boundary integral equation method. Despite usefulness in limited circumstances of the boundary integral equation method, the finite element method is usually used to analyze of cracked bodies [22].

The concept of this method is to subdivide the structures into discrete shapes which are called elements [22]. There are many element types including 1D beams, 2D plane stress or plane strain elements, and 3D bricks or tetrahedrons. Node points are the locations that the elements are connected. These points are enforced to have continuity of the displacement fields.

The stress analysis problems are normally solved by the stiffness finite element method. The outline below shows 2D plane stress or plane stain problems of an isoparametric continuum element that has both local and global coordinate axes. The local coordinates called parametric coordinates were between -1 and +1 over the element area. The node at the upper right-hand corner has parametric coordinates (+1, +1) and the lower left-hand corner is at (-1, -1). Moreover, the parametric coordinate system can be any shapes of quadrilateral. The global coordinates of a point on the element at (ξ, η) are given by

$$x = \sum_{i=1}^{n} N_i(\xi, \eta) x_i \tag{3.1}$$

$$y = \sum_{i=1}^{n} N_i(\xi, \eta) y_i \tag{3.2}$$

where $\mathbf{N_i}$ are shape functions corresponding to node i, whose coordinates are (ξ_i, η_i) in the parametric system and (x_i, y_i) in the global system.

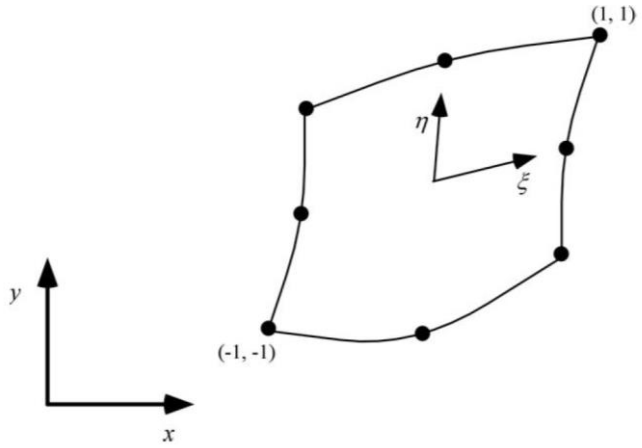

Figure 3.1 Local and global coordinates for a two-dimensional element [22].

The shape functions are polynomial whose degree depends on the number of nodes in the element and the value of shape functions can be interpolated from field quantities within the element. The displacements which are interpolated within an element are

$$u = \sum_{i=1}^{n} N_i(\xi, \eta) u_i \tag{3.3}$$

$$v = \sum_{i=1}^{n} N_i(\xi, \eta) v_i \tag{3.4}$$

where $\mathbf{u_i}$ is the nodal displacement in x direction and $\mathbf{v_i}$ is the nodal displacement in y direction. The strain matrix in global coordinates is given by

$$\begin{Bmatrix} \varepsilon_x \\ \varepsilon_y \\ \gamma_{xy} \end{Bmatrix} = [B] \begin{Bmatrix} u_i \\ v_i \end{Bmatrix} \tag{3.5}$$

Where matrix $[B]$ is

$$[B] = \begin{bmatrix} \frac{\partial N_i}{\partial x} & 0 \\ 0 & \frac{\partial N_i}{\partial y} \\ \frac{\partial N_i}{\partial y} & \frac{\partial N_i}{\partial x} \end{bmatrix} \tag{3.6}$$

And

$$\begin{Bmatrix} \frac{\partial N_i}{\partial x} \\ \frac{\partial N_i}{\partial y} \end{Bmatrix} = [J]^{-1} \begin{Bmatrix} \frac{\partial N_i}{\partial \xi} \\ \frac{\partial N_i}{\partial \eta} \end{Bmatrix} \tag{3.7}$$

where $[J]$ is the Jacobian matrix is given by

$$[J] = \begin{bmatrix} \frac{\partial x}{\partial \xi} & \frac{\partial y}{\partial \xi} \\ \frac{\partial x}{\partial \eta} & \frac{\partial y}{\partial \eta} \end{bmatrix} = \begin{bmatrix} \cdots \frac{\partial N_i}{\partial x} \cdots \\ \cdots \frac{\partial N_i}{\partial y} \cdots \end{bmatrix} \begin{bmatrix} \vdots \\ x_i y_i \\ \vdots \end{bmatrix} \tag{3.8}$$

The stress matrix can be computed from

$$\{\sigma\} = [D]\{\varepsilon\} \tag{3.9}$$

Where matrix $[D]$ is the stress-strain constitutive matrix.

$$\{\Delta\sigma\} = [D(\varepsilon, \sigma)]\{\Delta\varepsilon\} \tag{3.10}$$

The constitutive law and the nodal displacements can infer that the behavior of stress and strain distribute throughout the body. The nodal displacements depend on both the nodal forces and the element stiffness whose matrix is given by the following equation derived from the principle of minimum potential energy.

$$[k] = \int_{-1}^{1} \int_{-1}^{1} [B]^T [D][B] det|J| \, d\xi \, d\eta \tag{3.11}$$

The global stiffness matrix $[\mathcal{K}]$ is given from assembly of the elemental stiffness matrices. Furthermore, the relation of the global stiffness matrix, displacement matrix, and force matrix can be shown as follow:

$$[\mathcal{K}][u] = [F] \tag{3.12}$$

3.2 Design of welded transverse stiffeners by AASHTO (2012)

Transverse stiffeners are welded on either one or both sides of web [3]. The double-side stiffeners that are not used as connection plates or bearing stiffeners shall be fitted tightly or attached with only the compressive flange. Single-sided stiffeners should be attached to both flanges in order to retain the cross-sectional configuration of the beam when subjected to torsion and can avoid high localized bending within the web. This reason is the requirement of pairs of transverse stiffeners to attach to both flanges as shown in Figure 3.2.

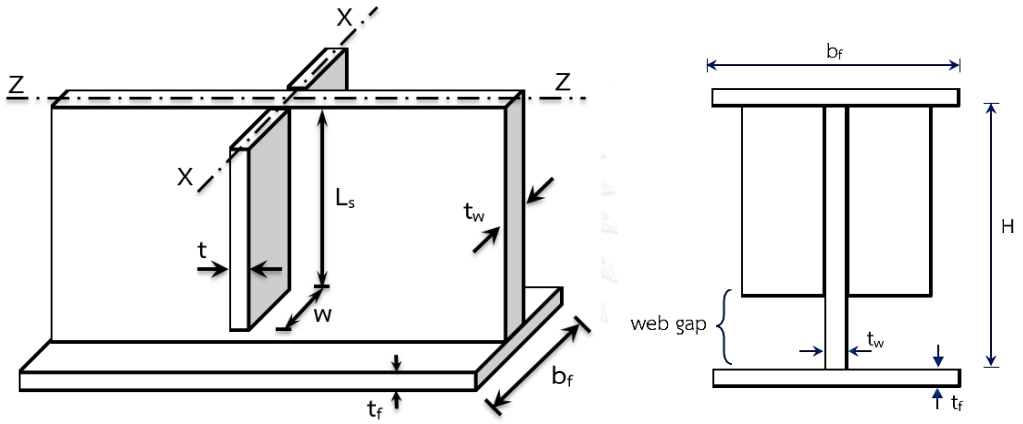

Figure 3.2 double-sided stiffeners

Projecting width, b_t, is required by AASHTO (2012) to prevent local buckling of the transverse stiffeners. The width of each projecting transverse stiffener shall satisfy the equations (3.13) and (3.14).

$$w \geq 2.0 + \frac{H}{30} \tag{3.13}$$

$$16t \geq w \geq b_f/4 \tag{3.14}$$

The web-gap length, which is the distance between the bottom end of web-to-stiffener weld and the tensile flange, shall not be less than four times of web thickness to relieve flexing of the unsupported of the web in order to avoid fatigue-induced cracking of the weld toe. However, this length shall not exceed the less of six times of web thickness and 4.0 in (100 mm) to avoid vertical buckling of the unsupported web as shown in the equation (3.15).

$$4t_w \leq web\ gap \leq 6t_w \tag{3.15}$$

The transverse stiffeners do not required when $H/t_w < 1.12\sqrt{Ek/F_{yw}}$ where k is shear-buckling coefficient. For transverse stiffener that panel support a shear force, V_u, is lower than the factor shear buckling resistance, $\phi_v V_{cr}$, the moment of inertia (I_{st}) of stiffener must satisfy the following limits

$$I_{st} \geq I_{st1} \tag{3.16}$$

and

$$I_{st} \geq I_{st2} \tag{3.17}$$

where

$$I_{st1} = bt_w^3 J \tag{3.18}$$

$$I_{st2} = \frac{H^4 \rho_t^{1.3}}{40}\left(\frac{F_{yw}}{E}\right)^{1.5} \tag{3.19}$$

where ρ_t is the large of F_{yw}/F_{crs} and 1.

$$J = \frac{2.5}{(a/H)^2} - 2.0 \geq 0.5 \tag{3.20}$$

The transverse stiffener of web that adequately develop the shear-buckling resistance or the combined the shear-buckling and post-buckling tension-field resistance requires having sufficient rigidity to maintain a vertical line of zero lateral deflection along stiffener line. For ratios of (a/H) less than 1.0, much larger values of I_{st} are used to develop the shear-buckling resistance represented by equation (3.16). The equation (3.16) and (3.19) give a constant for the I_{st} for web panel with a>H.

$$\frac{0.31E}{\left(\frac{w}{t}\right)^2} \leq F_{ys} \tag{3.21}$$

$$V_{cr} = CV_p \tag{3.22}$$

$$V_p = 0.58F_{yw}ht_w \tag{3.23}$$

where V_p, V_{cr}, V_u are plastic shear force, smaller of the nominal shear-buckling resistance of the adjacent web panel, and larger of the shears in the adjacent web panels from factor loads, respectively.

For transverse stiffener that panel support a shear force, V_u, is larger than the factor shear bulking resistance, $\phi_v V_{cr}$, or the tension-field resistance is required. The moment of inertia (I_{st}) of stiffener must satisfy the following limits.

$$I_{st2} > I_{st1} \tag{3.24}$$

then

$$I_{st} \geq I_{st1} + (I_{st2} - I_{st1})\left(\frac{V_u - \phi_v V_{cr}}{\phi_v V_n - \phi_v V_{cr}}\right) \tag{3.25}$$

The AASHTO (2012) recommended that the transverse stiffeners on I-girders that were designed for tension-field action are loaded predominantly in bending because of the restraint they provide to lateral deflection of web. Therefore, the moment of inertia in equation (3.25) is used instead of the transverse stiffener area requirement.

3.3 Flexural rigidity ratio

The flexural rigidity ratio is defined as the ratio of flexural rigidity (EI) of transverse stiffener about the centroid axis (x-axis) to flexural rigidity (EI) of the girder about z-axis as shown in Figure 3.3. So, the given equation is represented in equation (3.28).

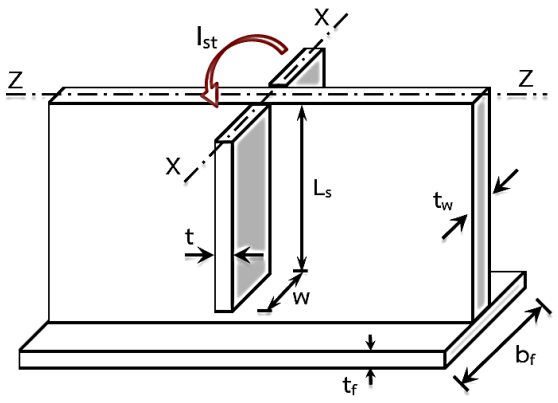

Figure 3.3 the moment of inertia of double-sided transverse stiffeners

$$I_{st} = \frac{1}{12} t[(2w + t_w)^3 - t_w^3] \quad (3.26)$$

and

$$I_{girder} = \frac{1}{12} t_w H^3 + 2\left[\frac{1}{12} b_f t_f^3 + \left(b_f t_f\right)\left(\frac{H + t_f}{2}\right)^2\right] \quad (3.27)$$

then

$$\textit{Flexural rigidity ratio} = {(EI)_{st}}\Big/{(EI)_{girder}} \quad (3.28)$$

3.4 Stress intensity factor

The tool which is used to determine the crack propagation and service life of steel bridge is stress intensity factor (K). The value of K can determine the stress, strain, and displacement fields in the near crack-tip area under linear elastic fracture mechanics (LEFM) assumptions. There are two categories of stress intensity factor techniques. First, direct approaches correlate the stress intensity factor with finite element method results directly. Second, energy approaches, which compute energy release rates have more accuracy and are often used to determine stress intensity factors. Nevertheless, the direct approaches are simple enough to hand calculation; therefore, they are used to check on energy approaches. [16]

Since the most effective method for discontinuous problem, especially the problem of fracture, is the extension of finite element method, M-integral is applied to calculate stress intensity factor by computing the stress and displacement field nearby the crack tip. [23]

3.4.1 M-integral technique for calculating stress intensity factor (energy approach)

This method can be used to calculate in case of mixed-mode stress intensity factor along 3D cracks in homogeneous materials [23]. The derivation of M-integral bases on the path-independent J-integral technique. The auxiliary displacement, stress, strain fields must be selected as the crack tip asymptotic field. The 2D relationship

between stress intensity factor and J-integral can be written for general mixed-mode problems.

$$J = \frac{K_I^2}{E^*} + \frac{K_{II}^2}{E^*} \tag{3.29}$$

Where E^* is defined as

$$E^* = \begin{cases} E & \text{for plane stress} \\ \dfrac{E}{1-\nu^2} & \text{for plane strain} \end{cases} \tag{3.30}$$

A cracked body is considered in two states. State1, $\left(\sigma_{ij}^{(1)}, \varepsilon_{ij}^{(1)}\, u_{ij}^{(1)}\right)$, and state2, $\left(\sigma_{ij}^{(2)}, \varepsilon_{ij}^{(2)}\, u_{ij}^{(2)}\right)$ relate to the present state and an auxiliary state. The J-integral which is the sum of two states is shown in

$$J^{(1+2)} = \int_\Gamma \left[\frac{1}{2}\left(\sigma_{ij}^{(1)} + \sigma_{ij}^{(2)}\right)\left(\varepsilon_{ij}^{(1)} + \varepsilon_{ij}^{(2)}\right)\sigma_{1j} - \left(\sigma_{ij}^{(1)} + \sigma_{ij}^{(2)}\right)\frac{\partial\left(u_i^{(1)} + u_i^{(2)}\right)}{\partial x_1}\right] n_j\, d\Gamma \tag{3.31}$$

Expanding and rearranging terms

$$J^{(1+2)} = J^{(1)} + J^{(2)} + M^{(1,2)} \tag{3.32}$$

Where $M^{(1+2)}$ is called the M-integral for state 1 and 2

$$M^{(1+2)} = \int_\Gamma \left[W^{(1,2)}\sigma_{1j} - \sigma_{ij}^{(1)}\frac{\partial u_i^{(2)}}{\partial x_1} - \sigma_{ij}^{(2)}\frac{\partial u_i^{(1)}}{\partial x_1}\right] n_j d\Gamma \tag{3.33}$$

where $W^{(1,2)}$ is the interaction strain energy.

$$W^{(1,2)} = \sigma_{ij}^{(1)}\varepsilon_{ij}^{(2)} = \sigma_{ij}^{(2)}\varepsilon_{ij}^{(1)} \tag{3.34}$$

The combined states are

$$J^{(1+2)} = J^{(1)} + J^{(2)} + \frac{2}{E^*}\left(K_I^{(1)}K_I^{(2)} + K_{II}^{(1)}K_{II}^{(2)}\right) \tag{3.35}$$

This equation gives the following relation.

$$M^{(1,2)} = \frac{2}{E^*}\left(K_I^{(1)}K_I^{(2)} + K_{II}^{(1)}K_{II}^{(2)}\right) \qquad (3.36)$$

Choosing state 2 as the mode-I asymptotic fields with $K_I^{(2)} = 1, K_{II}^{(2)} = 0$ give mode I of SIF in terms of M-integral.

$$K_I^{(1)} = \frac{2}{E^*}M^{(1,ModeI)} \qquad (3.37)$$

Also, choosing state 2 as the mode-II asymptotic fields with $K_I^{(2)} = 0, K_{II}^{(2)} = 1$ give mode II of SIF in terms of M-integral.

$$K_{II}^{(1)} = \frac{2}{E^*}M^{(1,ModeII)} \qquad (3.38)$$

3.4.2 Displacement correlation methods (direct approach)

Displacement correlation method is a direct approach for extracting the stress intensity factors from finite element method results. Chan, Tuba and Wilson (1970) stated that one of the simplest techniques was displacement correlation technique. The one point in the mesh of finite element displacements is replaced directly into the near-tip displacements of the analytical methods. Figure 3.4 shows the configuration for this simple technique. [16, 24, 25]

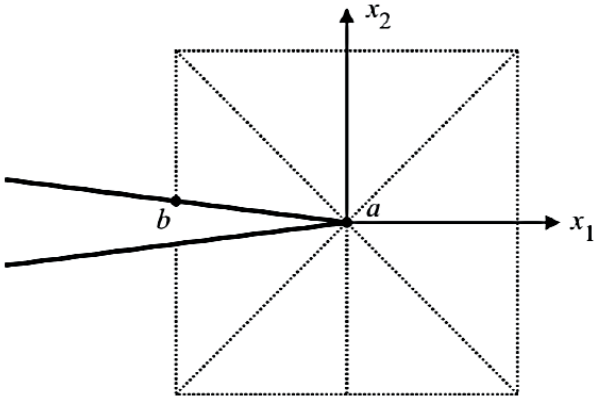

Figure 3.4 Possible sample point locations for simple displacement correlation [24]

In case of plane strain, the stress intensity factors can be expressed in following formulae.

$$K_I = \frac{\mu\sqrt{2\pi}(v_b - v_a)}{\sqrt{r}(2-2\nu)} \tag{3.39}$$

$$K_{II} = \frac{\mu\sqrt{2\pi}(u_b - u_a)}{\sqrt{r}(2-2\nu)} \tag{3.40}$$

$$K_{III} = \frac{\mu\sqrt{\pi}(w_b - w_a)}{\sqrt{2r}} \tag{3.41}$$

Where u_i, v_i, w_i are the displacements in x, y, and z axes at point i, μ is the shear modulus, ν is Poisson's ratio, and r is the length between crack tip and correlative point. This expression can be used in case of plane stress by replacement Poisson's ratio with $\nu = \nu/(1+\nu)$.

The accuracy of results can be improved by choosing the correlative point and having high refined mesh in the region of crack tip. One technique used for choosing the correlative point to compute stress intensity factors for a series of points which are very near the crack tip as shown in Figure 3.5. These results are plotted to be a curve and extrapolated to stress intensity factor value for r equal to zero.

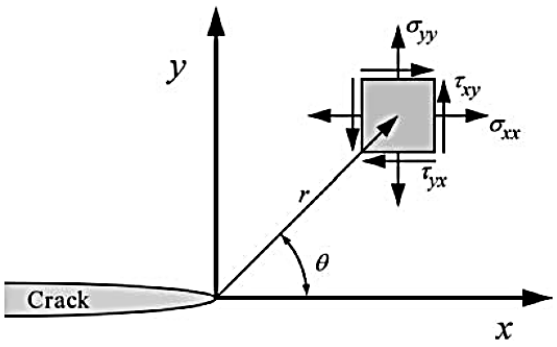

Figure 3.5 Definition of the coordinate axis ahead of a crack tip. The z direction is normal to the page [22]

Moreover, the accuracy of stress intensity factor value can be improved by using four nodes. The quarter-node b, c, d, and e present along the crack route. In this case, the displacement of all node can be used to compute the stress intensity factor as follows.

$$K_I = \frac{\mu\sqrt{2\pi}}{\sqrt{r}(2-2\nu)}[4(v_b - v_d) + v_e - v_c] \tag{3.42}$$

$$K_{II} = \frac{\mu\sqrt{2\pi}}{\sqrt{r}(2-2\nu)}[4(u_b - u_d) + u_e - u_c] \qquad (3.43)$$

3.5 Fatigue crack growth analysis

3.5.1 Fatigue loading types

The variables causing fatigue loading can be defined as the applied loads, vibrations, pressure changes, wave loads, and temperature changes. The structures are usually subjected to variable cyclic loading. Stress ranges and other stress parameters, such as, mean stress value and sequence of loading cycle, can be generated by these loads of varying amplitude. The variable amplitude stress ranges which are generated by real loads are very useful to deal with the complex loading situations. On the other hand, the constant amplitude stress ranges are easier to handle in design calculations. The stress and its parameters are shown in Figure 3.6 for both variable and constant amplitude fatigue loading.[1, 26]

Fatigue life describes the duration of structure depending on several parameters. The most important and primary parameter is the stress range($\Delta\sigma$). The cycle of stress damages accumulatively to the steel structures. In the case of constant amplitude fatigue loading, the loading is defined as cyclic loading with constant mean load ($\Delta\sigma_m$) and constant amplitude. The ratio of minimum and maximum stress is defined as the stress ratio (R) indicating the effect of mean stress, a secondary parameter influencing fatigue life. In the high residual stress condition, the fatigue design of welded components can neglect the effect of mean stress [27].

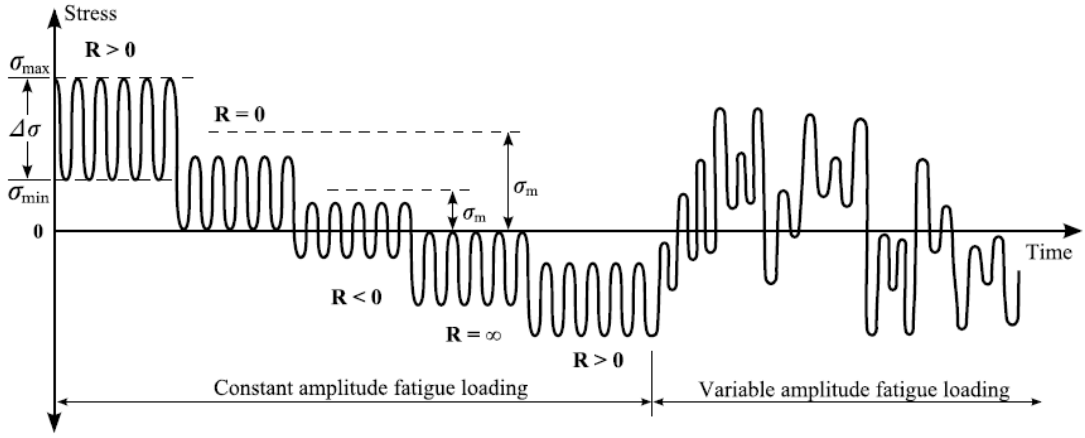

Figure 3.6 Stress parameters defined in fatigue loading [27]

3.5.2 Kink angle

The local direction of crack propagation is defined by the amount of deviation from self-similar direction, the measured in a plane perpendicular to the crack front called “kink” angle. The Figure 3.7 shows the kink angle (θ) [26].

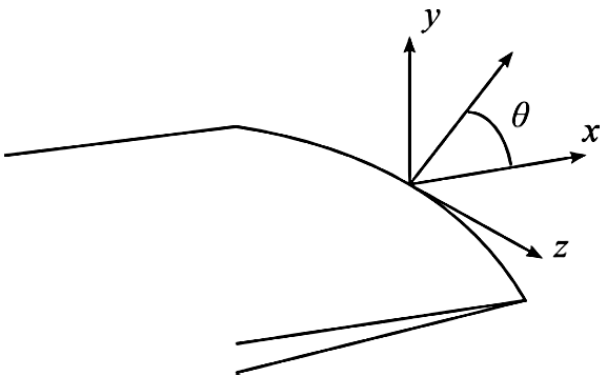

Figure 3.7 Schematic illustration of the definition of the kink angle [26]

3.5.2.1 Maximum tensile stress criterion

This concept proposed by Erdogan and Sih (1963) [28] is to predict the direction of crack propagation where the hoop stress, $\sigma_{\theta\theta}$, is maximum as shown in Figure 3.8. The hoop stress can be used to calculate the resolve mode-I stress intensity factor, K_I^r for an isotropic stiffness materials [26]. The toughness of the isotropic material can be estimated by numerical finding the θ angle that has maximum K_I^r and $\sigma_{\theta\theta}$.

$$K_I^r(\theta) = \sigma_{\theta\theta}\sqrt{2\pi r} = \cos\frac{\theta}{2}\left[K_I\cos^2\frac{\theta}{2} - \frac{3}{2}K_{II}\sin\theta\right] \qquad (3.44)$$

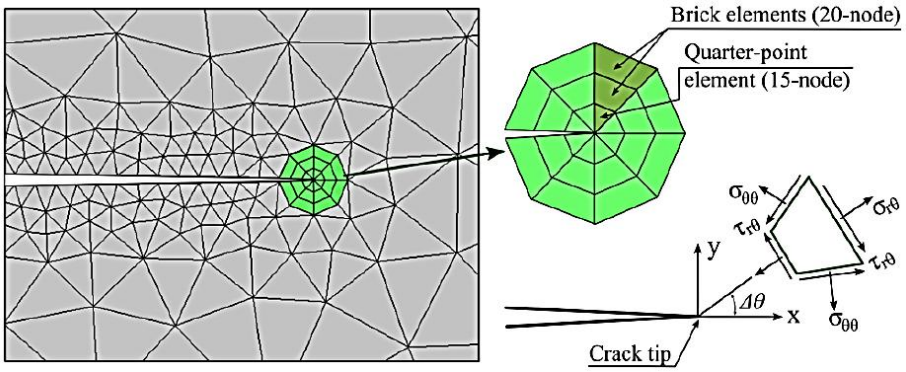

Figure 3.8 Definition of MTS criterion and crack direction at the crack tip [27]

The MTS criterion had been applied as the following equations.

$$\sigma_{\theta\theta} = \frac{1}{\sqrt{2\pi r}}\cos\frac{\theta}{2}\left[K_I\cos^2\frac{\theta}{2} - \frac{3}{2}K_{II}\sin\theta\right] \qquad (3.45)$$

$$\Delta\theta = 2\tan^{-1}\left(\frac{1-\sqrt{1+8(K_{II}/K_I)^2}}{4(K_{II}/K_I)}\right) \qquad (3.46)$$

The direction of maximum tensile stress obtained from equating the derivative of equation (3.45) to zero, as given in equation (3.46) [27].

3.5.2.2 Maximum shear stress criterion

In high shear loading condition at crack front, crack can grow in the high shear stress condition. This theory predicts the crack propagation in the direction that has maximum resolved shear stress, $\sigma_s = \sqrt{\sigma_{r\theta}^2 + \sigma_{z\theta}^2}$. The resolved mode-II and mode-III stress intensity factor have a relation to the components of shear stress for materials with isotropic stiffness properties. [26]

$$K_{II}^r = \sigma_{r\theta}\sqrt{2\pi r} = \frac{1}{2}\cos\frac{\theta}{2}[K_I\sin\theta - K_{II}(3\cos\theta - 1)] \qquad (3.47)$$

$$K_{III}^r = \sigma_{z\theta}\sqrt{2\pi r} = K_{III}\cos\frac{\theta}{2} \qquad (3.48)$$

The toughness of the isotropic material can be estimated by numerical finding the θ angle that has maximum K_s^r.

$$K_s^r(\theta) = \sqrt{\left(\beta_{II} K_{II}^r(\theta)\right)^2 + \left(\beta_{III} K_{III}^r(\theta)\right)^2} \qquad (3.49)$$

Where β_I and β_{II} are user supplied parameters for predicting shear crack growth direction which matches assumption or predicts behavior.

3.5.2.3 Maximum generalized stress criterion

This criterion predicts the direction of crack growth that corresponds with the greater resolved SIF K_I^r from the maximum tensile stress criterion or K_s^r from the maximum generalized stress criterion. [26]

In such a case, crack front is considered to be tensile fracture but shear fracture is in another part. This can cause abrupt discontinuity in the predicted kink angles. The crack cannot mesh successfully and crack geometries cannot be realistic. Therefore, the maximum tensile stress criterion and the maximum generalized stress criterion should be selected.

3.5.2.4 Maximum strain energy release rate criterion

The concept of this criterion is to predict the path that crack will grow in the direction that has maximum rate of change of potential energy in the system due to crack growth. [26]

The toughness of the isotropic material can be estimated by numerical finding the θ angle that has maximum the expression.

$$G(\theta) = \left(K_I^r(\theta)\right)^2 + \left(\beta_{II} K_{II}^r(\theta)\right)^2 + \left(\beta_{III} K_{III}^r(\theta)\right)^2 \qquad (3.50)$$

where K_I^r, K_{Ii}^r, K_{III}^r are the resolved mode-I, mode-II, and mode-III stress intensity factors respectively and can be calculated as the equations (3.44), (3.47), and (3.48) . The beta factors are described in 3.4.3.

3.5.2.5 Planar criterion

This criterion forces the crack propagation with a zero kink angle called self-similar growth. This option should be selected in the case of crack growth in plane. Computing the kink angle usually has small undulations developing in the predicted

crack surface due to numerical noise. Therefore, this option can reduce the small undulation. [26]

3.6 Paris law

The important factor estimating the fatigue life of structure is fatigue crack growth rate. The crack growth rate of metal is often used Paris law [29], which is the relationship between crack growth rate and stress intensity factor as follow.[1, 2]

$$\frac{da}{dN} = C(\Delta K)^n \qquad (3.51)$$

where C and n are material constants including the environmental effect which are determined by experiment. According to Paris and Erdogan (1963) experimental data, they suggest using an exponent of 4 (n=4)[29]. However, many investigations for most materials used in fatigue-load structures have shown that m are between 2 and 4 [22].

3.7 FRANC3D fatigue crack propagation

FRANC3D is a pre- and post-processor for simulation of crack growth in three dimension. Crack propagation in this software is based on point. The stress intensity factors are calculated along a crack front whose shape can be transformed. The algorithm of FRANC3D fatigue crack propagation can model both planar and nonplanar crack growth [17].

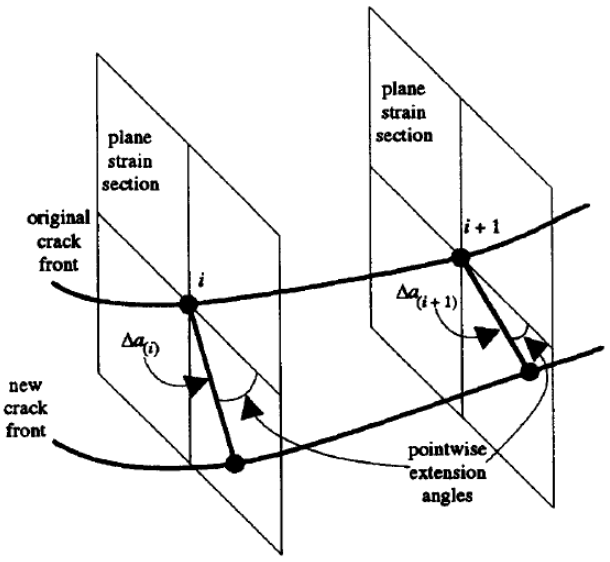

Figure 3.9 The simulation of three-dimensional fatigue crack propagation by FRANC3D [17]

Figure 3.9 summarized the process for numerical simulation of fatigue crack propagation in FRANC3D by prediction of crack shape and crack size. Treating the crack as a series of plane strain is used to predict the direction of propagation at each node along crack front. A criterion such as G_{max}, S_{min}, or maximum hoop stress is selected at each node. The crack growth increments are required when the direction are found. This approximation can be written as the equation of

$$\Delta a_i = \Delta a_{max} \frac{\frac{da_i}{dN}}{\left(\frac{da}{dN}\right)_{max}} \tag{3.52}$$

where da_i/dN is the crack growth rate at the node i using the local **Δ**K for calculation, $(da/dN)_{max}$ is the prediction of the crack growth rate along the crack front, and Δa_{max} is the maximum allowable crack growth increment that is input by user. Paris law is brought to substitute in equation (3.*52*) and obtain

$$\Delta a_i = \Delta a_{max} \left(\frac{\Delta K_i}{\Delta K_{max}}\right)^n \tag{3.53}$$

where ΔK_{max} is the maximum value of the stress intensity factor along the crack front and n is the Paris material component.

The second step is connection of the tips of the vectors of length Δa_i to define the new crack front. Crack surface is added from the area between the new crack front and the old crack front as shown in Figure 3.9. The software performs the local remeshing before a 3D stress analysis is performed on the new geometry. Then, the process is repeated.

The last step is to predict the number of load cycle which separate successive crack fronts. Fatigue life can be calculated if there exists a value of **Δ**K to represent each crack front and a value of **Δ**a to represent the difference between each pair of FRANC3D-predixcted crack fronts. FRANC3D extracts a series of **Δ**K and **Δ**a values from the series of FRANC3D-predicted crack fronts. **The Δ**K for the entire crack front is taken to be the average of **Δ**K over the entire crack front and the crack length increment **(Δ**a) between crack front is taken to be the average of Δa_i over the crack front. Therefore, FRANC3D predictions are based on this method of fatigue life integration.

CHAPTER IV

FRANC3D SIMULATION

4.1 Methodology

The following work flow represents the process for fatigue crack propagation analysis using ANSYS and FRANC3D software. (Refer to Appendix A)

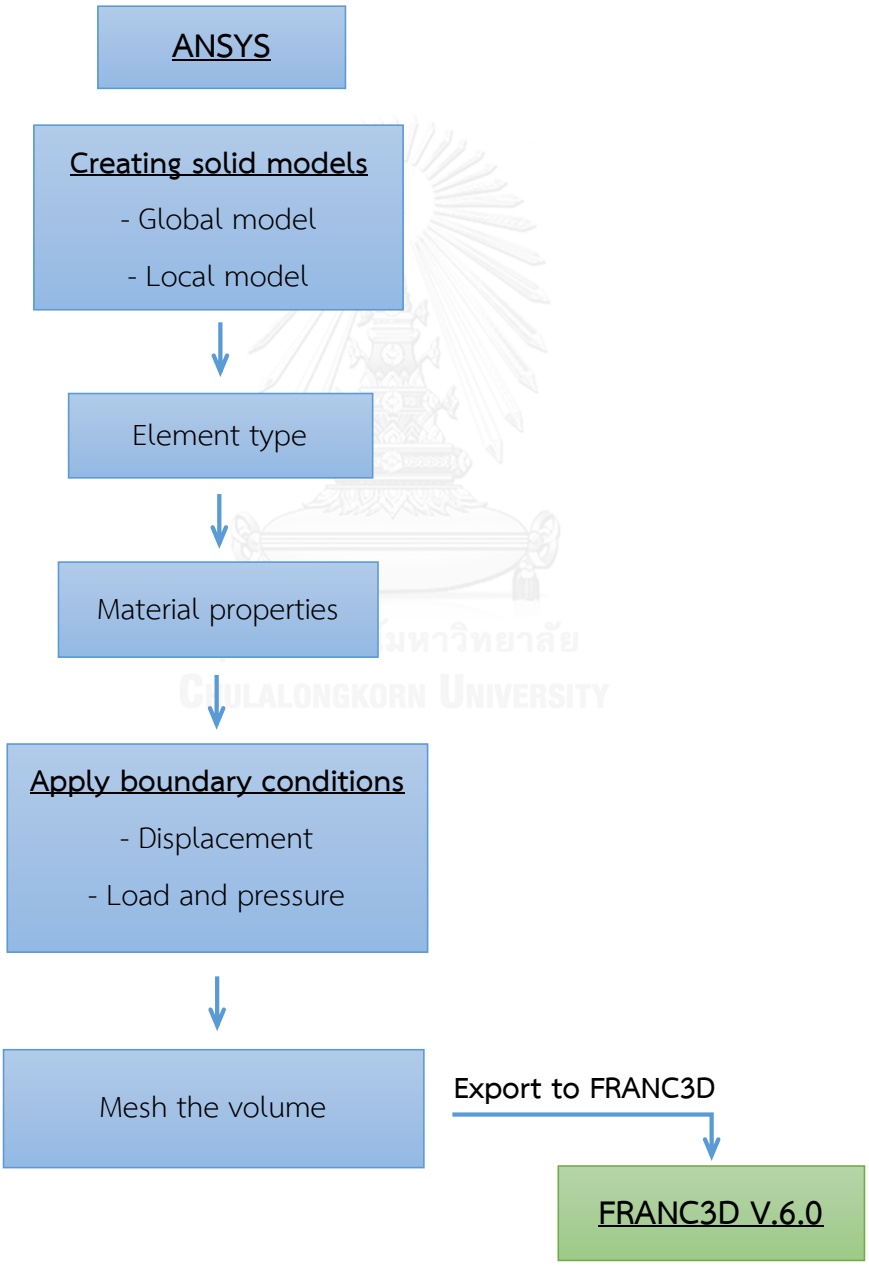

Figure 4.1 Work flow for crack-propagation analysis using ANSYS and FRANC3D

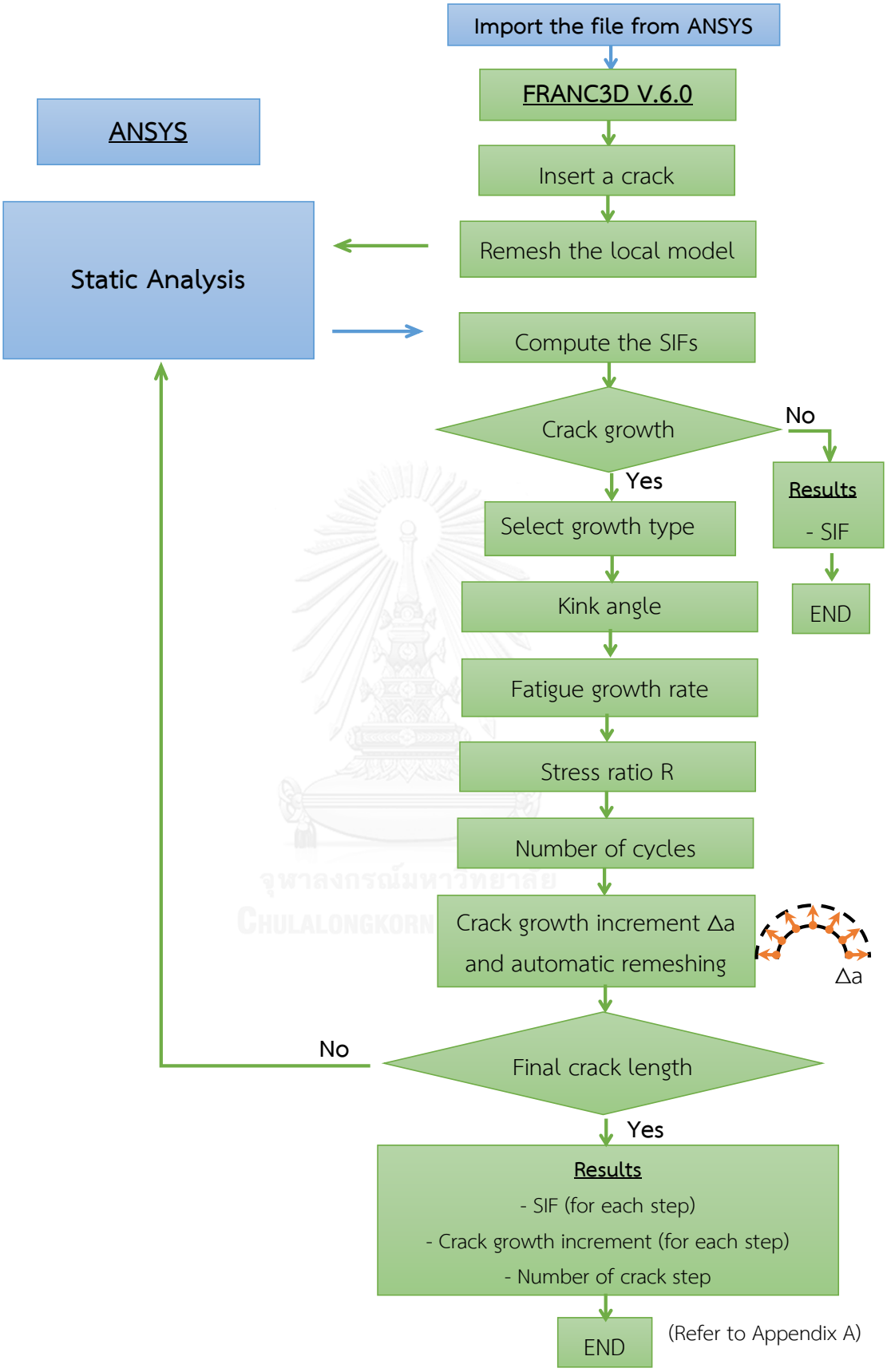

Figure 4.1 Work flow for crack-propagation analysis using ANSYS and FRANC3D (continued)

In this research, FRANC3D V.6.0 software developed by the Cornell fracture group is used to perform numerical simulation using the finite element analysis. However, other software used concurrently with FRANC3D is ANSYS software. In the first step, the model of steel beam with welded transverse stiffeners is created and defines both the element type and material property by ANSYS as shown in Figure 4.1. The boundary conditions, such as, point loads, distributed loads, bending moments, and structure supports are also assigned to the model. The model is divided into many elements and then is exported to FRANC3D software. Many types of cracks are able to be inserted into the model that FRANC3D performed remeshing. FRANC3D automatically sends the element model to ANSYS for performing the static analysis and then sending back to FRANC3D. In this step, the stress intensity factors along crack front can be computed for initial crack by FRANC3D using the results file obtained from ANSYS. FRANC3D continuously operates the crack growth analysis. The fatigue crack growth type, fracture growth rate, number of cycles, stress ratio, and kink angle are required to extend the crack growth increment Δa. The element model is automatically remeshed again for next static analysis. This process is repeated for the chosen number of crack steps. Finally, the obtained results are the stress intensity for each step, crack increment for each step, and the number of crack step.

4.2 Verification of three-dimensional finite element analysis

Fatigue crack occurs at the weld toe at the bottom end of transverse stiffeners that developed as a semicircular shape and then transformed into two-tip through-thickness shape. Accordingly, these two fatigue crack shapes can be studied in other cases in order to ensure the ability of the software.

4.2.1 Stress intensity factor for surface crack with semicircular shape under tension and bending

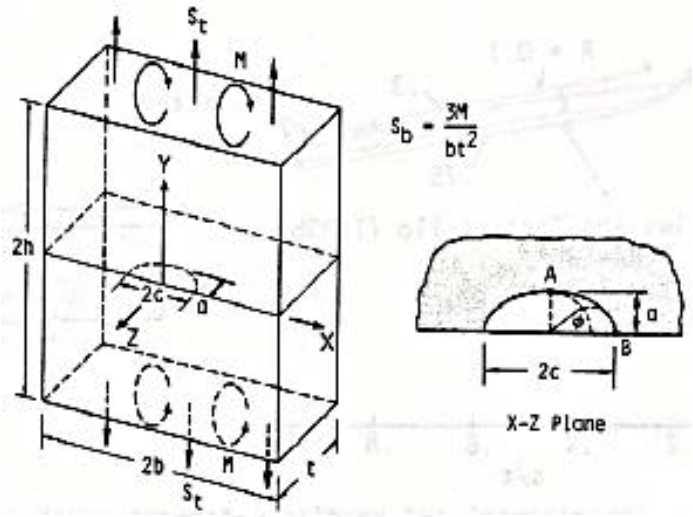

Figure 4.2 Coordinates and symbols of Surface crack in a plate [10].

Newman and Raju (1979) [8] studied the stress intensity factor of surface semi-elliptical crack under tension and bending as shown in Figure 4.2. There were many cases depending on the ratios of crack length in depth to width direction (a/c). This study chooses the cases of both tension and bending that a/c is equal to 1 (semicircular shape) as shown in Figure 4.3.

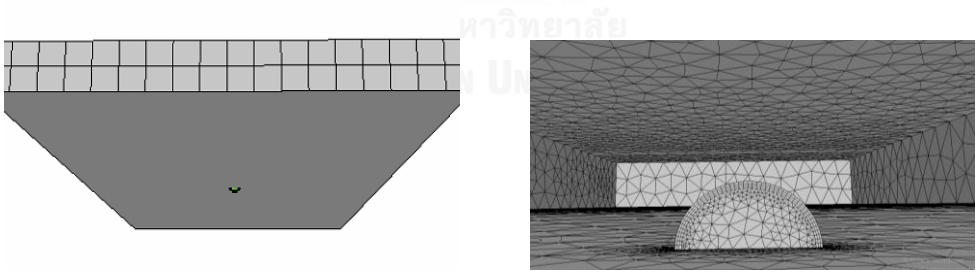

Figure 4.3 The initial semi-elliptical crack

For tension plate, the steel plates have the thickness of 2 mm, width of 30 mm, height of 50 mm. Tensile stress is applied of 1 MPa as shown in Figure 4.4. The ratios of crack length in depth to the thickness of steel plate (a/t) are equal to 0.2, 0.4, 0.6, and 0.8, respectively.

In case of bending plate, Newman and Raju (1979) [8] studied on a large steel plates which had the thickness of 9.5 mm, width of 80 mm (c/b=0.2), height of 140 mm (c/h=0.2). Bending stress is applied of 1 MPa at the crack position Figure 4.5. The ratios of crack length in depth to the thickness of steel plate (a/t) are equal to 0.2, 0.4, 0.6, and 0.8, respectively.

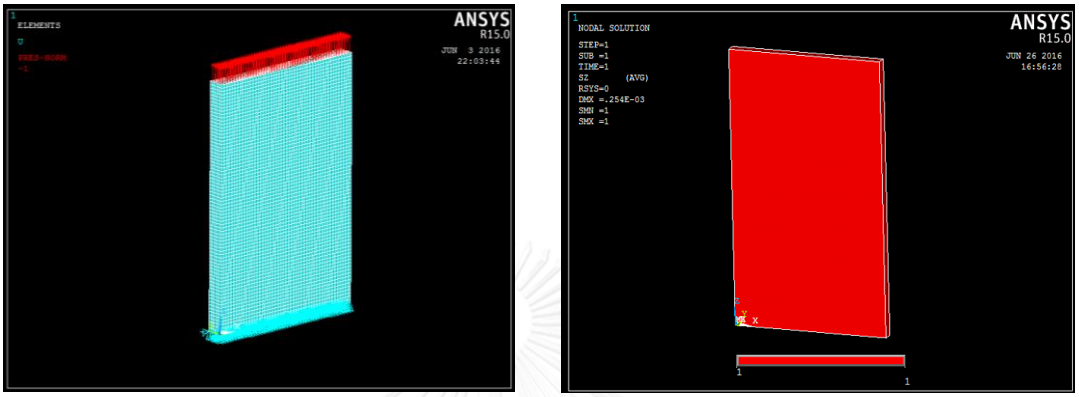

Figure 4.4 The model of steel plate under tension

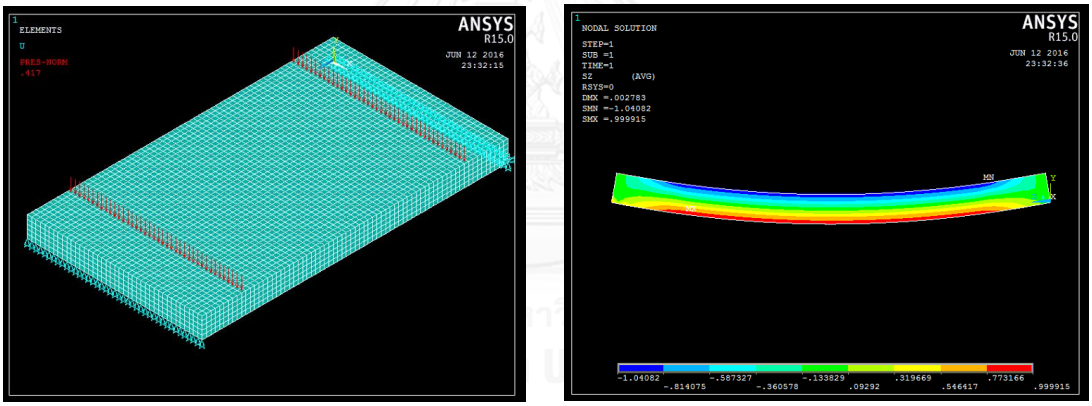

Figure 4.5 The model of steel plate under bending

The stress intensity factor values that are obtained from the FRANC3D simulation are compared with the results of Newman and Raju (1979) [8] and Liao and Atluri (1989) [12]. Moreover, The stress intensity factors are normalized to be unity as

$$Normalized\ KI = \frac{K}{S\sqrt{\pi \frac{a}{Q}}} \tag{4.1}$$

where S is the tension or bending stress and the shape factor (Q) is approximated by

$$Q = 1 + 1.464\left(\frac{a}{c}\right)^{1.65} \tag{4.2}$$

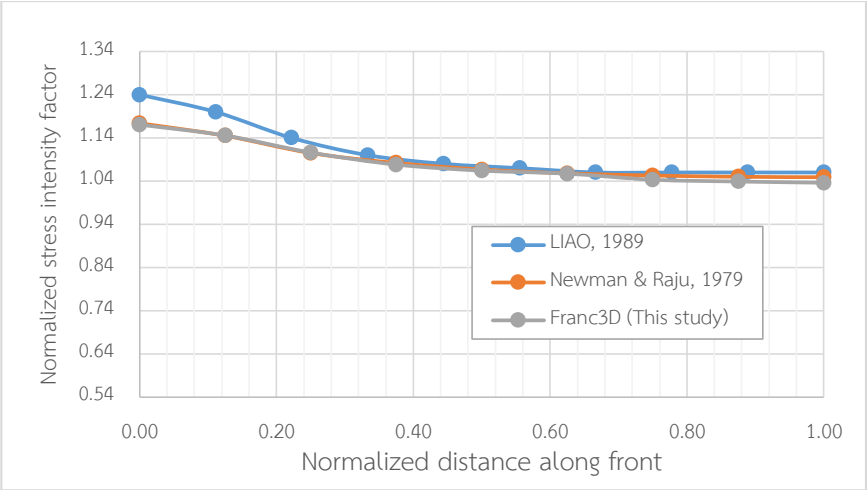
Normalized stress intensity factor
1.34
1.24
1.14
1.04
0.94
0.84
0.74
0.64
0.54
0.00
0.20
0.40
0.60
0.80
1.00
Normalized distance along front
LIAO, 1989
Newman & Raju, 1979
Franc3D (This study)

(a)

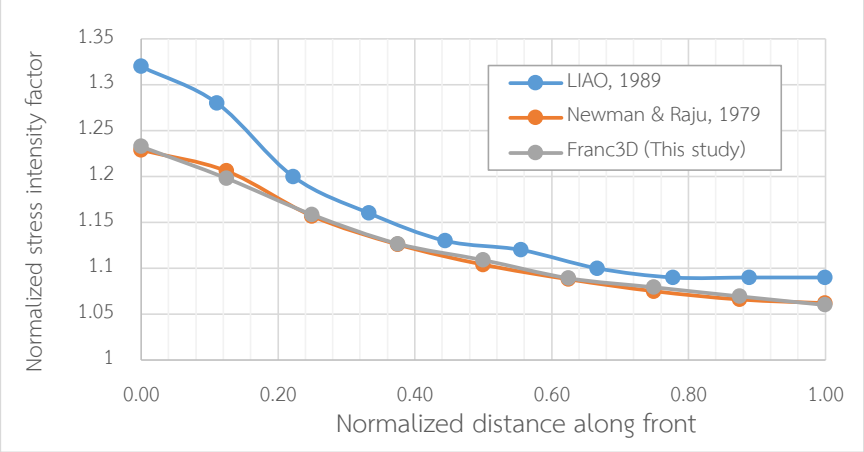
Normalized stress intensity factor
1.35
1.3
1.25
1.2
1.15
1.1
1.05
1
0.00
0.20
0.40
0.60
0.80
1.00
Normalized distance along front
LIAO, 1989
Newman & Raju, 1979
Franc3D (This study)

(b)

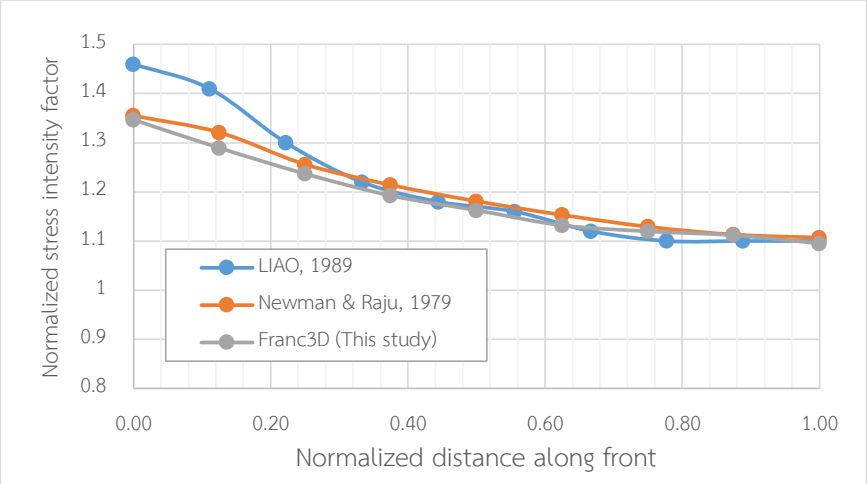
Normalized stress intensity factor
1.5
1.4
1.3
1.2
1.1
1
0.9
0.8
0.00
0.20
0.40
0.60
0.80
1.00
Normalized distance along front
LIAO, 1989
Newman & Raju, 1979
Franc3D (This study)

(c)

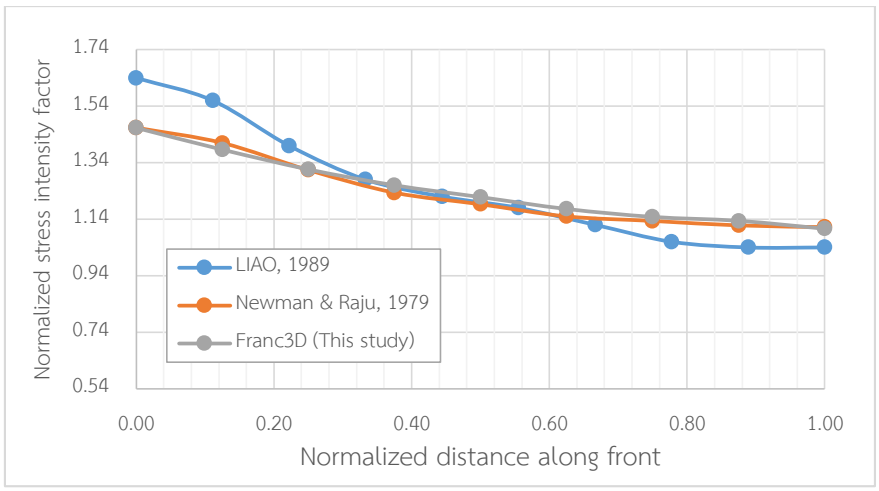

(d)

Figure 4.6 The results of the stress intensity factor along crack front under tension (a) a/t=0.2, (b) a/t=0.4, (c) a/t=0.6, and (d) a/t=0.8

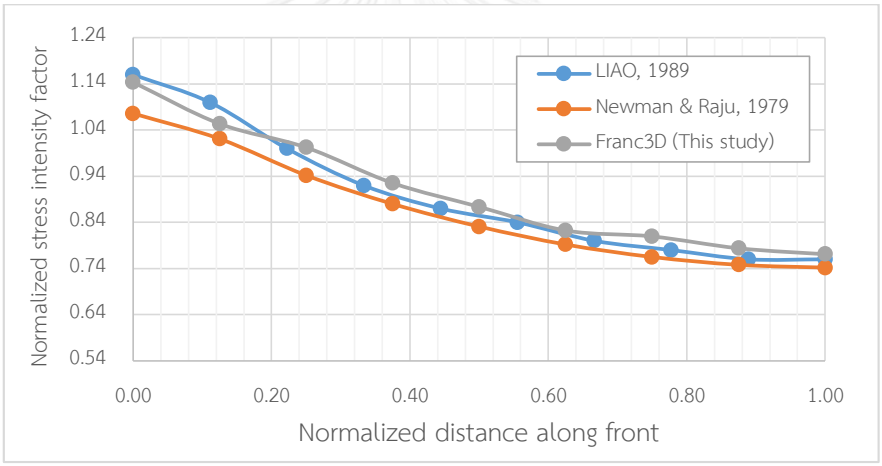

(a)

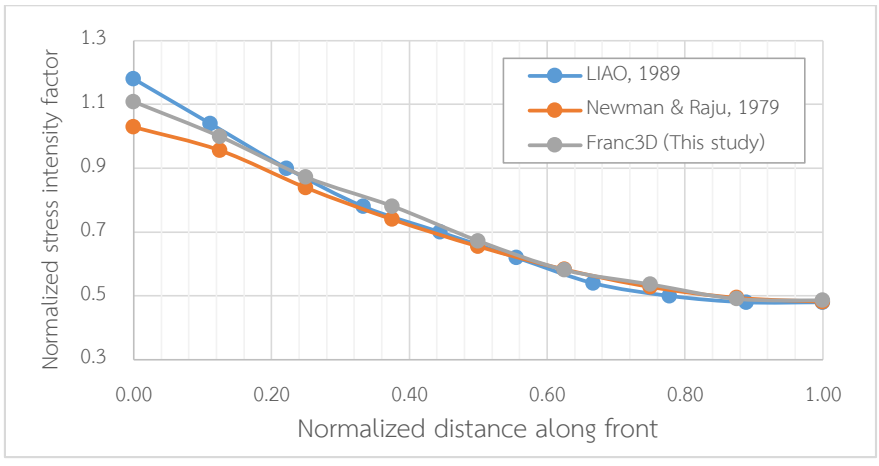

(b)

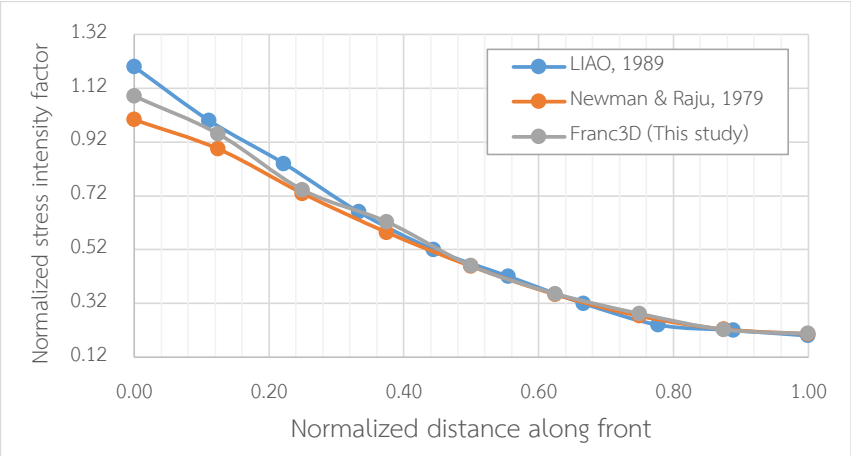

(c)

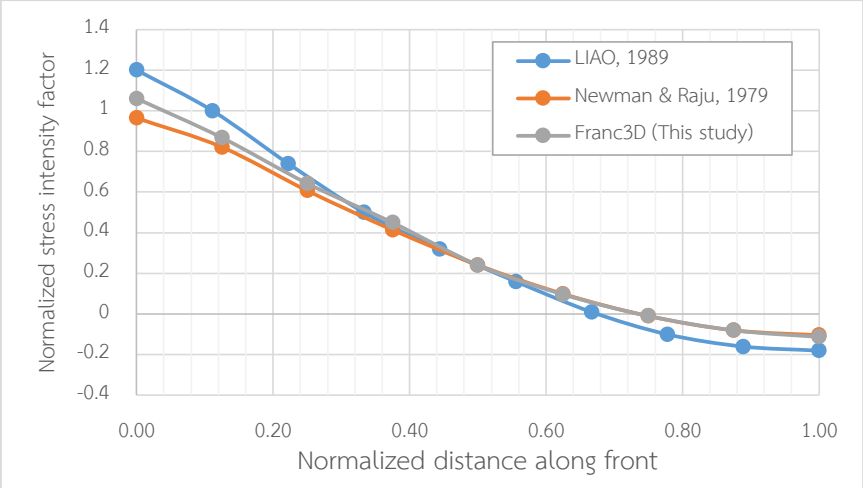

(d)

Figure 4.7 The results of the stress intensity factor along crack front under bending (a) a/t=0.2, (b) a/t=0.4, (c) a/t=0.6, and (d) a/t=0.8

Figure 4.6 and Figure 4.7 show the normalized stress intensity factors for the semicircular crack under tension and bending, respectively. Very good agreements are observed between FRANC3D results and Newman and Raju (1979) for all a/t except for a/t=0.2 under bending that is observed as fair agreement. So, FRANC3D may have enough performance to calculate the stress intensity factor for surface crack under both tension and bending.

4.2.2 Surface crack with semi-elliptical shape under tension

The problem form example 13 of FRANC3D/BES benchmarking [30] is selected to verify that FRANC3D V.6.0 is capable of providing accurate the stress intensity factor and life for surface crack with semi-elliptical shape problem. Stainless steel plate with semi-elliptical surface flaw has thickness of 19.75 mm, width (2b) of 180.3 mm, height (2h) of 400 mm as shown in Figure 4.8. The material properties include an elastic modulus of 210,000 MPa and a Poisson's ratio of 0.30. The initial surface crack with a/t is equal to 0.098 that is crack length (a) of 1.93 mm and a/c is equal to 0.78 that is crack length (c) of 2.47 mm as shown in Figure 4.9. The loading on steel plate is cyclic uniform tension with constant amplitude loading having max tensile stress of 245 MPa and stress ratio of 0.15. The Paris law [29] is used in prediction which C and n are equal to 1.14×10^{-15} and 3.85, respectively. Figure 4.10 shows the points on the crack front.

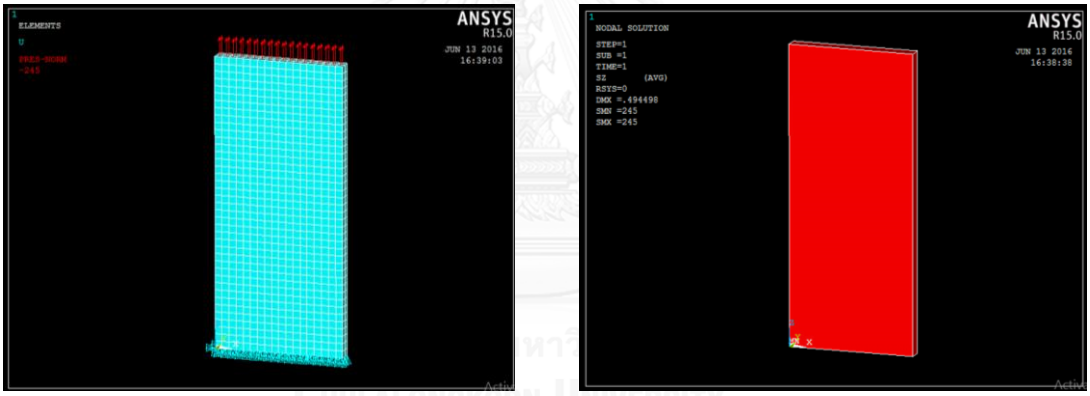

Figure 4.8 The modeling of plate under tension

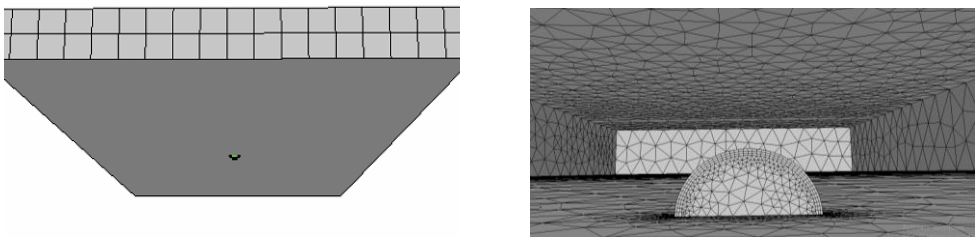

Figure 4.9 The initial semi-elliptical crack

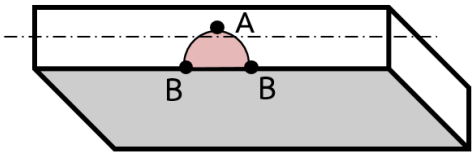

Figure 4.10 the studied positions of surface crack: the depth point (A) and the surface value (B)

Table 4.1 Comparison of the values of stress intensity factor at initial crack.

Methods	Surface value (point B) (MPA√mm)	Relative error %	Depth value (point A) (MPA√mm)	Relative error %
Experiment	445	-	457	-
FRANC3D (Benchmarking)	460	3.37	454	-0.66
FRANC3D (This study)	448	0.67	443	-3.06

Table 4.1 shows the values of stress intensity factor at initial crack for surface and the deepest point which is compared with experiment of Kawahara (1978) [31] and the obtained values from FRANC3D/BES benchmarking. The results obtained from FRANC3D V.6.0 has very good agreement with the relative error at surface point and the deepest point of 0.67 and -3.03 percent, respectively.

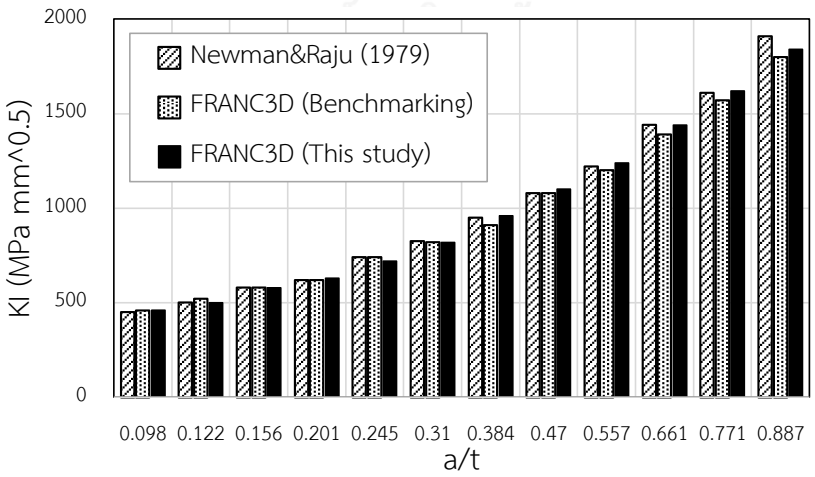

Figure 4.11 A comparison of the stress intensity factor KI at surface (point B) obtained from Newman & Raju (1979) [8], FRANC3D (Benchmarking) [30], and FRANC3D (This study).

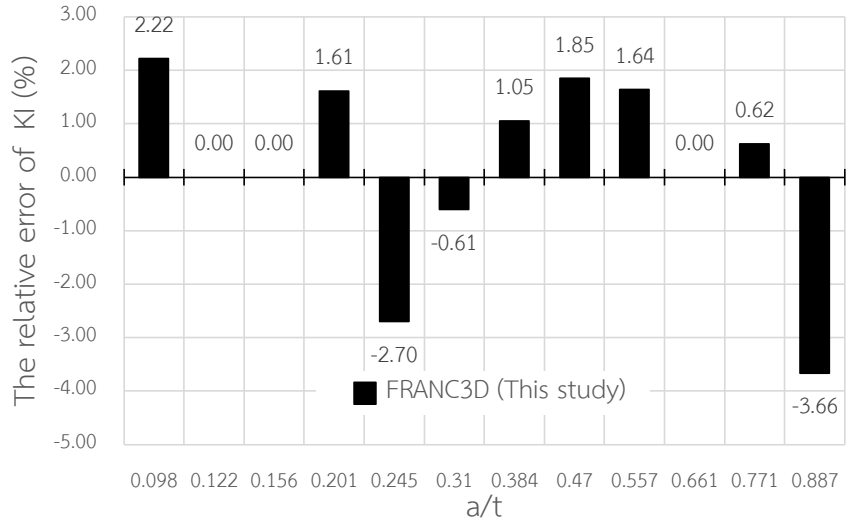

Figure 4.12 A relative error of stress intensity factor KI at surface of crack for FRANC3D (This study) compared to Newman & Raju (1979) [8]

Figure 4.11 and Figure 4.12 plot the different values and the relative errors of stress intensity factor at surface of crack against normalized crack length (a/t) that are calculated from three methods. The results indicate that the values of stress intensity factor obtained from each method are not quite different with all relative errors of FRANC3D compare with Newman & Raju (1979) below 4 percent.

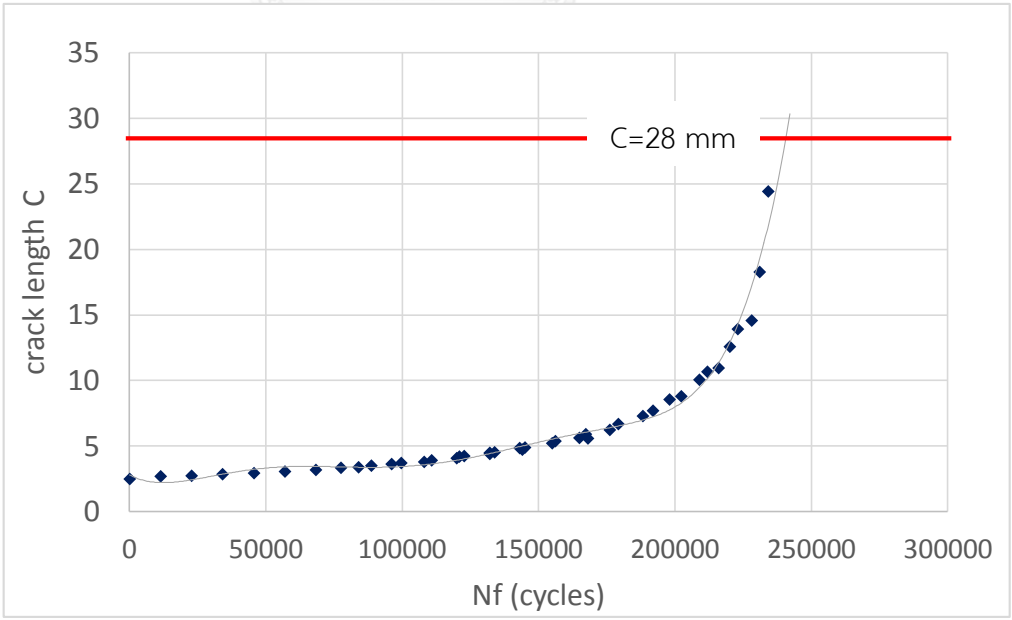

Figure 4.13 The predicted number of fatigue cycles obtained from FRANC3D (This study)

Table 4.2 the total number of fatigue cycles at crack length c of 28 mm (point B)

Methods	N_f (cycles)	Difference %
FRANC3D (Benchmarking) [30]	217,000	-
FRANC3D (This study)	230,000	5.99

The fatigue crack growth curve in the surface (c) is plotted in Figure 4.13 that the stress intensity factor solutions are incorporated into a fatigue life prediction. The comparison of benchmarking and FRANC3D surface crack growth that was predicted to 28 mm is shown in Table 4.2. The result of FRANC3D (This study) also has good agreement with benchmarking with the difference of 5.99 percent.

4.2.3 Two-tip through-thickness in structural steel I-beams under bending

A structural steel I-beam [15], W40x149 of 6 m length, 300 mm width, 949.2 mm depth, and 21.1 mm flange thickness, and 16 mm web thickness is selected as shown in Figure 4.14. The crack eccentricity is 250 mm with λ_w=0.2. Therefore, initial crack having two-tip through-thickness shape is 44.92 mm of length. Stress intensity factor and fatigue crack life have been calculated by FRANC3D and compare with those of finite element values by Albrecht et al (2008) [15].

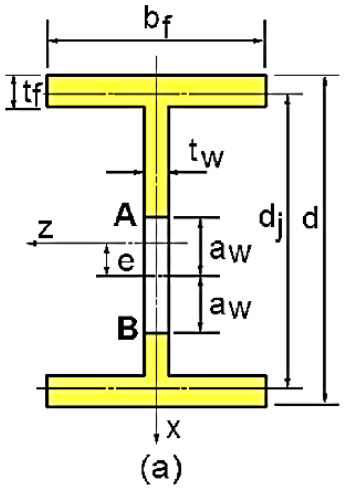

Figure 4.14 I-beam for two-tip web crack web crack [15]

In case of fatigue life, the Paris law [29] is used to calculate the number of load cycles by direct integration which C and n are $5x10^{8}$ and 1.5 as shown in equation (4.3).

$$N = \int_{a_0}^{a_f} \frac{da}{C(\Delta K)^n} \approx \sum_{a_0}^{a_f} \frac{\Delta a}{C(\Delta K)^n} \tag{4.3}$$

The stress intensity factor is

$$\Delta K = f^B(\lambda_w, \varepsilon, \beta)\Delta\sigma\sqrt{\pi a} \tag{4.4}$$

where $f^B(\lambda_w, \varepsilon, \beta)$ is a correction factor of two-tip web cracks in I-beams for lower crack tip under bending stress that used from [15] and $\Delta\sigma$ is bending stress at the flange-to-web junction.

Table 4.3 shows the results of stress intensity factor using the correction factor from Albrecht (2008) [15] and bring to compute the fatigue life by direct integration method. Because the equation (4.3) is very difficult to calculate the fatigue life, trapezoidal rule is used. The step sizes of trapezoidal rule must be considered to ensure the accurate values obtained from calculation. Moreover, the stress intensity factors for mode II and mode III have very little values and can be neglected.

Figure 4.15 and Figure 4.16 present difference and relative errors of the values of the stress intensity factor KI at any crack lengths by comparison the results obtained from Albrecht et al. (2008) [15] and the FRANC3D. Clearly, the analysis results indicate that the values of stress intensity factor obtained from both methods are not quite different with all relative errors below 6 percent.

Figure 4.17 and Figure 4.18 also present the difference and relative errors of the number of fatigue crack life at any crack lengths by comparison the results obtained from direct integration by using the correction factor form Albrecht et al. (2008) [15] and the FRANC3D. The small difference of the number of fatigue crack life obtained from both methods is shown and all relative errors do not exceed 12 percent.

Table 4.3 The results of stress intensity factor and fatigue life obtained from Albrecht (2008) and FRANC3D

Crack length (mm)	Stress intensity factor, KI (MPa mm^0.5)			Fatigue life, Nf (cycles)		
	Albrecht et al. (2008)	FRANC3D	Relative error (%)	Direct Integration	FRANC3D	Relative error (%)
44.9	3,758	3,900	3.8	0	0	0.0
50	4,006	4,150	3.6	492	500	1.6
55	4,243	4,400	3.7	935	950	1.6
60	4,474	4,600	2.8	1,342	1,400	4.3
65	4,700	4,850	3.2	1,719	1,800	4.7
70	4,922	5,150	4.6	2,090	2,200	5.3
75	5,140	5,400	5.1	2,398	2,500	4.3
80	5,354	5,600	4.6	2,707	2,850	5.3
85	5,565	5,800	4.2	2,997	3,200	6.8
90	5,774	6,000	3.9	3,271	3,550	8.5
95	5,979	6,300	5.4	3,532	3,900	10.4
100	6,182	6,500	5.1	3,779	4,200	11.1
105	6,382	6,750	5.8	4,014	4,500	12.1

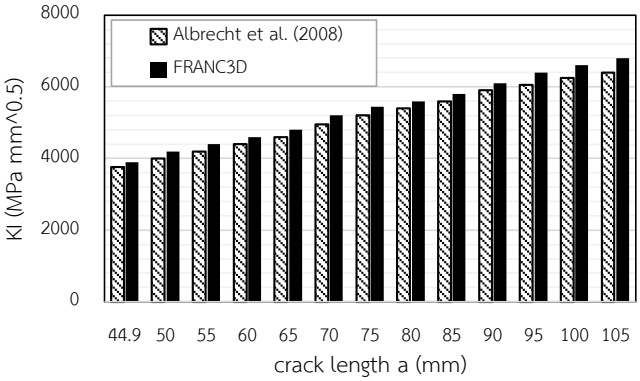

Figure 4.15 A comparison of the values of the stress intensity factor KI Albrecht et al. (2008) [15] and the FRANC3D.

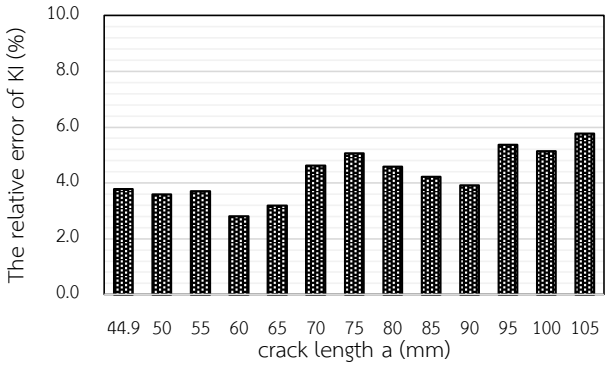

Figure 4.16 A relative error of stress intensity factor KI for both methods [15].

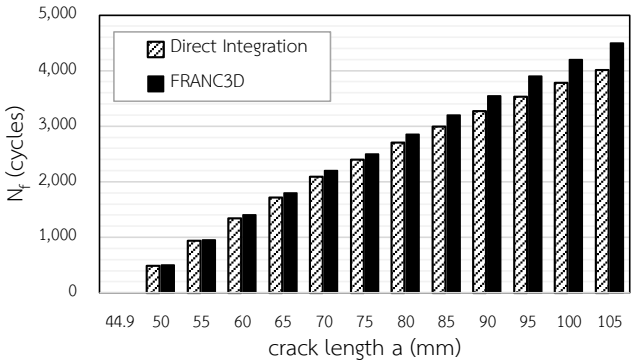

Figure 4.17 A comparison of the values of the number of fatigue cycles N_f using the direct integration [15] and the FRANC3D.

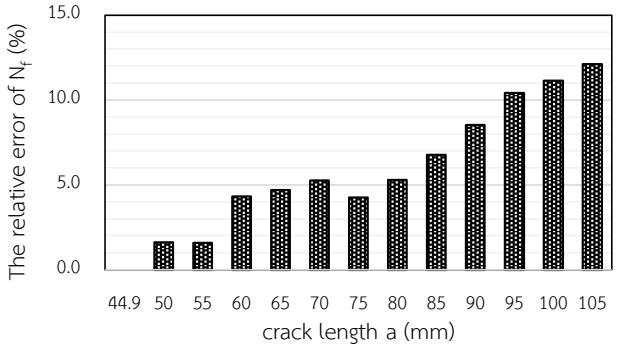

Figure 4.18 A relative error of the number of fatigue cycles N_f for both methods [15].

For these reasons, the obtained small different results may not significantly deform results of such analyses in the values of stress intensity factor and fatigue crack life. Accordingly, the FRANC3D software can work well and give the precise fatigue crack propagation results for steel structural calculations.

CHAPTER V
EFFECTS OF PARAMETERS ON FATIGUE LIFE OF WELDED TRANSVERSE STIFFENERS

5.1 Finite element models

The finite element method is one of the most well-known methods used for solving engineering problems with complicated geometries, boundary conditions, and material properties. Figure 5.1 shows that the steel beams are modelled as a combination of top flange plate, bottom flange plate, web plate, and welded transverse stiffener plates. Fillet welds are neglected. Eight-node solid elements – ANSYS designation of brick 8 node 185 – are selected. The element is defined by eight nodes which each node has three degrees of freedom: translations in the nodal x, y, and z directions. Approximately 105,000 elements are used for the entire model.

Since the most effective method for analyzing discontinuity problem, especially the problem of fracture, is the extension of finite element method, M-integral is applied to calculate stress intensity factor by calculating the stress and displacement field near the crack tip [23]. Furthermore, the fatigue life of steel structures can be estimated by using fatigue crack growth rate. The crack growth rate of metal is widely used the Paris law [29], which is the relationship between crack growth rate and stress intensity factor.

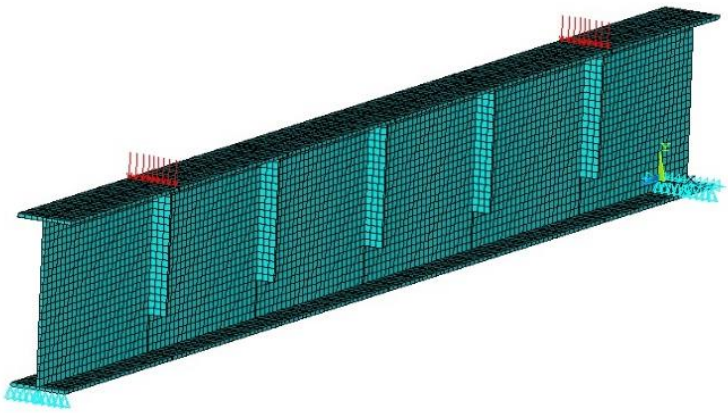

Figure 5.1 Finite element modeling of steel I-beams with welded transverse stiffeners

5.2 Materials and parameters

5.2.1 Materials

Numerical simulations study on plate of ASTM A36 steel which is a standard steel alloy and is often used as structural steel. It has excellent welding properties and is suitable for many general applications. Young's modulus for A36 steel is 200 GPa., poisson's ratio is 0.29, and a fracture toughness is 90 ksi√(in.) (3,165 MPa√(mm)) [32].

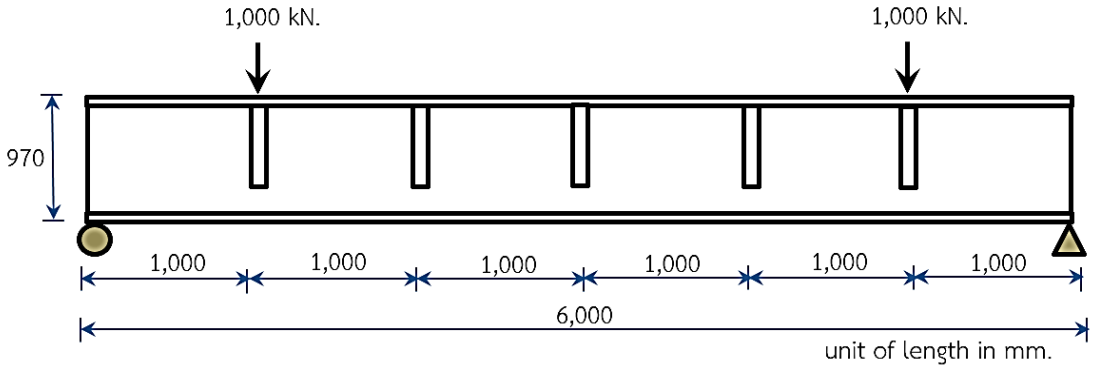

Figure 5.2 The model of Steel I-beam

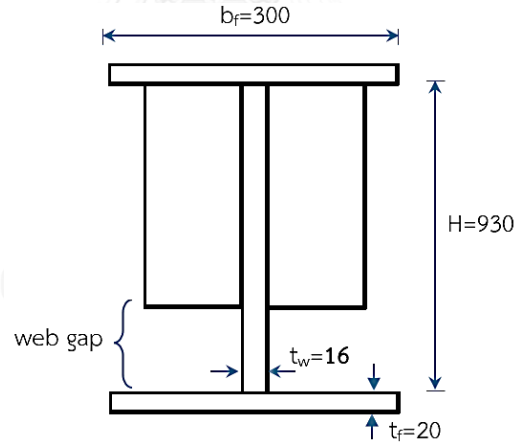

Figure 5.3 Cross section of steel I-beam

5.2.2 Steel I-beams with welded transverse stiffeners

A model of the steel I-beam with welded transverse stiffeners is used to predict fatigue life as shown in Figure 5.2 and Figure 5.3. It has I-sectioned steel plate beam of 6 m length, 300 mm width, 930 mm depth, 20 mm flange thickness, and 16 mm web thickness with welded transverse stiffeners of 100 mm width and 12 mm thick attached both sides on the web plate with a web gap of 90 mm.

5.2.3 Parameters

- **Initial crack sizes**

According to the recommendation of FHWA [33], the length of initial crack size is 0.25 mm (0.01 in) but the analysis of very small crack requires accurate knowledge of stress concentration factor of notch. Therefore, the initial cracks have semicircular shape with a/c=1 and their sizes are 1, 2, 4, 8, 12 mm for surface cracks and initial crack size of two-tip through-thickness shape is 16 mm. The steel beams have I-sectioned steel plate beam of 6 m length, 300 mm width, 930 mm depth, 20 mm flange thickness, and 16 mm web thickness with welded transverse stiffeners of 100 mm width and 12 mm thick attached both sides on the web plate with a web gap of 90 mm. The flexural rigidity ratio of this steel beam is equal to 2.66×10^{-3}.

- **Web-gap lengths**

The web-gap lengths are equal to 90, 215, and 340 mm, respectively as presented in Figure 5.4. The steel beams have I-sectioned steel plate beam of 6 m length, 300 mm width, 930 mm depth, 20 mm flange thickness, and 16 mm web thickness with welded transverse stiffeners of 100 mm width and 12 mm thick attached both sides on the web plate. The initial crack size is 1 mm for semicircular shape and 16 mm for the two-tip through-thickness shape. The flexural rigidity ratio of this steel beam is equal to 2.66×10^{-3}.

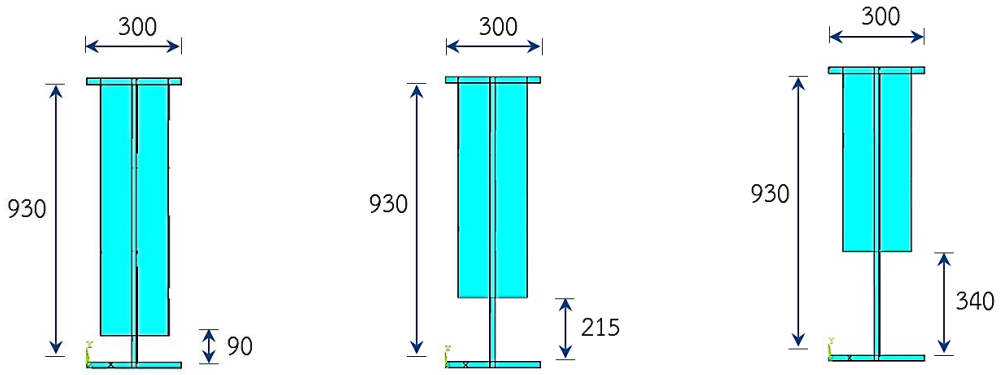

Figure 5.4 Cross section of steel I-beams with different wed gap lengths (a) 90 mm (b) 215 mm (c) 340 mm

- **Flexural rigidity ratios**

The flexural rigidity ratios are equal to $2.66x10^{-3}$, $4.44x10^{-3}$, $5.92x10^{-3}$, and $7.39x10^{-3}$, respectively. The steel beams have I-sectioned steel plate beam of 6 m length, 300 mm width, 930 mm depth, 20 mm flange thickness, and 16 mm web thickness with welded transverse stiffeners whose dimensions depend on the values of the flexural rigidity ratios as shown in Figure 5.5. The initial crack size is 1 mm for semicircular shape and 16 mm for the two-tip through-thickness shape. The web-gap length is equal to 90 mm.

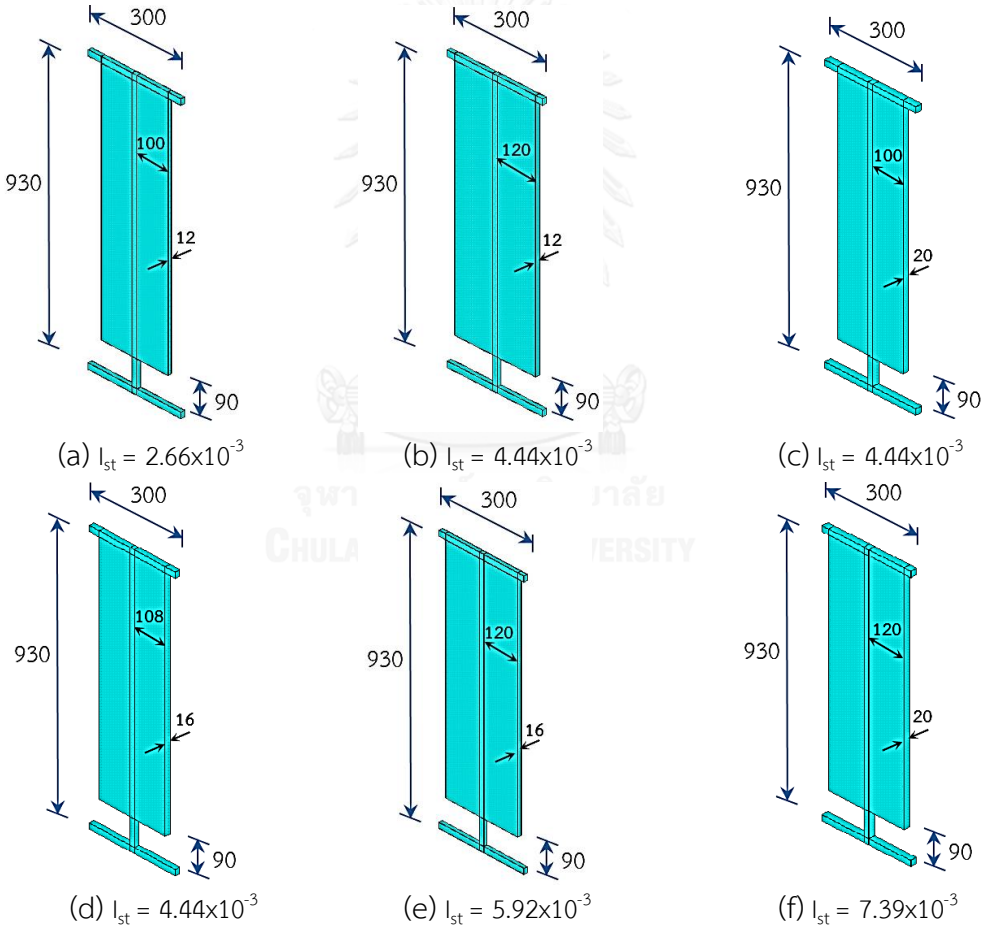

Figure 5.5 Cross section of steel I-beams with different flexural rigidity ratios (a) $2.66x10^{-3}$ (b), (c), (d) $4.44x10^{-3}$ (e) $5.92x10^{-3}$ and (f) $7.39x10^{-3}$

5.2.4 Fatigue loadings

The models are conducted under constant amplitude loading in a four-point bending condition with stress ratio of 0.1. Fatigue crack growth rate of metal usually applies the Paris law shown in equation (3.51) [29] . In this study, C and n which are material constants used to estimate fatigue crack propagation and life are assumed to be equal to $5x10^{-8}$ and 1.5, respectively. The fatigue crack increment is recommended using approximately less than twenty times of total fatigue life.

5.3 The effect of initial crack sizes

The service life of the steel beams can be described by number of cyclic loadings starting from crack initiation until the stress intensity factor reaching the fracture toughness. The initial crack sizes might influence fatigue crack life, especially very small initial crack size. The sizes of initial crack were assigned of 1, 2, 4, 8, 12 mm, respectively, as a surface crack with semicircular shape (a/c=1) as shown in Figure 5.6.

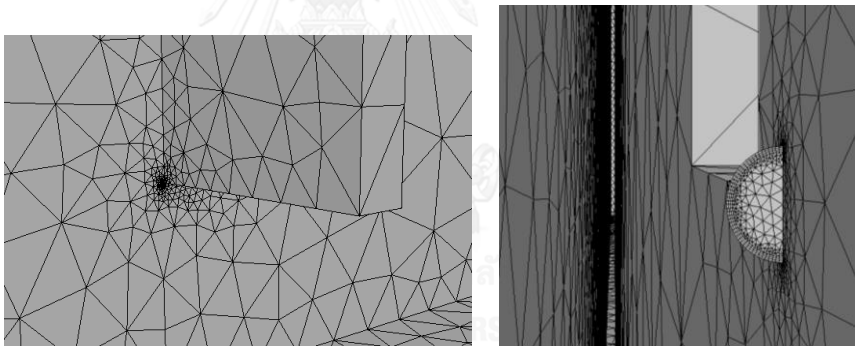

Figure 5.6 initial crack configuration

Figure 5.7 shows the transitional stage when the fatigue crack propagated until penetrating through the web plate, the initial crack of phase II having two-front through-thickness shape has started of 16 mm. Then, let fatigue crack propagates until the stress intensity factor reaching their fracture toughness. Eventually, the results of cycle counting of phase I is compared to phase II.

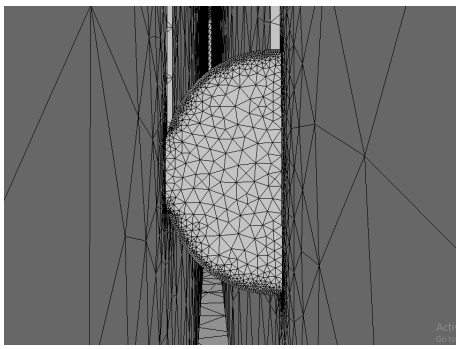

Figure 5.7 Transition of fatigue crack from phase I (surface crack) to phase II (two-tip through-thickness crack)

Figure 5.9 plots the stress intensity factors of the lower crack front of web crack tip for the steel I-beam with welded transverse stiffeners with web-gap length of 90 mm with different initial crack sizes. The crack length of phase I, semicircular shape, increases to 16 mm which is the end of web thickness and continuously propagates in different shape, two-tip through-thickness shape in Phase II. Moreover, the stress intensity factors for mode II and mode III have very little values and can be neglected.

At the transition state (a=16 mm), the crack shape transforms its shape from semicircular at surface crack to be two-tip through-thickness. The stress intensity factor values at this point obtained from both shapes are not equal. Jump discontinuous values occur because the shape of fatigue crack is changed into the other shape. Moreover, Figure 5.8 shows the studied point on the crack front.

Because the fatigue life is governed by the fracture toughness of ASTM A36 steel that is equal to 3,165 MPa$\sqrt{}$(mm) [32], the final crack size is equal to 18 mm. The number of load cycles of phase I having initial crack size of 1 mm is about 8,500 cycles and phase II is about 800 cycles read from Figure 5.10 that is plotted the number of load cycles against the crack sizes. The results of fatigue life influenced by different initial crack sizes as shown in Table 5.1.

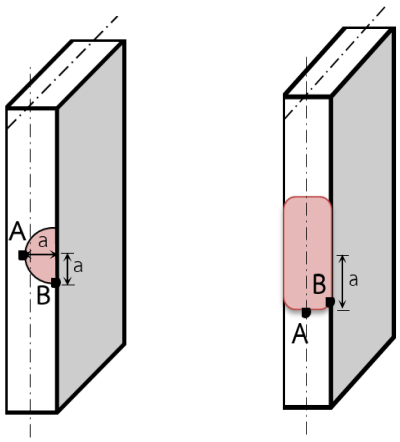

Figure 5.8 the studied positions of surface crack and through-thickness crack at the web plate

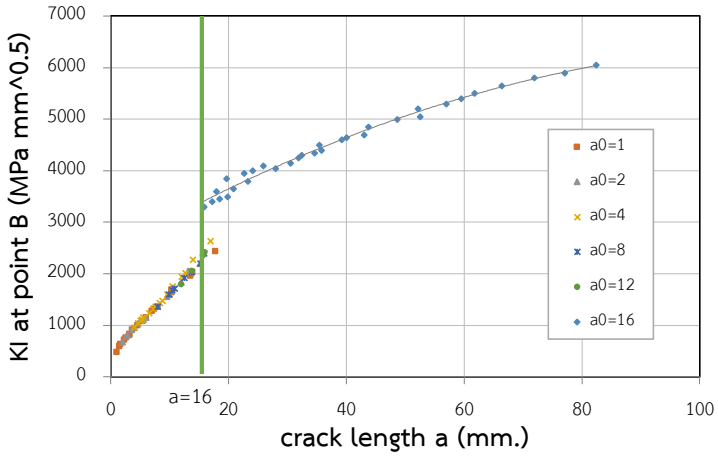

Figure 5.9 The result of the stress intensity factor depending on the fatigue crack lengths for web-gap length of 90 mm

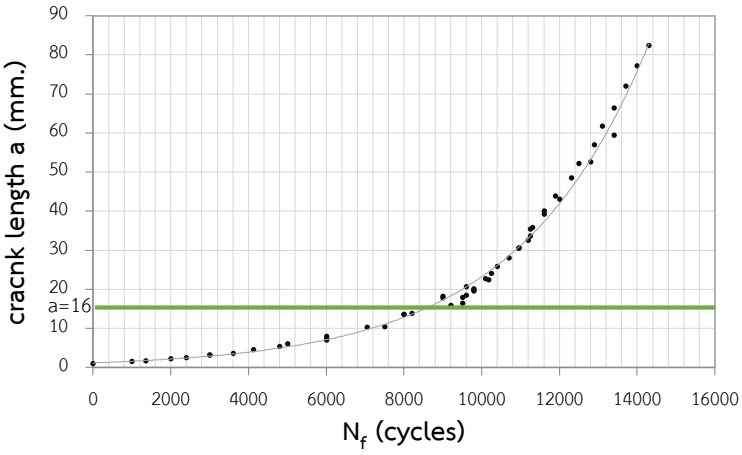

Figure 5.10 The result of the fatigue life depending on the number of load cycles for web-gap length of 90 mm

Table 5.1 The results of fatigue life influenced by different initial crack sizes.

Phase I (semicircular shape)		Phase II (two-tip through-thickness shape)		Phase I / Phase II	
Initial crack sizes (mm.)	Fatigue life (cycles) (from initial crack to the end of web)	Initial crack sizes (mm.)	Fatigue life (cycles) (from the end of web to toughness, af=18)	Crack lengths (a0/af)	Fatigue life
1	8,500	16	800	0.06	10.63
2	6,700	16	800	0.11	8.38
4	4,800	16	800	0.22	6.00
8	2,400	16	800	0.44	3.00
12	1,000	16	800	0.67	1.25

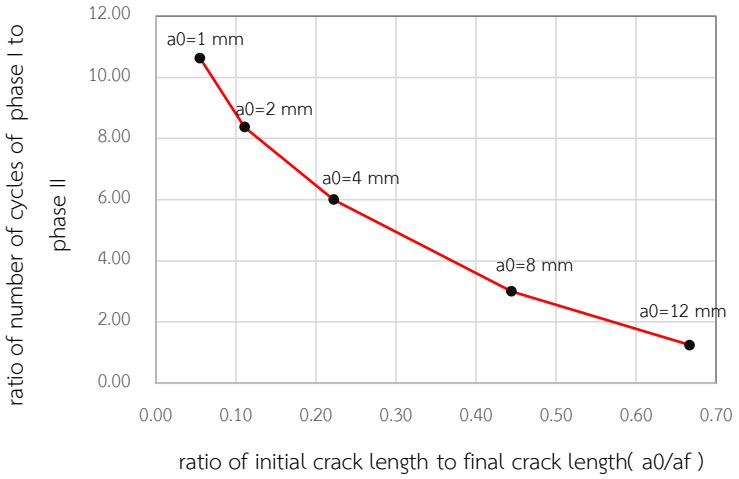

Figure 5.11 Influence of initial crack sizes on fatigue crack life

So, Figure 5.11 shows that the ratio of number of cycles of phase I to phase II for web-gap length of 90 mm with initial crack size of 1 mm (ratio of initial crack length to final crack of 0.06) is equal to 10.63. In addition, the ratio of the number of cycles of phase I to phase II for web-gap length of 90 mm with other initial crack sizes of 2, 4, 8, and 12 mm (ratio of initial crack length to final crack of 0.11, 0.22, 0.44, and 0.67) are 8.38, 6.00, 3.00, and 1.25, respectively.

Therefore, the influence of initial crack sizes on fatigue crack life can be described that the very small crack will be subjected to very high number of load cycles in the initial state and severely decreases when the crack size is larger.

5.4 The effect of web-gap lengths

The design guides of AASHTO (2012) recommend the web-gap length using four to six times as thick as web thickness for the strength of steel beams but do not consider the effects of fatigue crack to the life span of the steel beams and might finally cause the fracture of the bridge. The web-gap length of 90, 215, 340 mm. is studied by starting at initial crack a_0 = 1 mm as surface crack having semicircular shape. Then, fatigue crack continuously propagates until reaching their fracture toughness. Eventually, the results of cycle counting summary phase I and phase II of all web gaps are compared.

Table 5.2 The results of fatigue life influenced by different web-gap lengths.

Web-gap lengths (mm.)	Normalized web-gap lengths	Phase I (semicircular shape, a0=1 mm)		Phase II (two-tip through-thickness shape, a0=16 mm)		Fatigue life (Phase I + Phase II)	Normalized fatigue life
		Final crack (mm)	Fatigue life (cycles)	Final crack (mm)	Fatigue life (cycles)		
90[a]	0.19	16	8,500	18	800	9,300	0.14
215[b]	0.46	16	16,200	42	4,700	20,900	0.32
340[c]	0.73	16	33,000	101	32,000	65,000	1.00

[a] The results show in Figure C.1 and Figure C.2. [b] The results show in Figure C.3 and Figure C.4.

[c] The results show in Figure C.5 and Figure C.6.

Table 5.2 indicates that the results of total fatigue crack life for the web-gap lengths of 90, 215, 340 mm are equal to 9300, 20900, and 65000 cycles, respectively. The results that calculated by FRANC3D are plotted as described in APPENDIX C.

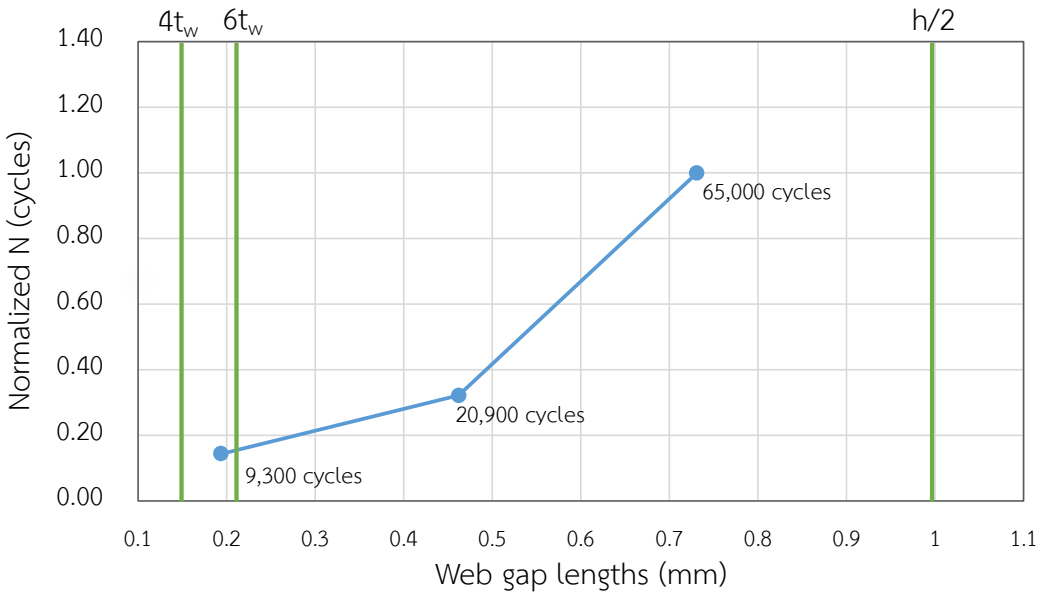

Figure 5.12 Influence of web-gap lengths on fatigue crack life

Figure 5.12 presents that the normalized web-gap lengths of 0.19, 0.46, and 0.73 mm (normalized with H/2= 465 mm) corresponded with the normalized number of load cycles of 0.14, 0.32, and 1.00, respectively (normalized with 65,000 cycles). An initial crack with smaller web-gap length has a higher value of stress intensity factor which shortens the fatigue life. However, the larger web-gap length can provide the longer life. The effect of web-gap length is nonlinear.

5.5 The effect of transverse stiffener dimensions

The transverse stiffeners must have sufficient rigidity for keeping the cross section of steel beam in shape in order to ensure the nodal line formation during web buckling and develop the shear-buckling resistance. The web panel boundary is assumed that it does not deflect laterally perpendicular to the plane of web when the steel beam is subject to external loads [5]. So, all transvers stiffeners are required to have proper rigidity in that direction whereas the effects of fatigue crack are not taken into consideration.

Table 5.3 The results of fatigue life influenced by different stiffener dimensions.

Flexural rigidity ratios	Stiffeners dimensions (mm.)		Phase I (semicircular shape, a0=1 mm.)		Phase II (two-tip through-thickness shape, a0=16 mm.)		Fatigue life (Phase I + Phase II)	Normalized fatigue life
	Thick-ness	Width	Final crack (mm)	Fatigue life (cycles)	Final crack (mm)	Fatigue life (cycles)		
[a]2.66×10^{-3}	12	100	16	8,500	18	800	9,300	1.00
[b]4.44×10^{-3}	12	120	16	8,800	17	300	9,100	0.98
[c]4.44×10^{-3}	16	108	16	5,700	-	-	5,700	0.61
[d]4.44×10^{-3}	20	100	12	3,500	-	-	3,500	0.38
[e]5.92×10^{-3}	16	120	16	5,900	-	-	5,900	0.63
[f]7.39×10^{-3}	20	120	13	3,400	-	-	3,400	0.37

[a]The results show in Figure C.1 and Figure C.2. [b]The results show in Figure C.9 and Figure C.10.

[c]The results show in Figure C.15 and Figure C.16. [d]The results show in Figure C.11 and Figure C.12.

[e]The results show in Figure C.7 and Figure C.8. [f]The results show in Figure C.13 and Figure C.14.

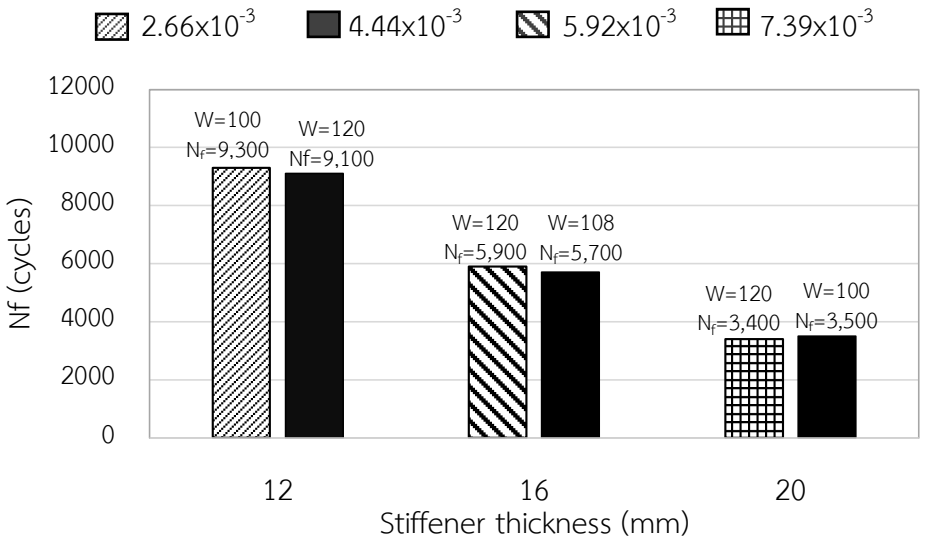

Figure 5.13 The fatigue crack life of steel I-beams with different flexural rigidity ratios

The steel beams are studied by starting at initial crack a_0 = 1 mm as surface crack having semicircular shape and using web-gap length of 90 mm. Table 5.3 presents the results of total fatigue crack life for each stiffeners dimensions. The results that calculated by FRANC3D are plotted as described in APPENDIX C.

Figure 5.13 indicates that the flexural rigidity ratios do not have an influence fatigue life of steel I-beams with welded transvers stiffeners. Despite the same of flexural rigidity ratio, the fatigue lives are different represented as the black bars. On the other hand, the factor that is investigated having an effect to fatigue life instead of the flexural rigidity ratio is stiffener thickness (t_s).

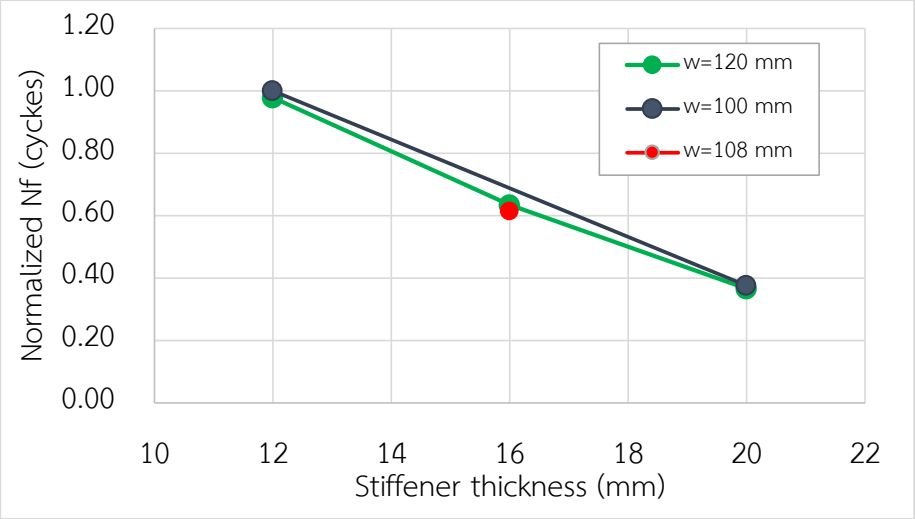

Figure 5.14 Influence of Stiffener thickness on fatigue crack life

Figure 5.14 presents that the stiffener thickness of 12, 16, and 20 mm corresponded with the normalized number of load cycles of 0.98, 0.63, and 0.37, respectively, for stiffener width of 12 mm (normalized with 9300 cycles). For the stiffener thickness of 12 and 20 mm with the stiffener width of 100 mm are predicted the normalized number of load cycles of 1.00 and 0.38, respectively. The last width of 108 mm with the stiffener thickness of 16 mm is predict the life of 0.61.

The results indicate that the thickness of transverse stiffeners has the effect on fatigue crack life because the stress intensity factor may be more concentrated in the larger thickness of transverse stiffeners. Therefore, the influence of stiffener thickness on fatigue crack life can be described that the small thickness provides very high number of load cycles and severely decreases when the stiffener thickness is larger.

CHAPTER VI
CONCLUSIONS

6.1 Behavior of fatigue crack propagation for steel I-beams with welded transverse stiffeners under in-plane loading

Long life fatigue numerical simulation is carried out using 6 m long steel I-beams with welded transverse stiffeners, under constant amplitude loading. The obtained results clearly show that taking into consideration the different initial crack sizes and web-gap lengths have the influences on the fatigue durability of steel structures. The following conclusions are drawn from this study:

1. In the initial state, the propagation of very small crack requires very high number of load cycles. The defects should be minimized and the welding at the end of transverse stiffener should be very careful to increase the service life of the steel beams.

2. An initial crack with smaller web-gap length has a higher value of stress intensity factor which shortens the fatigue life.

3. The propagation of transverse stiffeners with larger thickness has a tendency to decrease the fatigue life of steel I-beams, whereas the flexural rigidity ratios do not affect to the fatigue life.

6.2 Recommendation for welded transverse stiffener details

As the result, steel I-beams with welded transverse stiffeners could be ensured to have the least defects in the process of fabrication because the sizes of defects have a strong influence fatigue life on steel structures. Also, the web-gap length is recommended by AASHTO (2012) [4] to use of four to six times as thick as web thickness for the strength of steel beams. This research suggests that the web-gap length could use six times as thick as web in order to increase the life of steel beams for fatigue effects. Furthermore, the thickness of transverse stiffeners should use as small as possible. If the transverse stiffeners can provide sufficient rigidity to steel beams, the use more thickness does not recommend from this research.

Recommendation for future works

This study concentrates on numerical simulation of in-plane fatigue crack propagation at the web-gap of steel I-beams in steel bridge. According to the limitations on this study, there are still many works that could be extended from this research, as follows,

- The shape of crack in all stage is only studied as the growth of semicircular crack. So, other cracks could be studied, such as, semi-elliptical crack, edge crack, double semicircular shape, etc.

- The mode of loadings, mode II, mode III, or mixed mode can take into consideration to study their effects on the welded steel structures.

- Variable amplitude loadings should be applied into account instead of constant amplitude loading for more accurate results of predicted fatigue life.

- Not only the rectangular shape of welded transverse stiffener can be studied, but other shapes can also be used in simulation to study their effects to steel structures.

- Residual stresses which arise from the welding could take into consideration in simulations, especially the welded steel structures.

- Improvement of the welded details on the connection between transverse stiffener and web plate is a useful method to obtain the more accuracy results.

- Environmental effects, e.g., temperature change, humidity, and corrosion should be considered to affect the fatigue crack propagation.

REFERENCES

[1] Aygül, M., Al-Emrani, M., Barsoum, Z., and Leander, J. Investigation of distortion-induced fatigue cracked welded details using 3D crack propagation analysis. International Journal of Fatigue 64 (2014): 54-66.

[2] Dinh, H.T. Analysis of Distortion-Induced Fatigue crack at the web gap of I-beam in steel bridges. doctor's degree, Department of Civil Engineering Chulalongkorn University, 2012.

[3] AASHTO. LRFD Bridge Specifications, ed. 6th. Washington, D.C., 2012.

[4] AISC. Specification for Structural Steel Buildings. 2010: Chicago.

[5] Huang, J.S., Yen, B. T. Stiffener requirements for plate girders. 1968, Fritz Laboratory Reports.

[6] Fisher, J.W., Albrecht, P. A., Yen, B. T., Klingerman, D. J., and McNamee, B. M. Fatigue strength of steel beams with welded stiffeners and attachments. 1974, Transportation Research Board: Washington, D.C.

[7] Sakano, M. and Wahab, M.A. Fatigue strength of welded transverse stiffener joints under variable amplitude loading. International Journal of Pressure Vessels and Piping 75(15) (1998): 1037-1045.

[8] Newman Jr, J.C. and Raju, I.S. Analyses of surface cracks in finite plates under tension or bending loads. NASA Technical Paper (1578) (1979).

[9] Raju, I.S. and Newman Jr, J.C. Stress-intensity factors for a wide range of semi-elliptical surface cracks in finite-thickness plates. Engineering Fracture Mechanics 11(4) (1979): 817-829.

[10] Newman Jr, J.C. and Raju, I.S. Prediction of fatigue crack-growth patterns and lives in three-dimensional cracked bodies. in The 6th International Conference on Fracture, pp. 1597-1608. New Delhi, India, 1984.

[11] Bouchard, P.O., Bay, F., and Chastel, Y. Numerical modelling of crack propagation: Automatic remeshing and comparison of different criteria. Computer Methods in Applied Mechanics and Engineering 192(35-36) (2003): 3887-3908.

[12] Liao, C.Y. and Atluri, S.N. Stress intensity factor variation along a semicircular surface flaw in a finite-thickness plate. Engineering Fracture Mechanics 34(4) (1989): 957-976.

[13] Newman, J.C. and Raju, I.S. An empirical stress-intensity factor equation for the surface crack. Engineering Fracture Mechanics 15(1) (1981): 185-192.

[14] McFadyen, N.B., Bell, R., and Vosikovsky, O. Fatigue crack growth of semi-elliptical surface cracks. International Journal of Fatigue 12(1) (1990): 43-50.

[15] Albrecht, P., Lenwari, A., and Feng, D. Stress intensity factors for structural steel I-beams. Journal of Structural Engineering 134(3) (2008): 421-429.

[16] Duchaczek, A. and Maήko, Z. Determination of the value of stress intensity factor in fatigue life of steel military bridges. European Journal of Environmental and Civil Engineering 19(8) (2014): 1015-1032.

[17] Riddell, W.T., Ingraffea, A.R., and Wawrzynek, P.A. Experimental observations and numerical predictions of three-dimensional fatigue crack propagation. Engineering Fracture Mechanics 58(4) (1997): 293-310.

[18] Kotsikos, G. and Grasso, M. Assessment of Fatigue Cracks in Rails. Procedia - Social and Behavioral Sciences 48 (2012): 1395-1402.

[19] Zong, L., Shi, G., and Wang, Y. Experimental investigation and numerical simulation on fatigue crack behavior of bridge steel WNQ570 base metal and butt weld. Construction and Building Materials 77 (2015): 419-429.

[20] Storgärds, E., Simonsson, K., and Sjöström, S. Three-dimensional crack growth modelling of a Ni-based superalloy at elevated temperature and sustained loading. Theoretical and Applied Fracture Mechanics 81 (2016): 2-10.

[21] Seifi, R. and Omidvar, N. Fatigue crack growth under mixed mode I + III loading. Marine Structures 34 (2013): 1-15.

[22] Anderson, T.L. Fracture Mechanics : Fundamentals and Applications. Boca Raton: CRC Press, 2005.

[23] Liang, R.Z., Rui, Z. C., Liang, Z. Y., & Bo, Z. H. M-integral for Stress Intensity Factor Base on XFEM. in International Symposium on Electronic Commerce and Security Workshops, pp. 226-230. Guangzhou, P.R. China, 2010.

[24] Ingraffea, A.R., & Wawrzynek, P. A. Finite Element Methods for linear elastic fracture mechanics. Chapter 3.1 in comprehensive structural integrity. [online]. 2003. Available from: http://www.cfg.cornell.edu/pdf/Comprehensive_Structural_integrity.pdf [September 10]

[25] Chan, S.K., Tuba, I.S., and Wilson, W.K. On the finite element method in linear fracture mechanics. Engineering Fracture Mechanics 2(1) (1970): 1-17.

[26] FRANC3D. Reference manual for version 6. Fracture Analysis Consultants, Inc. (2011).

[27] Aygül, M. Fatigue evaluation of welded details using the finite element method. CIvil and Environmental Engineering Chalmers university of technology, 2013.

[28] Erdogan, F. and Sih, G.C. On the Crack Extension in Plates Under Plane Loading and Transverse Shear. Journal of Basic Engineering 85(4) (1963): 519-525.

[29] Paris, P., and Erdogan, F. A Critical Analysis of Crack Propagation Laws. Journal of Basic Engineering 85(4) (1963): 528-533.

[30] FRANC3D. FRANC3D/BES Benchmarking. (2003).

[31] Kawahara, M. Study on Assessment of Safety Against Fatigue Crack Propagation in Nuclear Pressure Vessels and Piping Circuits. in AFC Submittee: Japan Welding Engineering Society, 1978.

[32] Nagoju, M.K.S.K., Gopinath, V. Computation of Stress Intensity Factor and Critical crack length of ASTM A36 steel using Fracture Mechanics. International Journal of Engineering Research & Technology (IJERT) 2(9) (2013).

[33] FHWA. Manual for repair and retrofit of fatigue cracks in steel bridges. March 2013, U.S.Department of Transportation.

APPENDIX

APPENDIX A

A STEP-BY-STEP CRACK PROPAGATION ANALYSIS BY FRANC3D

STEP 1: Finite Element Modeling

Create the finite element modeling as shown in Figure A.1 and define both the element type and material property by ANSYS. The boundary conditions, such as, point loads, distributed loads, bending moments, and structure supports are also assigned to the model. The model is divided into many elements and do volume meshing.

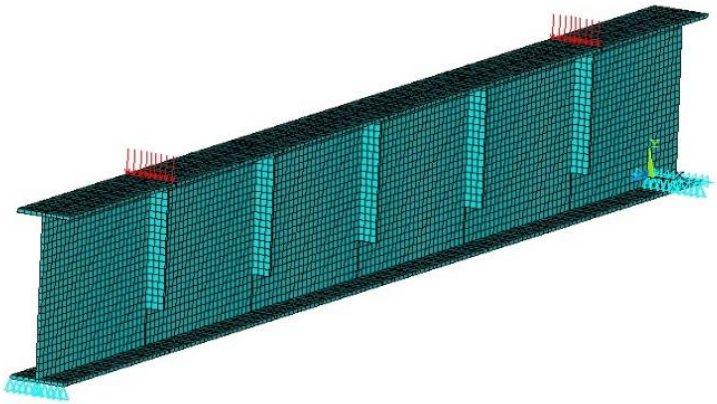

Figure A.1 Finite element modeling of steel I-beams with welded transverse stiffeners by Ansys

STEP 2: Import the File

Import the file to the FRANC3D software as shown in Figure A.2.

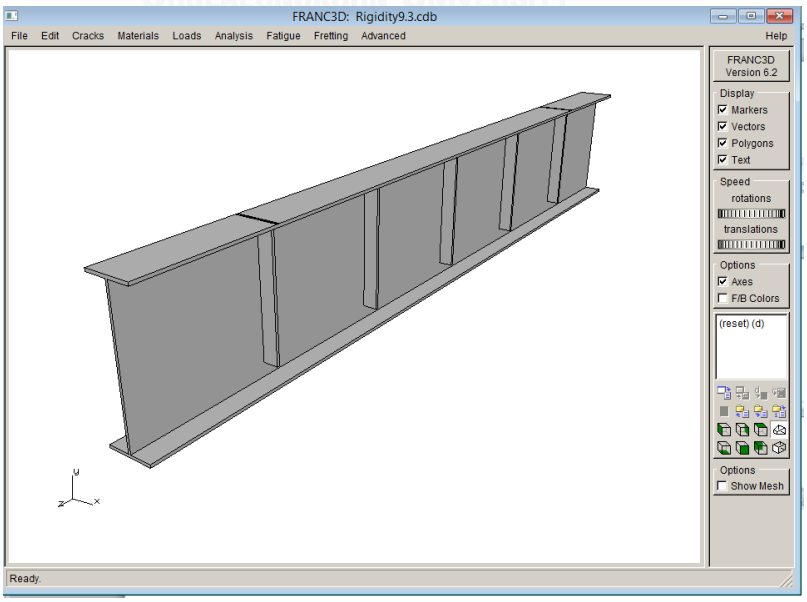

Figure A.2 the model is imported to FRANC3D software

STEP 3: insert an initial crack

Many types of cracks are able to be inserted into the model as shown in Figure A.3.

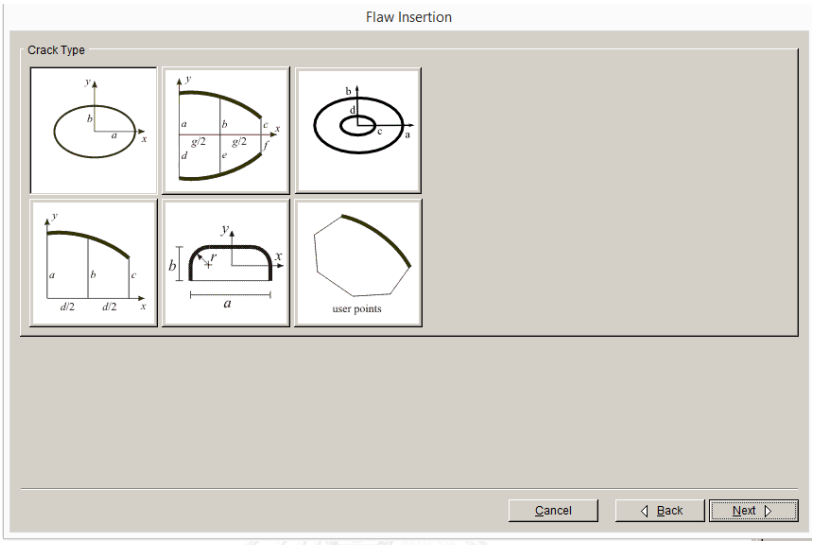

Figure A.3 Crack types

Define the initial crack size as shown in Figure A.4.

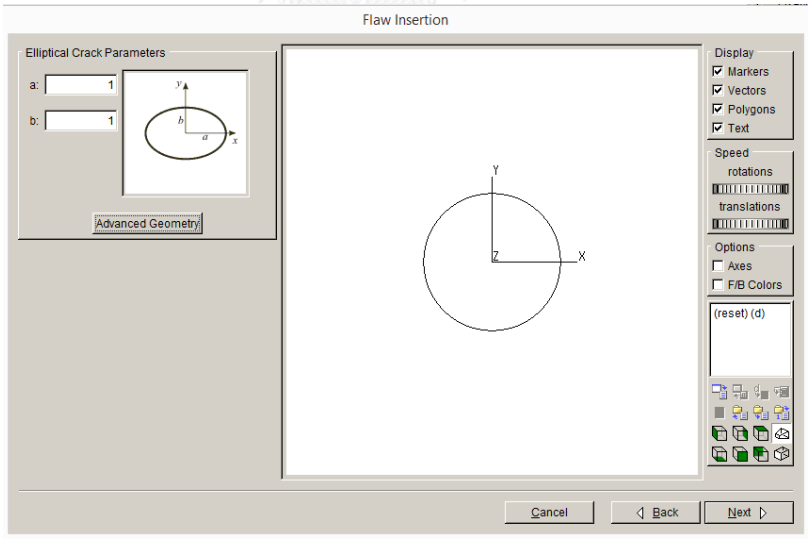

Figure A.4 Define an initial crack size

Define the location and the direction of the initial crack as shown in Figure A.5.

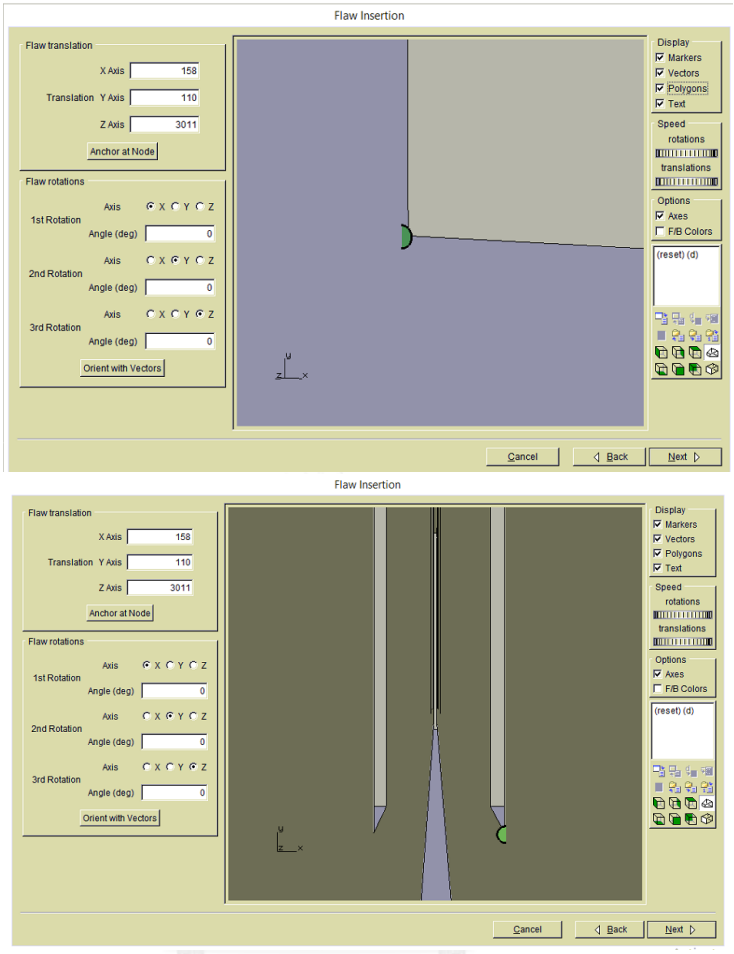

Figure A.5 The location and direction of the initial crack

Define the crack-front template (default is less than ten times of crack size) as shown in Figure A.6.

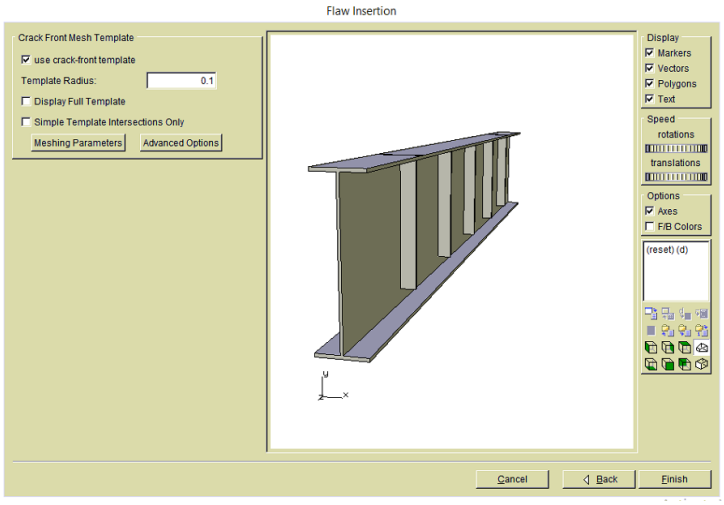

Figure A.6 The crack-front template

Figure A.7 shows that the FRANC3D begins the process of inserting the crack into the solid model by doing the geometric intersections, surface meshing, volume meshing, and final mesh smoothing. Wait a few minutes for operating.

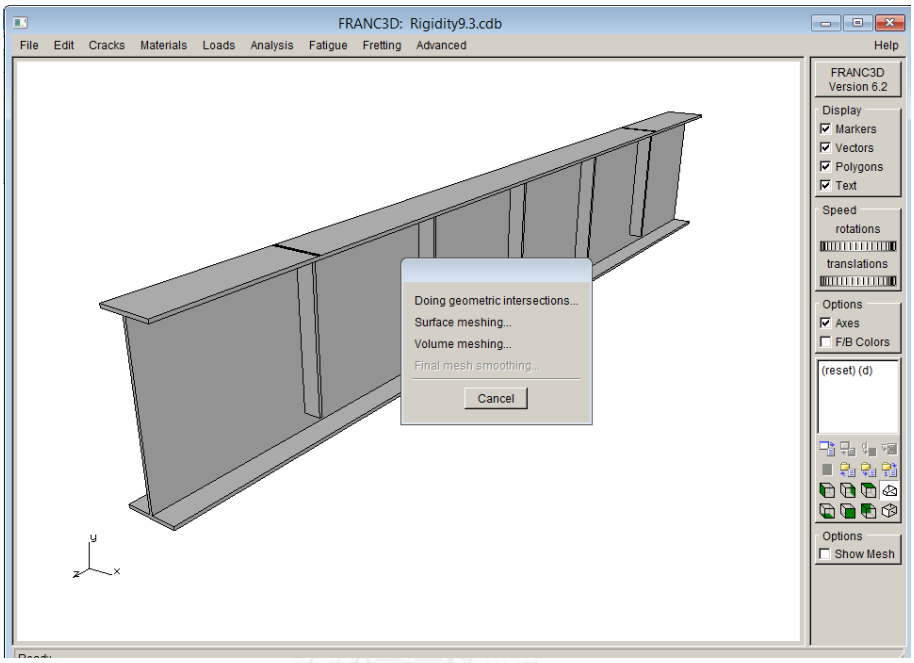

Figure A.7 Crack insertion status

FRANC3D automatically remesh when the new crack is inserted as shown in Figure A.8.

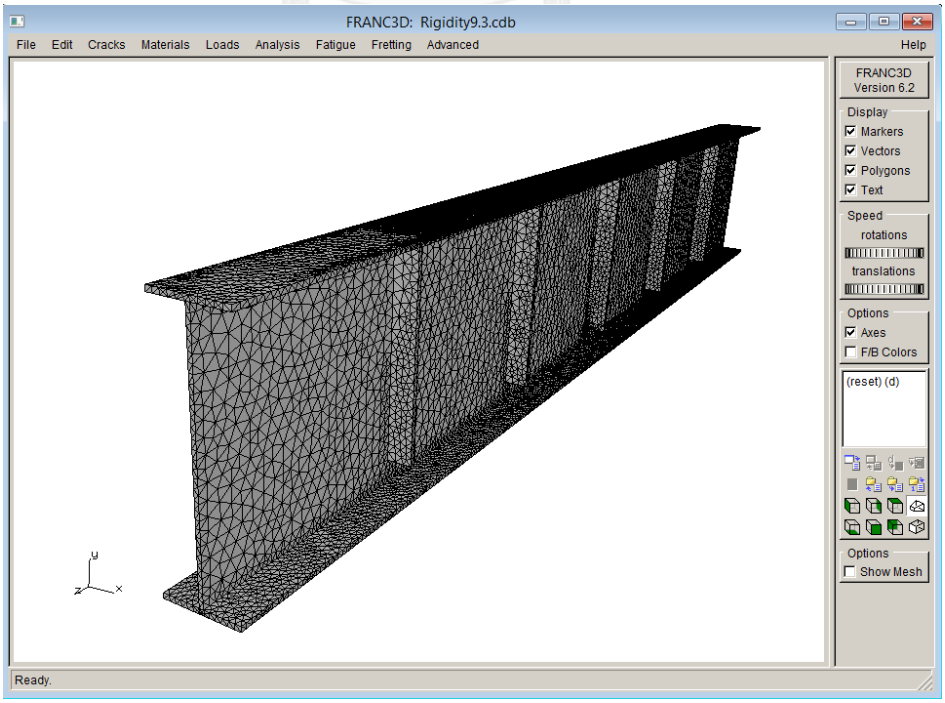

Figure A.8 Mesh model with initial crack

The obtained initial crack is located at the lower end of transverse stiffeners beside the weld toe as shown in Figure A.9.

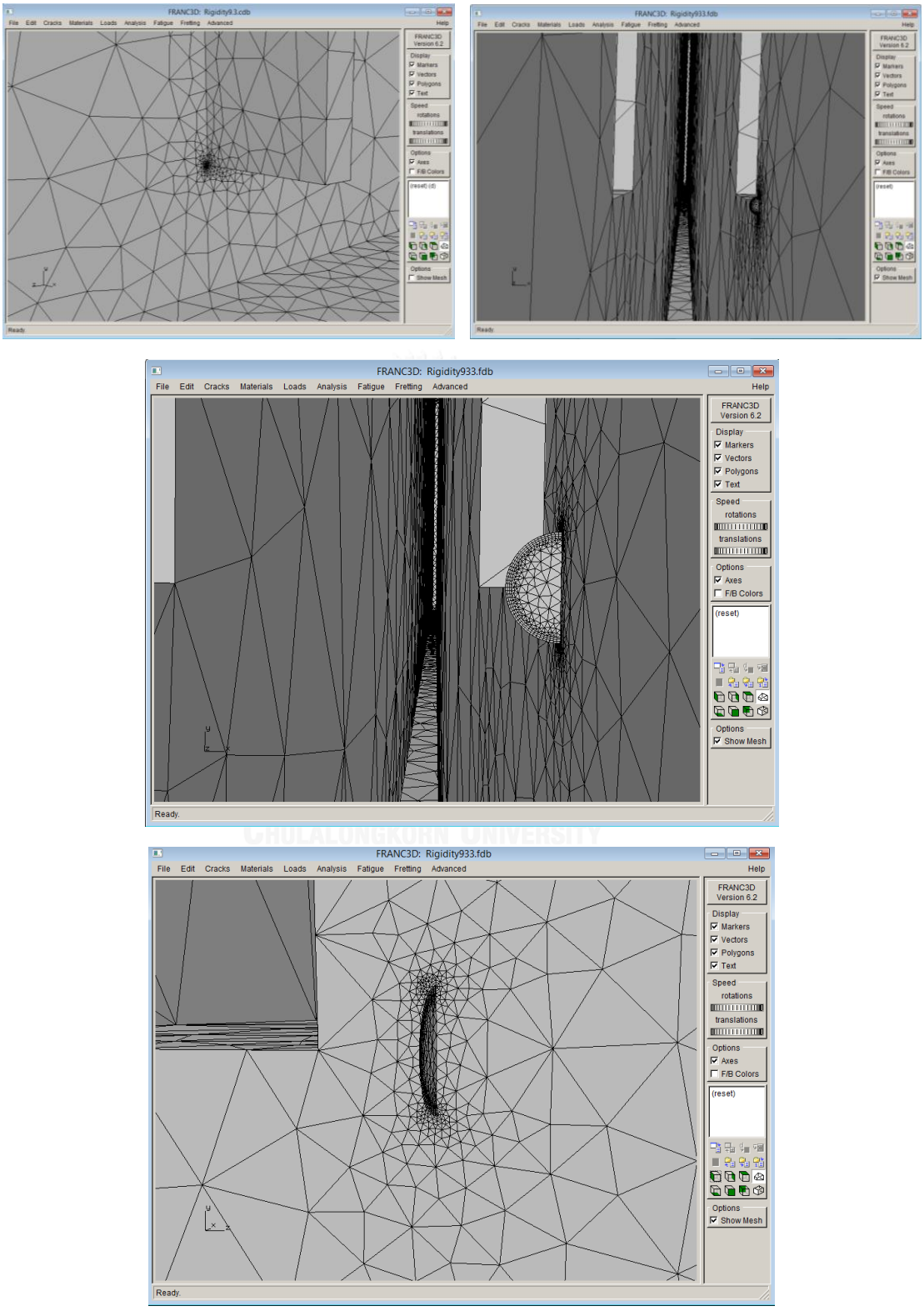

Figure A.9 Crack insertion results

STEP 4: Static analysis and stress intensity factor

Select the static analysis menu. FRANC3D automatically sends the element model to ANSYS for performing the static analysis and then sending back to FRANC3D. Select the method to compute the stress intensity factor for the initial stage in the panel as shown in Figure A.10 by FRANC3D using the results file obtained from ANSYS. Figure A.11 shows the obtained results.

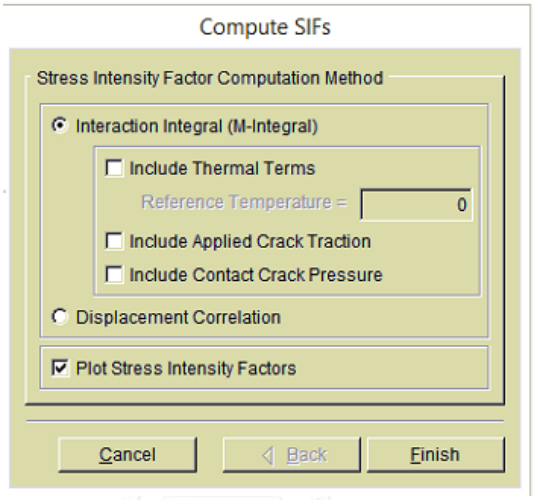

Figure A.10 compute the stress intensity factor panel.

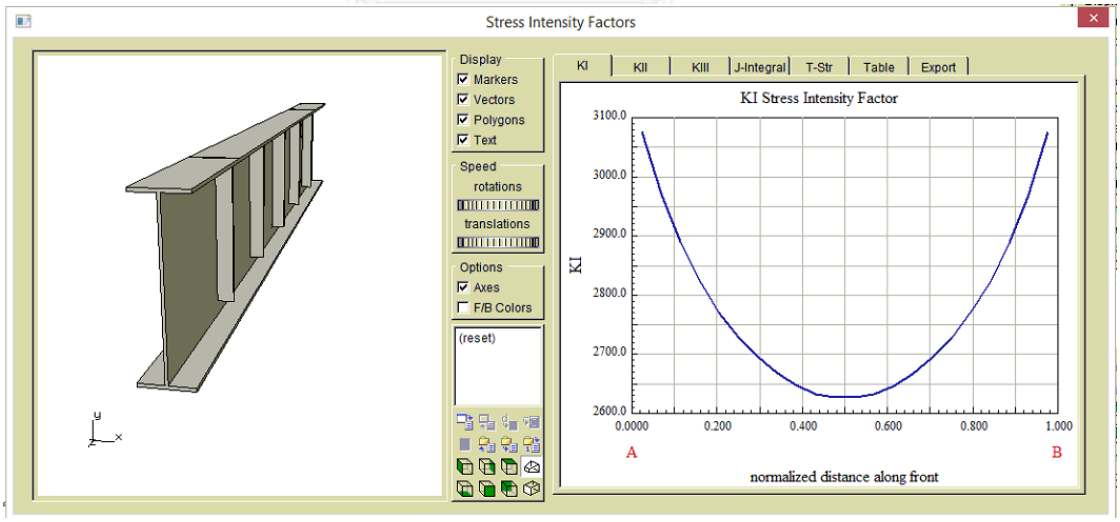

Figure A.11 The result of stress intensity factor

STEP 5: Crack growth analysis

Select the units, fatigue crack growth type, kink angle, and then input the material constant of Paris law as shown in Figure A.12.

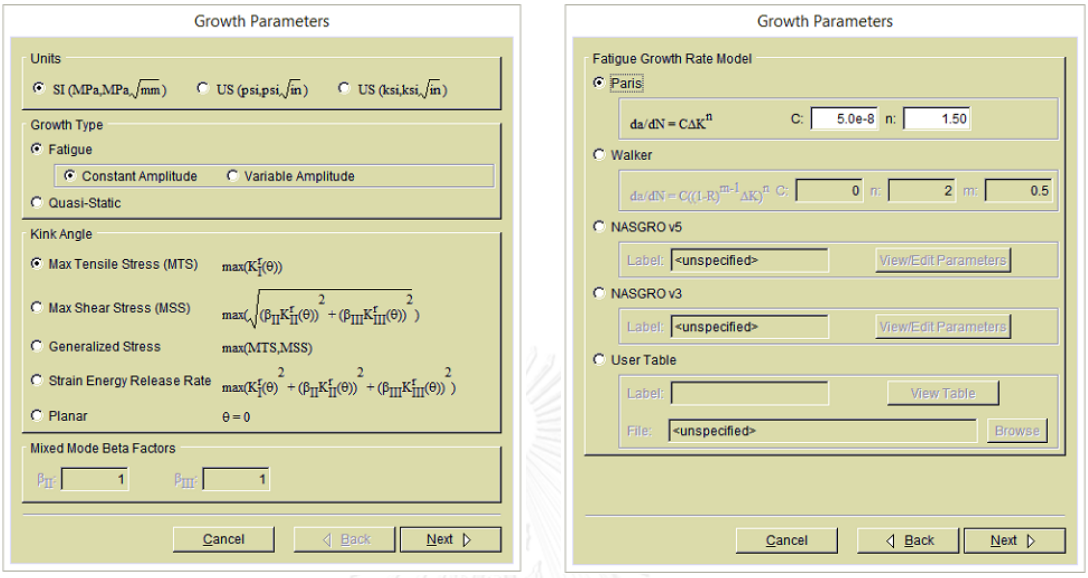

Figure A.12 Growth parameters panel

Select the crack extension type and input the constant amplitude stress ratio (R), the number of crack growth steps, and the constant cycles count increments for each step as shown in Figure A.13.

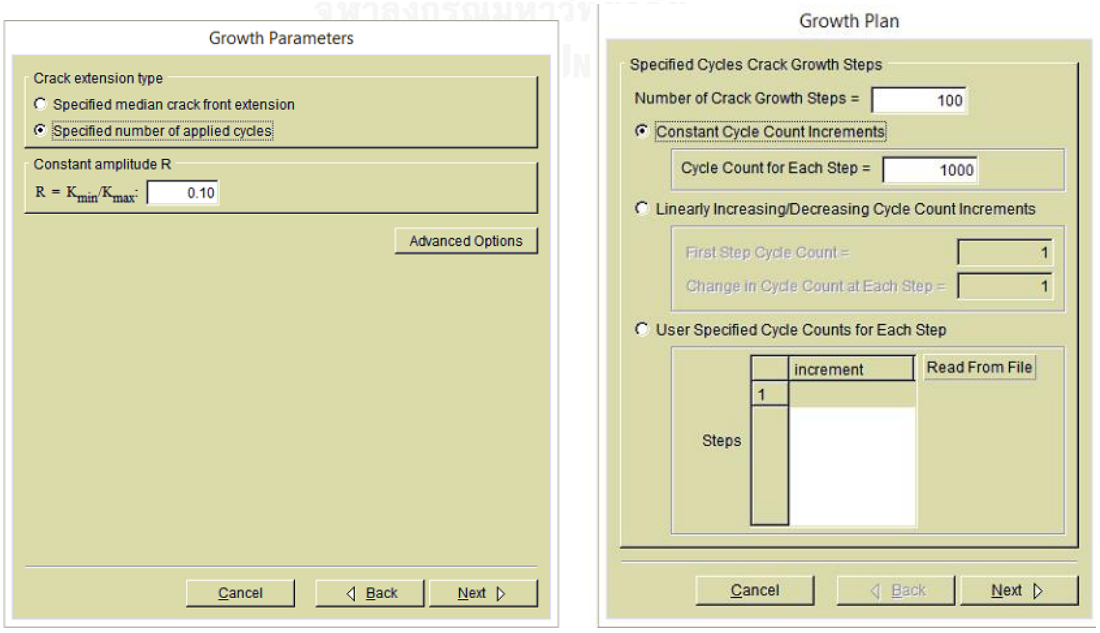

Figure A.13 Growth parameters panel (2)

The crack increment **Δ**a is extended and the element model is automatically remeshed again for next static analysis. This process is repeated for the chosen number of crack steps. Finally, the obtained results are the stress intensity for each step, crack increment for each step, and the number of crack step as presented in Figure A.14.

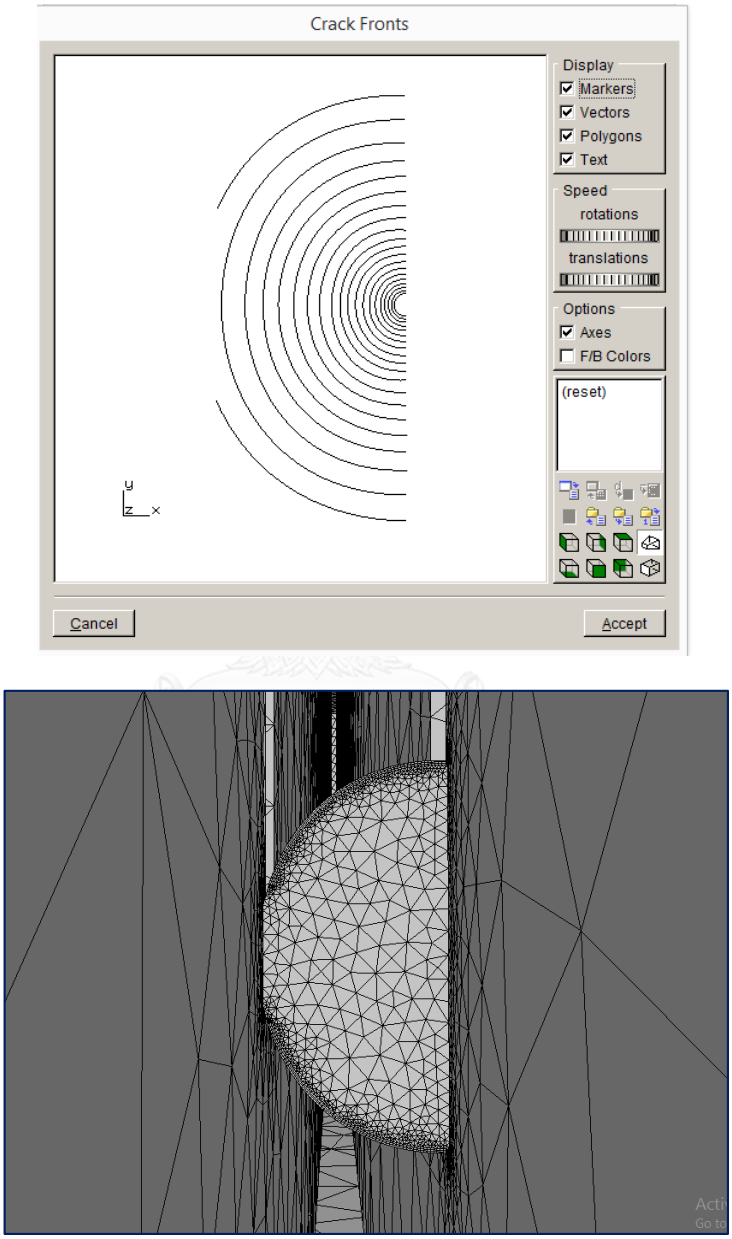

Figure A.14 Crack fronts result

Perform the analysis for the two-tip through-thickness crack

The method is repetition of the step 3-5 again but changes the crack configuration as shown in Figure A.15 and Figure A.16.

STEP 3: insert an initial crack

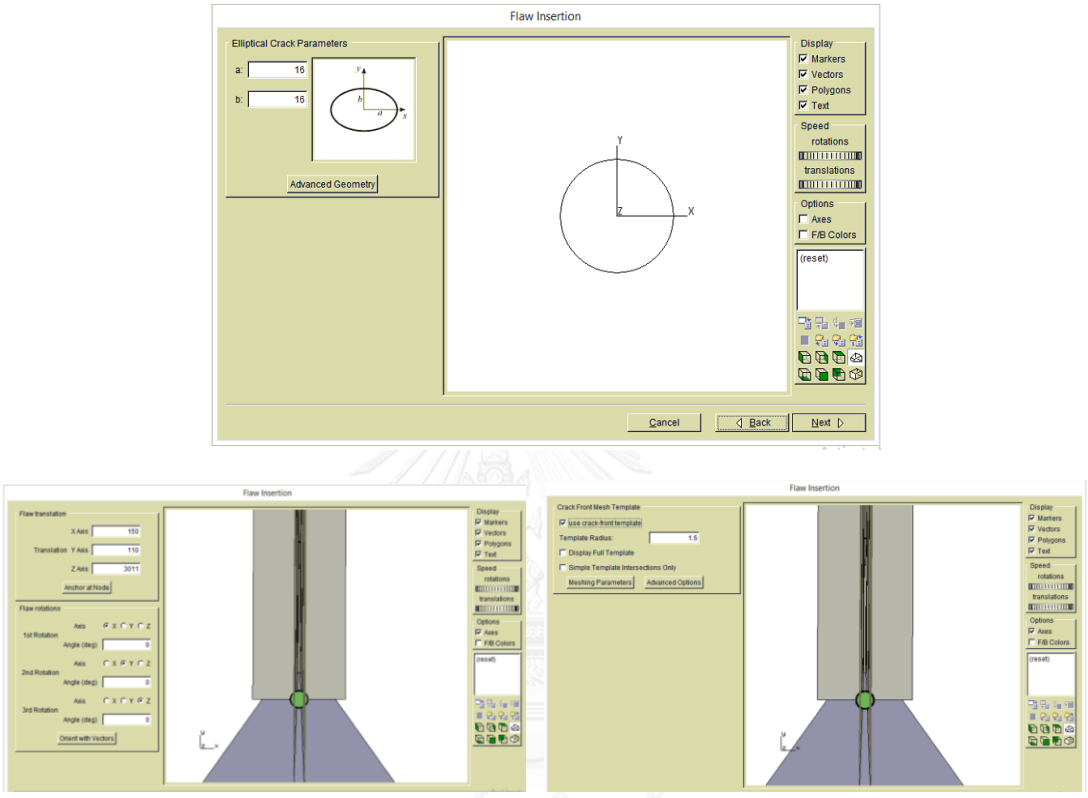

Figure A.15 The insertion of two-tip through-thickness crack

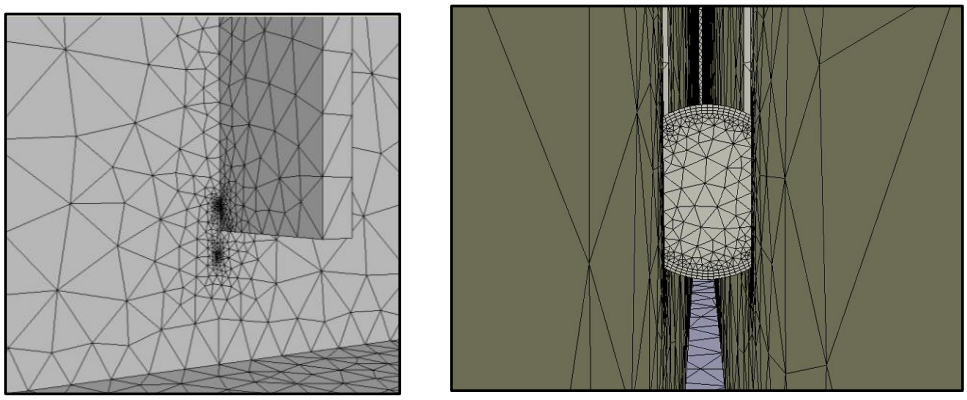

Figure A.16 crack insertion results

STEP 4: Static analysis and stress intensity factor

Select the static analysis menu. FRANC3D automatically sends the element model to ANSYS for performing the static analysis and then sending back to FRANC3D. Select the method to compute the stress intensity factor for the initial stage by FRANC3D using the results file obtained from ANSYS as shown in Figure A.17.

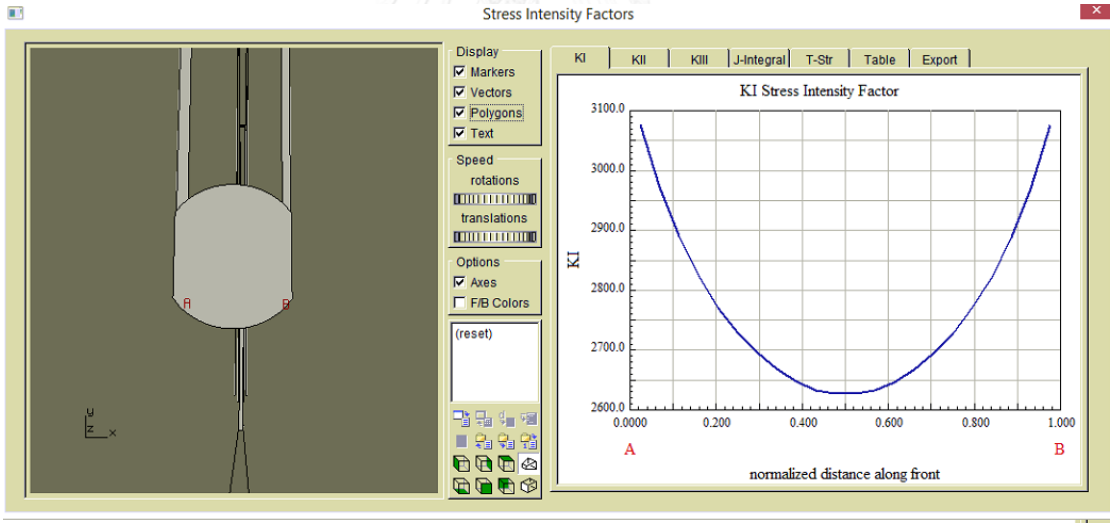

Figure A.17 The result of the stress intensity factor

STEP 5: Crack growth analysis

Finally, the obtained results are the stress intensity for each step, crack increment for each step, and the number of crack step as presented in Figure A.18.

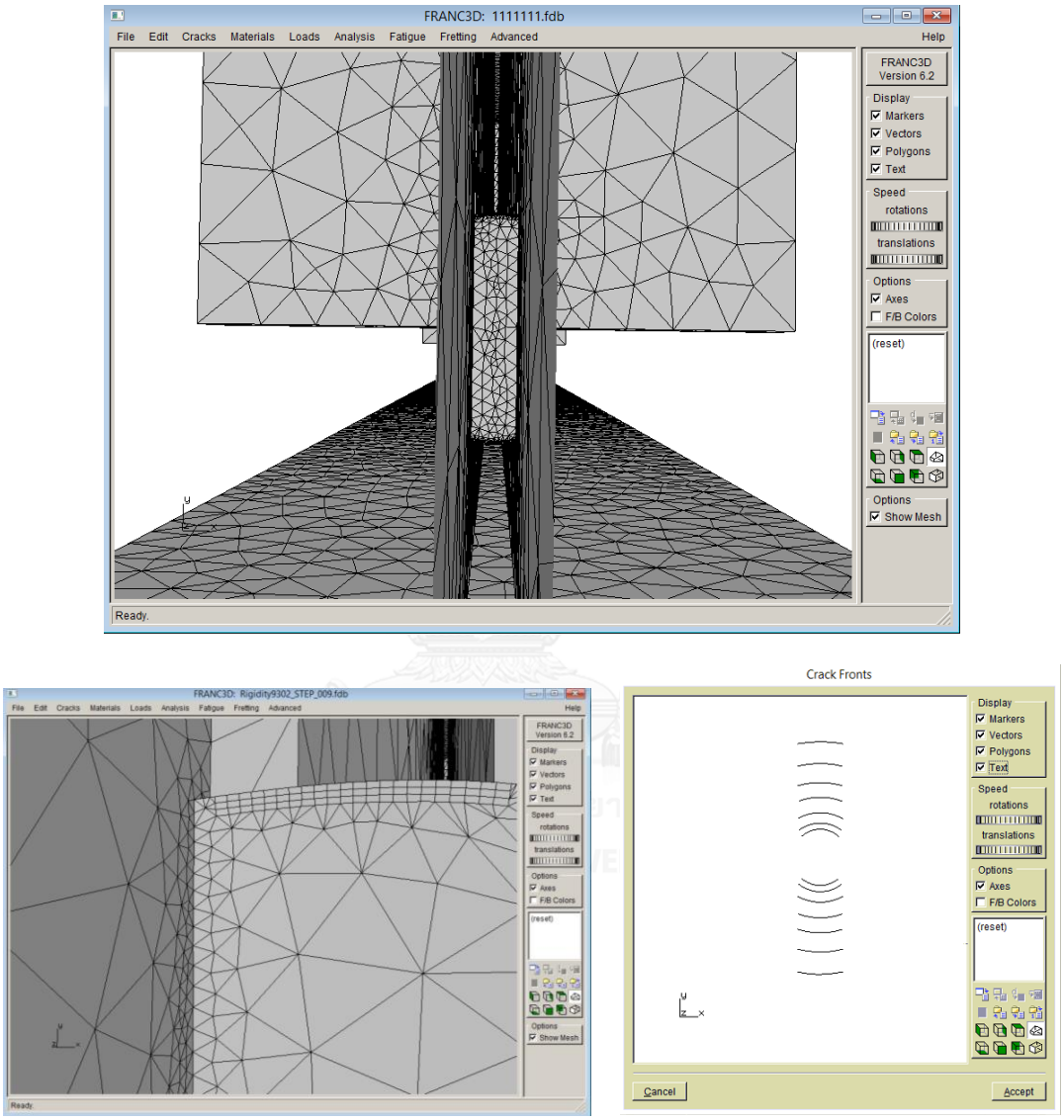

Figure A.18 Crack fronts results

APPENDIX B

THE COMPARISON OF THE RESULTS OF THE STRESS INTENSITY FACTOR BETWEEN STEEL I-BEAMS WITH AND WITHOUT WELDED TRANSVERSE STIFFENERS OBTAINED FROM FRANCE3D

The steel beams have I-sectioned steel plate beam of 6 m length, 300 mm width, 930 mm depth, 20 mm flange thickness, and 16 mm web thickness with and without welded transverse stiffeners of 100 mm width and 12 mm thick attached both sides on the web plate with a web gap of 90 mm. The initial crack size is 1 mm for semicircular shape and 16 mm for the two-tip through-thickness shape. The flexural rigidity ratio of the steel beam with welded transverse stiffeners is equal to 2.66×10^{-3}.

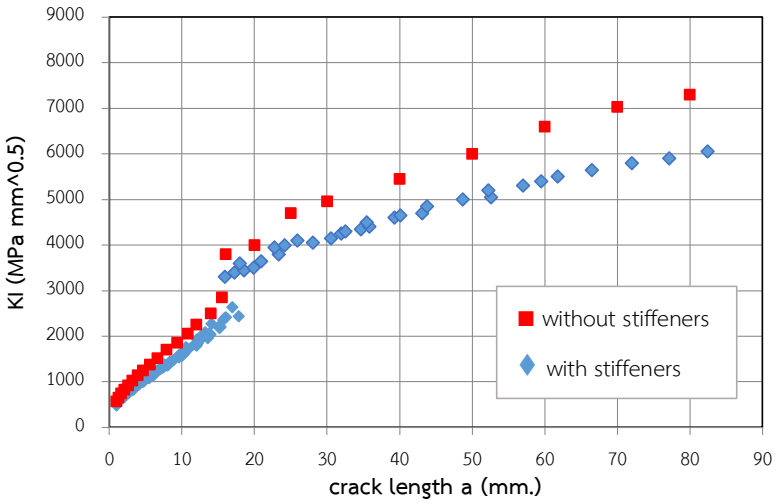

Figure B.1 The comparison of the results of the stress intensity factor between steel I-beams with and without transverse stiffeners

Figure B.1 indicates that the results of stress intensity factor of steel I-beams with welded transverse stiffeners have lower values than steel I-beams without transverse stiffeners along crack lengths. Because the transverse stiffeners are able to increase the rigidity of the steel beams, the stress intensity factor of the steel I-beams with welded transverse stiffeners decreases.

APPENDIX C

THE RESULTS OF THE STRESS INTENSITY FACTOR AND FATIGUE LIFE OBTAINED FROM FRANC3D SIMULATIONS

The steel I-beams with welded transverse stiffeners that are simulated with different parameters are investigated the stress intensity factor and the fatigue life.

- <u>Parameters : Web-gap lengths</u>

web-gap lengths = 90 mm **initial crack size = 1 mm**

flexural rigidity ratio = 2.66×10^{-3} **stiffener thickness = 12 mm, width = 100 mm**

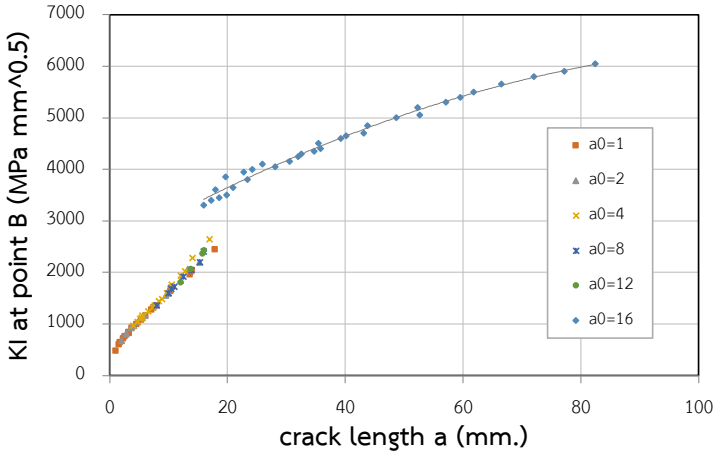

Figure C.1 The result of the stress intensity factor for web-gap length of 90 mm

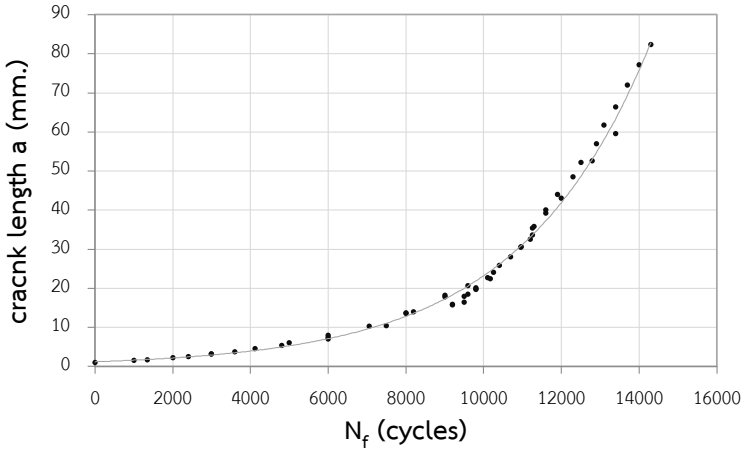

Figure C.2 The result of the fatigue life for web-gap length of 90 mm

web-gap lengths = 215 mm initial crack size = 1 mm

flexural rigidity ratio = 2.66×10^{-3} stiffener thickness = 12 mm, width = 100 mm

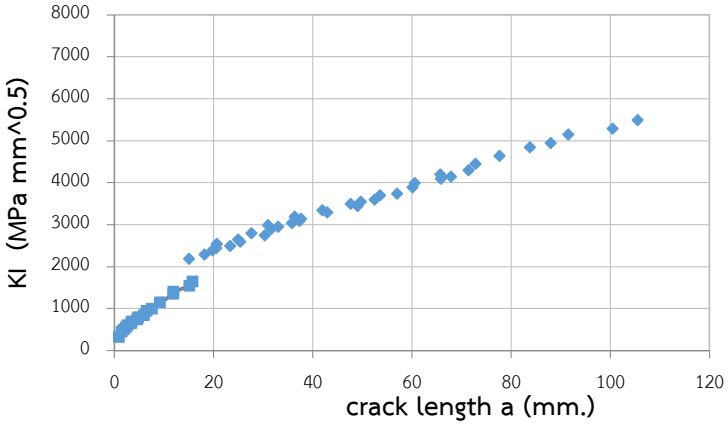

Figure C.3 The result of the stress intensity factor for web-gap length of 215 mm

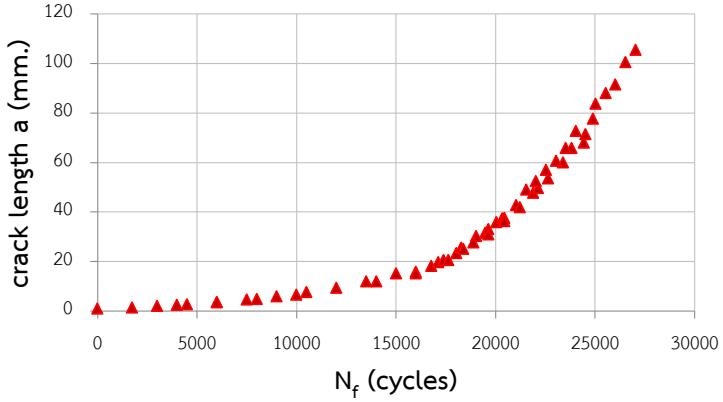

Figure C.4 The result of the fatigue life for web-gap length of 215 mm

web-gap lengths = 340 mm initial crack size = 1 mm

flexural rigidity ratio = 2.66×10^{-3} stiffener thickness = 12 mm, width = 100 mm

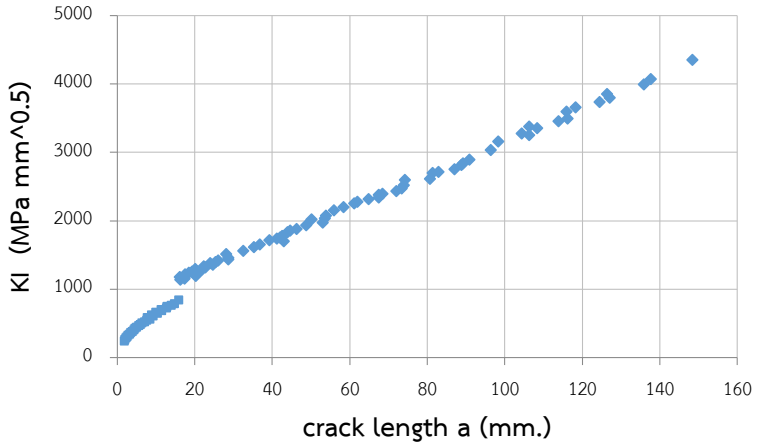

Figure C.5 The result of the stress intensity factor for web-gap length of 340 mm

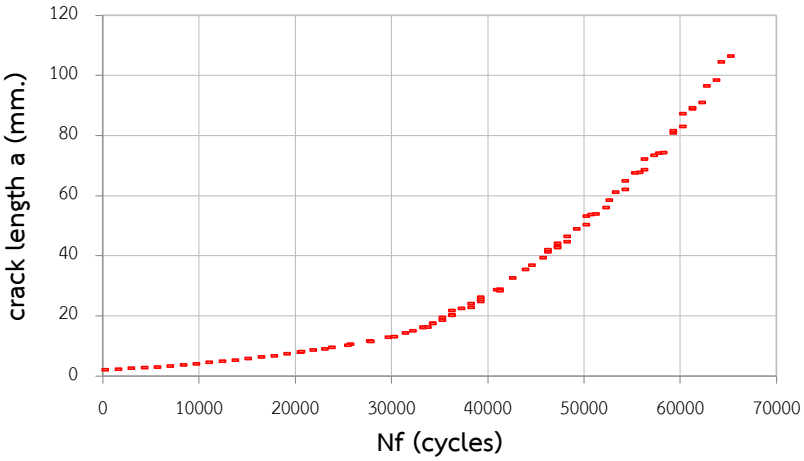

Figure C.6 The result of the fatigue life for web-gap length of 340 mm

- Parameters : Flexural rigidity ratios

web-gap lengths = 90 mm initial crack size = 1 mm

flexural rigidity ratio = 5.92×10^{-3} stiffener thickness = 16 mm, width = 120 mm

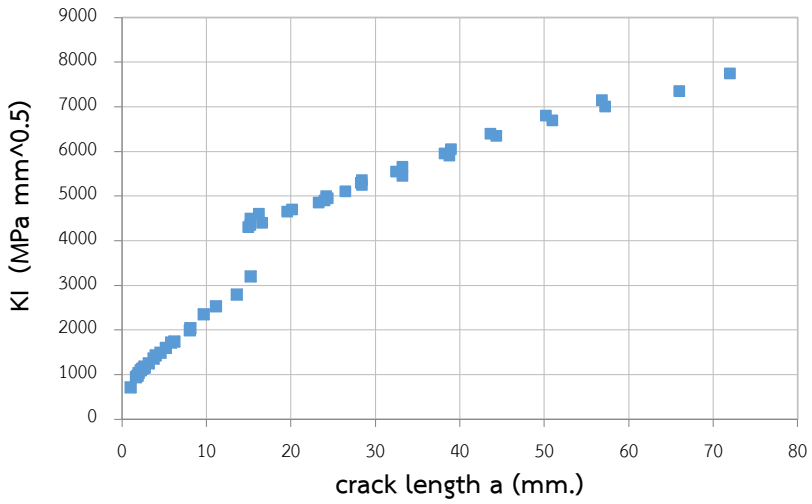

Figure C.7 The result of the stress intensity factor for flexural rigidity ratio of 5.92×10^{-3} (stiffener t=16 mm, w=120 mm)

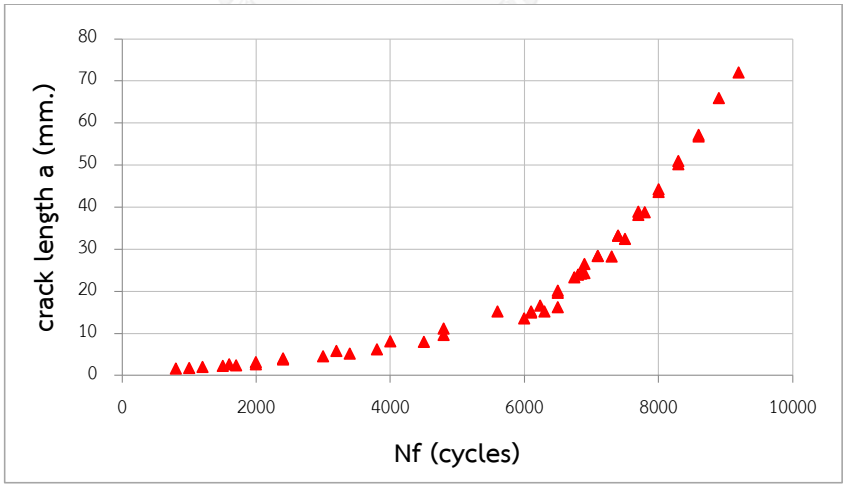

Figure C.8 The result of the fatigue life for flexural rigidity ratio of 5.92×10^{-3} (stiffener t=16 mm, w=120 mm)

web-gap lengths = 90 mm initial crack size = 1 mm

flexural rigidity ratio = 4.44×10^{-3} stiffener thickness = 12 mm, width = 120 mm

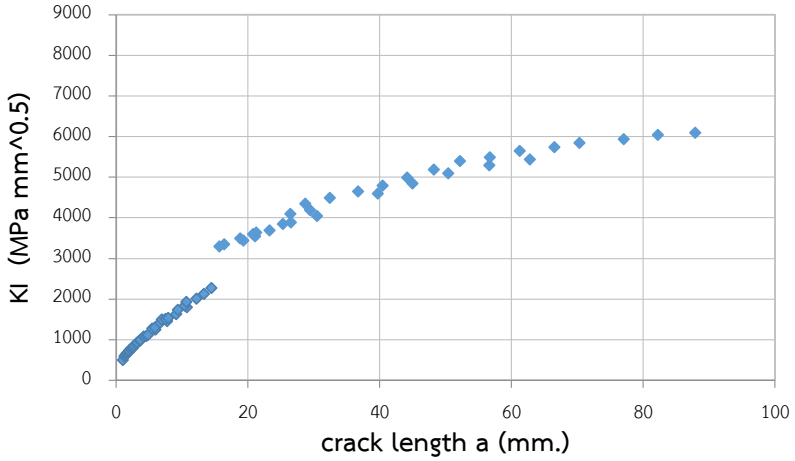

Figure C.9 The result of the stress intensity factor for flexural rigidity ratio of 4.44×10^{-3} (stiffener t=12 mm, w=120 mm)

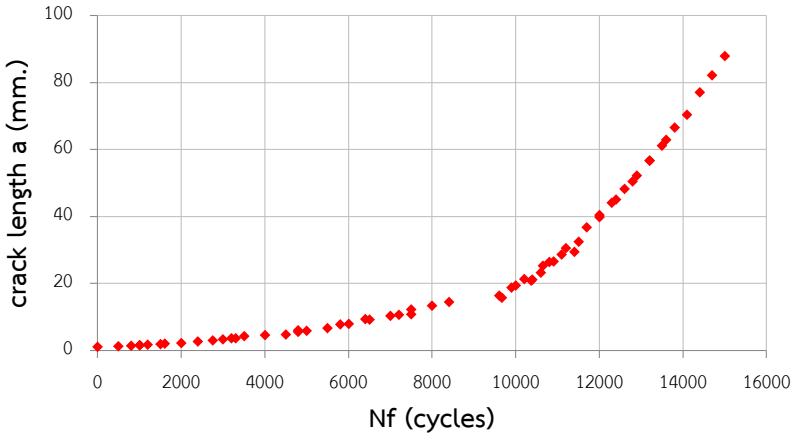

Figure C.10 The result of the fatigue life for flexural rigidity ratio of 4.44×10^{-3} (stiffener t=12 mm, w=120 mm)

web-gap lengths = 90 mm initial crack size = 1 mm

flexural rigidity ratio = 4.44×10^{-3} stiffener thickness = 20 mm, width = 100 mm

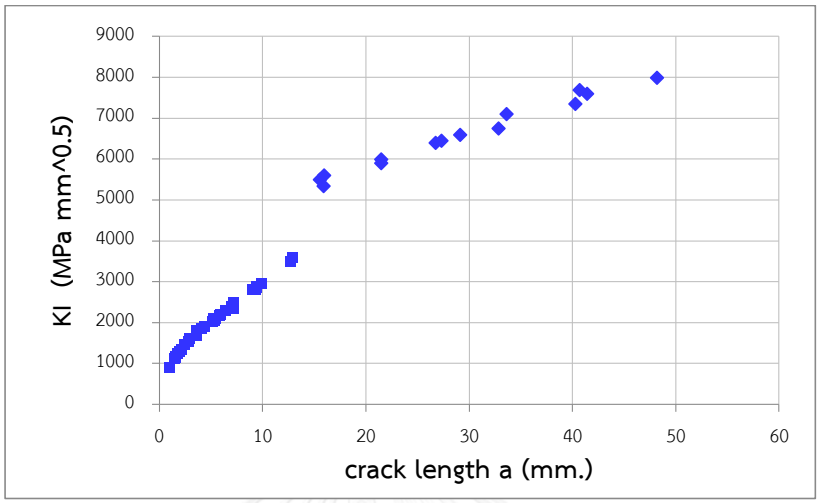

Figure C.11 The result of the stress intensity factor for flexural rigidity ratio of 4.44x10-3 (stiffener t=20 mm, w=100 mm)

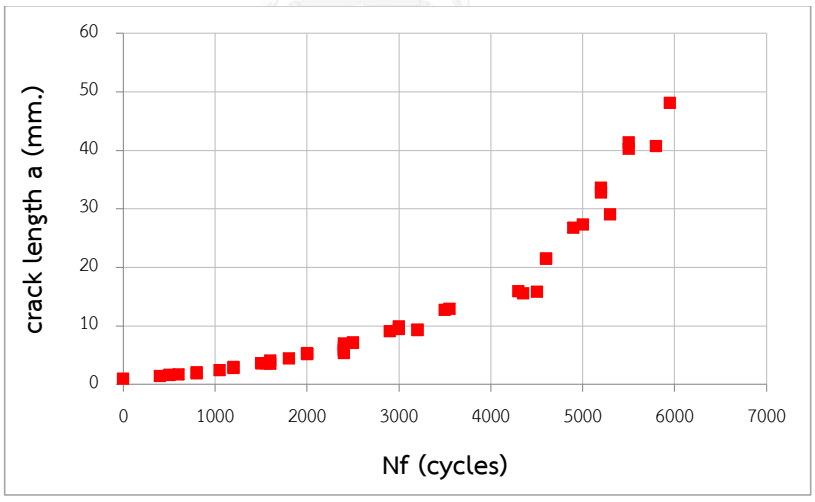

Figure C.12 The result of the fatigue life for flexural rigidity ratio of 4.44×10^{-3} (stiffener t=20 mm, w=100 mm)

web-gap lengths = 90 mm initial crack size = 1 mm

flexural rigidity ratio = 7.39×10^{-3} stiffener thickness = 20 mm, width = 120 mm

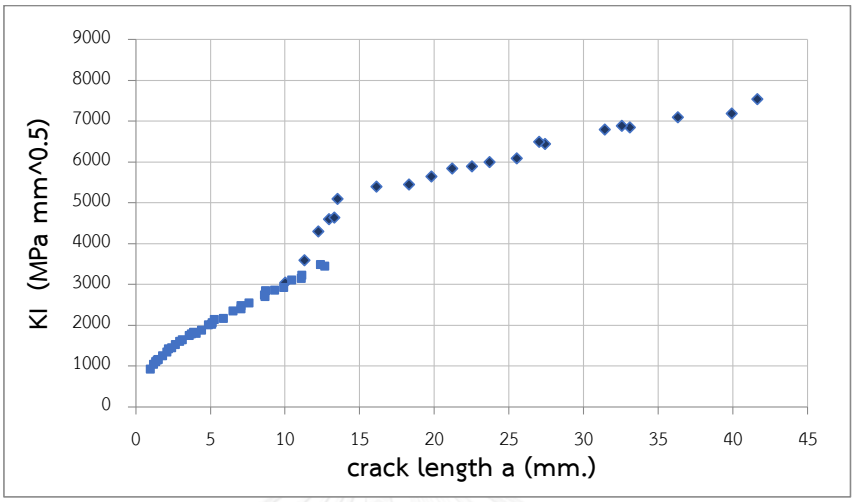

Figure C.13 The result of the stress intensity factor for flexural rigidity ratio of 7.39×10^{-3} (stiffener t=20 mm, w=120 mm)

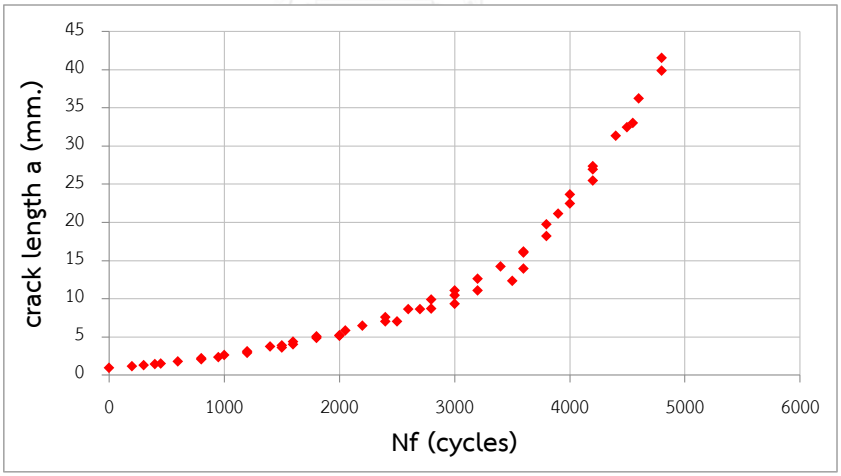

Figure C.14 The result of the fatigue life for flexural rigidity ratio of 7.39×10^{-3} (stiffener t=20 mm, w=120 mm)

web-gap lengths = 90 mm initial crack size = 1 mm

flexural rigidity ratio = 4.44×10^{-3} stiffener thickness = 16 mm, width = 108 mm

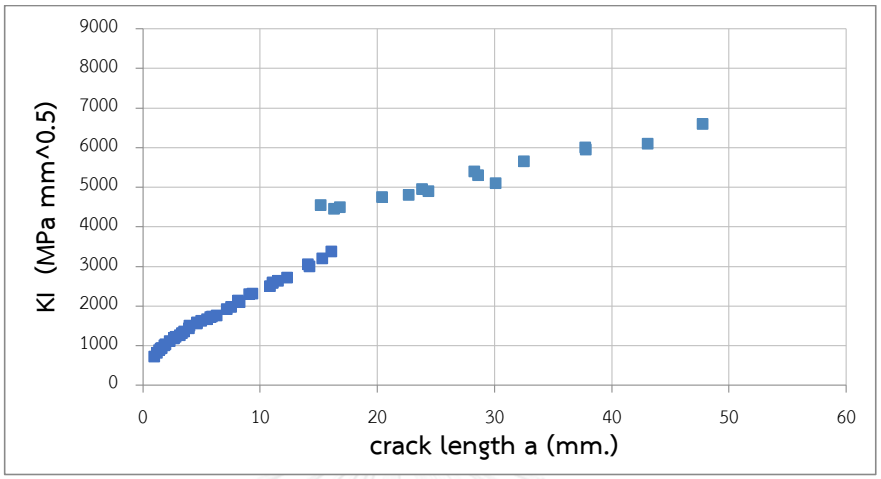

Figure C.15 The result of the stress intensity factor for flexural rigidity ratio of 4.44×10^{-3} (stiffener t=16 mm, w=108 mm)

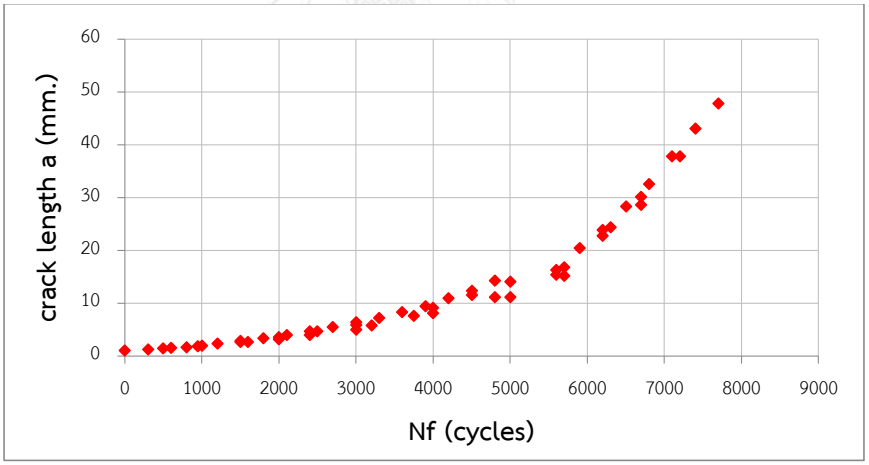

Figure C.16 The result of the fatigue life for flexural rigidity ratio of 4.44×10^{-3} (stiffener t=16 mm, w=108 mm)

VITA

Wanchalerm Triamlumlerd was born in Bangkok province, Thailand on 5th December, 1990. He graduated from Chulalongkorn University with a Bachelor's degree in Civil Engineering in April, 2013. After his graduation, he had worked as an Engineer at THAI SHIMIZU CO., LTD. for 1 year. In July, 2014, he was studying in Master Degree of Civil Engineering (Structural Engineering) at Chulalongkorn University.